Design and Development of Zinc Oxide thin film based Schottky Diodes and TFTs and their application as UV Detectors

Submitted in

fulfillment of the requirements for the degree of

Doctor of Philosophy

by

Tarun Varma

ID: 2010REC505

Under the Supervision of

Prof. Dharmendar Boolchandani

DEPARTMENT OF ELECTRONICS AND COMMUNICATION ENGINEERING

MALAVIYA NATIONAL INSTITUTE OF TECHNOLOGY JAIPUR, INDIA

December 2017

Certificate

This is to certify that the thesis entitled **"Design and Development of Zinc Oxide thin film based Schottky Diodes and TFTs and their application as UV Detectors"** being submitted by **Tarun Varma (2010REC505)** is a bonafide research work carried out under my supervision and guidance in fulfillment of the requirement for the award of the degree of **Doctor of Philosophy** in the Department of Electronics & Communication Engineering, Malaviya National Institute of Technology, Jaipur, India. The matter embodied in this thesis is original and has not been submitted to any other University or Institute for the award of any other degree.

Place: Jaipur
Date:

Dharmendar Boolchandani
Professor
Dept. of Electronics and Communication
M.N.I.T., Jaipur

i

DECLARATION

I, **Tarun Varma**, declare that this thesis titled, "**Design and Development of Zinc Oxide thin film based Schottky Diodes and TFTs and their application as UV Detectors** " and the work presented in it, are my own. I confirm that:

- This work was done wholly or mainly while in candidature for a research degree at this university.

- Where any part of this thesis has previously been submitted for a degree or any other qualification at this university or any other institution, this has been clearly stated.

- Where I have consulted the published work of others, this is always clearly attributed.

- Where I have quoted from the work of others, the source is always given. With the exception of such quotations, this thesis is entirely my own work.

- I have acknowledged all main sources of help.

- Where the thesis is based on work done by myself, jointly with others, I have made clear exactly what was done by others and what I have contributed myself.

Date:

Tarun Varma
(2010REC505)

ACKNOWLEDGEMENT

ABSTRACT

Zinc Oxide (ZnO) semiconductor material has wide range of applications for energy transformation and UV sensing with suitable properties for optoelectronics devices. It has an excellent transparency with a wide band gap of 3.37 eV and high carrier mobility along with quantum confinement effects that makes it preferable material for ultra-violet photo-detectors, solar cells and transparent electronics applications. Various types of well aligned ZnO nanostructures can be synthesized using novel RF sputtering deposition process, at low temperatures, in a controlled manner.

Simulation studies were undertaken with various software tools to optimize the device characteristics and improve the performance. ZnO based Schottky diodes were evaluated with different types of metal contacts, such as Gold (Au), Platinum (Pt) and Palladium (Pd) under different temperature conditions, doping concentrations and channel thicknesses. Simulations studies were also carried out to evaluate the optimized parameters for the bottom-gate TFT structure, with varying channel lengths.

Sputtered ZnO thin films were grown on silicon (Si) wafers for fabrication of Schottky photo-diodes (PD) and Thin Film Transistors (TFTs) to detect UV light. Characterization techniques, like Atomic Force Microscopy (AFM), Scanning Electron Microscopy (SEM), X-ray Diffraction (XRD) were used to analyze the micro structural properties along with the surface morphology, crystalline orientation and surface roughness.

Metal contacts of Gold (Au) and Palladium (Pd) were chosen for contacts in case of Schottky photo-diodes. Transmittance, rectification ratio, ideality factor, barrier height and series resistance were measured to comprehensively study the electro-optical responses of these Schottky photo-diodes, with current-voltage (I-

V), capacitance-voltage (C-V) curves at various frequencies. Further their UV responses were investigated with various performance parameters such as, contrast ratio, responsivity, photo-conductive gain and detectivity to extract the working performance of these Schottky photo-diodes.

Thin Film Transistors (TFTs) were also fabricated for applications as high response UV Photo-detectors with bottom gate structure, grown on silicon, at room temperature, with RF magnetron sputtering process. Performance of these detectors were explored by varying the W/L ratio. The channel width was taken as 40 μm and the lengths were varied as 6μm and 12 μm. Various electrical characteristics, such as leakage current, threshold voltage, ON-OFF ratio, field effect mobility and sub-threshold swing were evaluated with the help of output and transfer characteristics. Further, the TFTs were tested for device stability, by subjecting them to both positive and negative bias-stress conditions and their performance was evaluated. The TFTs were further tested for UV photo-response.

The structural and surface morphological properties were investigated using various characterization equipments such as AFM, XRD and SEM. Semiconductor Device Analyser was used to measure the electrical properties of both the devices.

This study consolidates that the ZnO thin film grown on n-Si substrate, using RF Magnetron Sputtering technique, with an (100) orientation is an excellent n-type semiconductor for further fabricating the Schottky diodes and TFTs, to be utilised in UV detection applications.

The majority of the fabrication and the device characterization work of ZnO Schottky diodes and the TFTs was carried out at National Nano Fabrication Center, Centre for Nano Science and Engineering (CeNSE), Indian Institute of Science (IISc), Bangalore.

Contents

List of Figures

List of Tables

ABBREVIATIONS

Au	Gold
Al	Aluminium
AFM	atomic force microscopy
SEM	scanning electron microscopy
ZnO	Zinc oxide
PL	photoluminescence
UV	ultraviolet
XRD	X-ray diffraction
GaN	Gallium nitride
Si	Silicon
SRH	Shockley-read-hall
UV-Vis	ultraviolet-visible

Chapter 1

Introduction

With UV radiation being a serious health hazard these days, there is a sincere need to design and develop efficient and highly sensitive photo sensors at relatively lower costs. An emerging class of materials that satisfy this need is the metal oxide semiconductors. Devices fabricated from these fundamental blocks of nano-structures possess unique properties that has attracted a huge attention in the last few decades.

Functional oxides of such materials such as SnO_2, Ga_2O_3, PbO_2, In_2O_3 and ZnO possess unique structural, physical, chemical and electro-optical properties that can be fine tuned for a wide range of applications in the diverse fields such as superconductor, magnetics and optoelectronic applications. Advantages of oxide semiconductors over the established a-Si:H technology include electrical-stress stability, higher field-effect mobility, and lower power consumption.

Nano-structures are similar when compared with a single continuous crystal, with the same lattice constants, as can be observed with the X-ray diffractions and transmission electron microscopy. They differ significantly in contrast to the arrangement of the structure in the bulk material due to the presence of defects, although they retain many of its bulk material properties. The major difference lies in its significantly large surface-to-volume-ratio, that begets it to possess remarkably distinct structural and electroptical properties as compared to its

bulk structure counterpart. The increased electronic density of states enhances the electron-hole and electron-phonon interactions, thereby causing the quantum confinement effects. Typical structures that result are the two-dimensional quantum wells (thin layers), one-dimensional quantum wires, and zero-dimensional quantum dots.

Recent research has extensively focussed on synthesising potential devices from the III-V and II-VI compounds that are wide band-gap semiconductors with distinctive properties suitable for developing applications in the UV region. Among these semiconductor materials, Zinc Oxide (ZnO) has attracted much attention for application in UV detection and solar cell applications with its high direct band-gap, good bonding strength, favourable thermal conductivity, large exciton binding energy and excellent transparency. Wide band-gap semiconductors, with a $E_g > 2eV$, are suitable for emission in the blue, green or UV region of the frequency spectrum and their use in high temperature and high power applications.

Zinc oxide (ZnO), from the group of transparent conducting oxides (TCO), is a promising semiconductor material for use as an active channel layer [3] due to to its exciting electroptical properties. It has a high bandgap of 3.37 eV, large exciton energy of 60 meV, at room temperature, with mobilities of 2.5 $cm^2V^{-1}sec^{-1}$, even surpassing that of the conventional silicon devices [4]. It also exhibits excellent semiconductor and piezo-electrical properties, with a dual behaviour both as an active and a passive component.

This chapter discusses the basic structural, optical and electrical properties of ZnO as a semiconductor material. Semiconductor contacts have been discussed, next, followed by the significance of UV detection in the context of increased solar radiation.

2

1.1 Semiconductor oxides

Research has focussed on the II-VI semiconductor materials to synthesise potential devices. Functional oxides of such materials possess unique structural, physical, chemical and electro-optical properties that can be fine tuned for a wide range of applications in the diverse fields such as superconductor, magnetics and opto-electronic applications.

Nano crystalline materials like carbon nano tubes, along with the II-VI semiconductor compounds have attracted much attention in the field of nano scale devices. II-VI wide band gap semiconductor materials with their extraordinary physical, chemical, optical and electrical properties have provided the necessary impetus for the researchers to investigate the Silicon Carbide (SiC), Gallium nitride (GaN) and Zinc oxide (ZnO) thoroughly.

Functional semiconductor metal oxides such as SnO_2, Ga_2O_3, PbO_2, In_2O_3 and ZnO can be used to fabricate different nano structures such as nano-rods, nano-sheets, nano-tubes, nano-belts, nano-rings, nano-needles and nano-wires. The electrical and optical properties of such oxides can also be tuned, thereby providing a scope of fabricating a wide variety of smart devices for huge range of applications. Among these the ZnO is of the binary system from which ternary alloys such as indium-zinc-oxide (IZO) or quaternary alloys like and indium-gallium-zinc-oxide (IGZO) can be derived.

ZnO semiconductors have a band-gap that is greater than 2 eV, that lies in the range between that of the semiconductors and semi-insulators. Such a band gap makes the ZnO based semiconductors suitable for emission in the blue, green or UV region of the frequency spectrum for use in high temperature and high power applications. It also permits development of optoelectronic devices, such as photo-diodes, light emitting diodes (LEDs), laser diodes and photo detectors. Advantages of oxide semiconductors over the established a-Si:H technology in-

clude electrical-stress stability, higher field-effect mobility, and lower power consumption.

1.2 ZnO: a suitable semiconductor material

Ionic bonding in the metal oxide semiconductors, such as the Zinc Oxide (ZnO) has a huge electrostatic potential between the zinc and oxygen that causes a wide band-gap of 3.37 eV. A unique ionic bonding exists in the ZnO that is responsible for the large electron mobility.

Zinc Oxide (ZnO) has a direct band-gap, high binding energy of 60 meV, high electron mobility and high thermal conductivity, good transparency. Wide band-gap of 3.37 eV ensures low leakage currents and high voltage operation in unipolar power devices [5]. The ease of growth of ZnO in one or two dimensional nano structures permits us to fabricate, with high reproducibility, various types of two-dimensional nano-sheets, nano-walls, & nano-flakes and also the one dimensional nano-rods, nano-wires, nano-tubes, nano-belts & nano-rings. It has a broad chemistry thereby providing many opportunities for wet chemical etching. The features of the nano-structures can be fine tuned with controlled processing parameters. This makes it a highly suitable material for use in lasers, spintronics, gas sensing, piezo-electronic nano generator, solar cells and UV detection applications. The nanostructural features of ZnO can be properly tuned by employing different processing parameters.

A large variety of semiconductors, such as Gallium Arsenide (GaAs), Gallium Nitride (GaN), Zinc Selenide (ZnSe), Zinc Sulphide (ZnS) and Zinc Oxide (ZnO) have the requisite band-gap for optical applications. Gallium Nitride (GaN) and Zinc Oxide (ZnO) are the two wide band-gap semiconductor materials that have many matching properties for optical application, but ZnO has a distinct edge

over GaN. Table 1.1 below shows some important properties of these materials. From the table we observe that ZnO has better potential for optoelectronic applications. It also has excellent stability of exciton as indicated by its binding energy of 60 meV. Further, it possesses superior bond strength, is extremely hard with a very good transmittance around 90%, and is also radiation hard.

ZnO also possesses the property of radiation hardness that makes it suitable for hostile environments, such as missile detection systems. The bandgap of 3.37 eV (368 nm) at room temperature corresponds to the ultra violet spectrum that makes it suitable for UV detection applications, with an added advantage of being visible blind.

Table 1.1: Comparison of properties of ZnO with other wide band-gap semiconductor materials

Semiconductor Material	Crystal structure	Melting point (K)	Cohesive energy (eV)	Exciton binding energy (meV)	Bandp-gap energy (eV)	Electron affinity (eV)	Electron Mobility (cm²/V.sec.)	Hole Mobility (cm²/V.sec.)	Thermal conductivity λ (W/cm. K)
GaN	Wurtzite	1973	2.24	21	3.39	4.1	1250	850	1.3
GaAs	Zincblende	1511	—	—	1.42	4.07	8500	400	0.46
ZnS	Wurtzite	2013	1.59	39	3.80	—	—	—	—
ZnSe	Zincblende and wurtzite	1793	1.29	20	2.70	—	—	—	—
ZnO	Wurtzite	2248	1.89	60	3.37	4.55	200	180	1.3

1.3 Material properties of ZnO

Much of the focus from the family of II-VI semiconductor oxides has fallen on ZnO due to its distinct structural, optical and electrical properties, as listed in Table 1.2.

Table 1.2: Material properties of ZnO

Parameters	Values
Molecular Formula	ZnO
Crystal Structure	Wurtzite, Zinc blende, Rock salt
Molar mass	81.40 g/mole
Appearance	Yellowish white/Amorphous white
Melting Point	1975°C
Boiling Point	2360°C
Effective mass of electrons	0.24 m_0
Effective mass of holes	0.59 m_0
Electron mobility (at 300 K)	200 cm^2/V.sec
Hole mobility (at 300 K)	5-50 cm^2/V.sec
Density	5.606 g/cm^3
Intrinsic carrier concentration (per cm^3)	10^{16} to 10^{20}
Solubility in water	0.16 mg/100 mL
Energy Gap	3.37 eV (Direct Band-gap)
Refractive Index	2.0041
Relative dielectric constant	8.66
Lattice constants	a = b = 3.25 Å, c = 5.20 Å
Exciton Binding energy	60 meV
Cohesive energy	1.89 eV
Typical impurities	Ga, Al, H, In, Mg, Cd
Typical defects	Zinc vacancies, Zinc interstitial, Oxygen vacancies

1.3.1 Structural properties

Zno can be grown into various crystal structures, such as cubic zincblende, hexagonal wurtzite and cubic rock salt, though the hexagonal wurtzite structure (B4 type) is the most stable one under ambient conditions, as shown in the Fig. 1.1.

Although the zinc blende structure is unstable in natural conditions, but it can
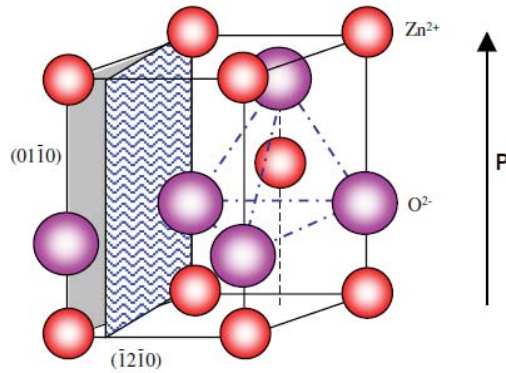
Figure 1.1: Wurtzite crystal structure of ZnO. [1]

be stabilized by developing ZnO layer on substrates in cubic lattice structure, wherein both the zinc and additionally oxide centres have a tetrahedral struc-ture.

The rock salt (NaCl-sort) structure is uncommon that has been recently observed at very high pressure (approx. 10 GPa) [6]. Various crystal structures are por-trayed in Fig. 1.2.

The wurtzite structure of ZnO comprises of a number of alternating planes com-posed of tetrahedrally coordinated Zn^{2+} and O^{2-} ions, arranged alternatively along the c-axis. Four essential terminations are obtained from this kind of lat-tice structure - both of the polar Zinc end and oxygen ended (0001) confronts, the (1010) confronts and the non-polar (1120)(a-axis). A good number of its prop-erties, including the piezoelectric & pyroelectric, can be assigned to this polar symmetrical nature of arrangement of the two inter-connecting sub-lattices of the Zn^{2+} and O^{2-} ions.

With these fundamental structures Zinc oxide (ZnO) can be induced to produce a vast variety of crystalline shapes utilizing specialised growth techniques such as Laser Deposition and RF sputtering. The exact crystal shape relies on the tech-nique which is used to grow the ZnO film. In regular type of zinc oxide these shapes shift between acicular needles and plate shaped crystals to nano-pipes, nano-flowers, nano-combs and so on. We have utilized the RF magnetron sput-

8
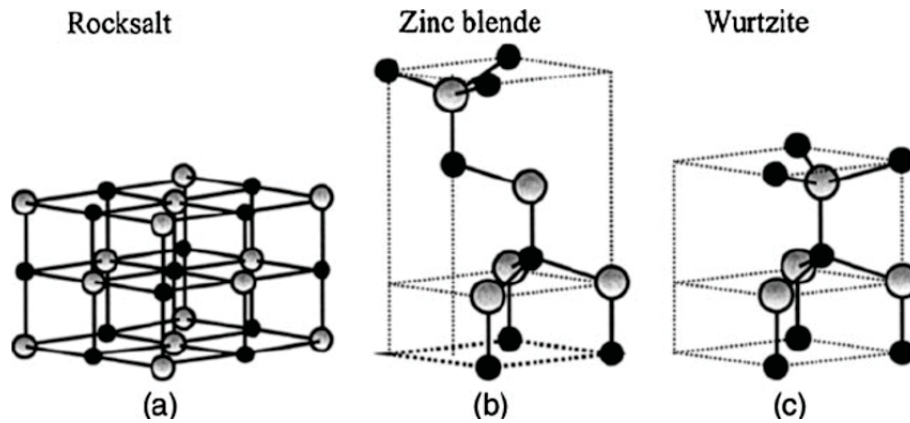
Figure 1.2: Schematic representation of ZnO crystal structures (a) hexagonal wurtzite, (b) cubic zinc blende, and (c) cubic rocksalt [2]

tering method to grow the ZnO thin film. This technique is considered as the most preferred method to produce uniform ZnO thin film. Further to refine the crystalline quality of grown ZnO thin film, annealing technique is used.

1.3.2 Thermal properties

The thermal properties of wurtzite ZnO have been discussed, that include the thermal conductivity and specific heat.

Thermal conductivity is needed for operation of semiconductor devices in high-power and high temperature. This is primarily due to the point defects in the ZnO crystal that causes phonon-phonon scattering and the values lie typically in the range $k = 0.6 - 1$ Wcm^{-1}K^{-1} [2]. The lattice deformation in the semiconductor material is described by the thermal expansion coefficients α_a and α_c, defined at the room temperature [7]. The lattice vibrations, free carriers, impurities and structural defects within the material are responsible for the specific heat. A wide range of values for the specific heat capacity of ZnO has been reported as 40.3 J mol^{-1}K^{-1} at a constant pressure [8].

1.3.3 Optical properties

The high density of electronic states in the Zinc Oxide semiconductor material enhances the electron-hole and electron-phonon interactions, thereby causing the quantum confinement effects. The nano materials behave in an entirely new way due to such quantum confinement and lattice vibrations. Typical structures that result are the two-dimensional quantum wells, one-dimensional quantum wires, and zero-dimensional quantum dots.

ZnO is a suitable material for applications related to the blue and ultra-violet optical devices. Zinc Oxide has a band-gap of 3.37 eV that is sufficient for emission in high frequencies, specially in the the blue, green or UV region of the frequency spectrum, that permits development of optoelectronic devices, such as photodiodes, light emitting diodes (LEDs), laser diodes and photo detectors.

1.3.4 Electrical properties

Large variation exist in the reported electrical properties of ZnO. As the carrier concentration of the n-type ZnO varies with the different layer deposition processes. Typical values range from 10^{16} cm^{-3} to 10^{20} cm^{-3}. Although doping of p-type in the ZnO semiconductor material has also been reported but these are yet to be verified [9]. The exciton binding energy is 60 meV at room temperature that is suitable for optoelectronic device applications. The typical electron mobility at room temperature for low doped n-ZnO μ = 200 cm^2 V^{-1} S^{-1} [10].

1.3.5 Doping and defects

Zinc oxide possesses n-type conductivity without any dependence on the deposition technique. Its intrinsic n-type nature were earlier presumed to due to the intrinsic defect, including oxygen vacancies and zinc interstitials. Studies now show that the intrinsic nature of its n-type behaviour may not be due to these ef-

fects. Instead the unintentional hydrogen interstitial impurities may be the cause, that act as shallow donors in ZnO. Efforts are continuing by the researchers to investigate the cause of n-type conductivity in ZnO [11,12].

P-type doping is still a difficult task in the ZnO wide band-gap semiconductor due to compensatory effects of the intrinsic/ interstitial defects in its crystal structure, the oxygen vacancies or the hydrogen impurities. Its low-soluble nature and the deep impurity levels prevents it to form shallow acceptor levels so as to be doped as p-type. Some researchers have reported p-type doping with copper, silver and gold. The oxygen lattice sites can also be substituted by group-V elements to make it p-type. Doping of the p-type is still a unstable and unreliable process [13,14].

1.4 Semiconductor contacts

Optoelectronic Schottky barrier structures can be fabricated in a variety of ways. Classification of such structures, based on different type of junctions, are the metal semiconductor (MS) junctions, metal-interfacial layer-semiconductor (MIS) junctions and the semiconductor-interfacial layer-semiconductor (SIS) junctions. Among these, the devices based on metal semiconductor Schottky junctions are easy to fabricate with low temperature deposition processes, thereby retaining the semiconductor properties. However, MIS and SIS structures possess charge in their interfacial layer to modify the barrier height, resulting in instability of such devices. Such structures have not been discussed further.

Metal semiconductor (MS) structures have a single semiconductor material of the same doping. The barrier that gets built up at the semiconductor junction is depleted of majority carriers with a high electric field [15]. Upon formation of a metal semiconductor contact an electro-chemical potential gets built up on reaching the thermodynamic equilibrium condition. Two different type of junctions

form based on the doping of the semiconductor material. Schottky contact gets formed for lightly doped semiconductor and and ohmic contact is formed when the semiconductor is heavily doped.

When two different materials are placed in contact with each other and a condition of thermodynamic equilibrium is established, electrostatic potential energy develops at the metal semiconductor interface. MS contacts of two types can be classified depending upon relative work functions of the metal ϕ_m and that of the semiconductor ϕ_s. A number of advantages are offered by such simple structures for optoelectronic applications where a single doped semiconductor material forms the barrier. Also the deposition processes can be low temperature processes that does not effect its properties. Certain disadvantages of such MS contacts are the reduction of incoming light that can be minimized by reducing the metal thickness.

1.4.1   Schottky contacts

The energy band diagrams for the metal and n-type semiconductor shown in Fig. 1.3 (a) for $\phi_m > \phi_s$ where ϕ_m and ϕ_s are the work functions of the metal and semiconductor respectively. A Schottky-Mott junction is formed due to creation of a dipole charge layer and an electrostatic potential energy barrier develops at the interface. After the equilibrium condition is established the energy band diagram is modified, as depicted by Fig. 1.3 (b). The band bending that takes place is the difference between the work functions of the metal and semiconductor. The contact potential (V_i) of the junction develops, given by $qV_i = (\phi_m - \phi_s)$. The corresponding barrier potential of the junction and the surface potential of the semiconductor are given by [16]:

$$\phi_B = (\phi_m - \chi_s) \tag{1.1}$$
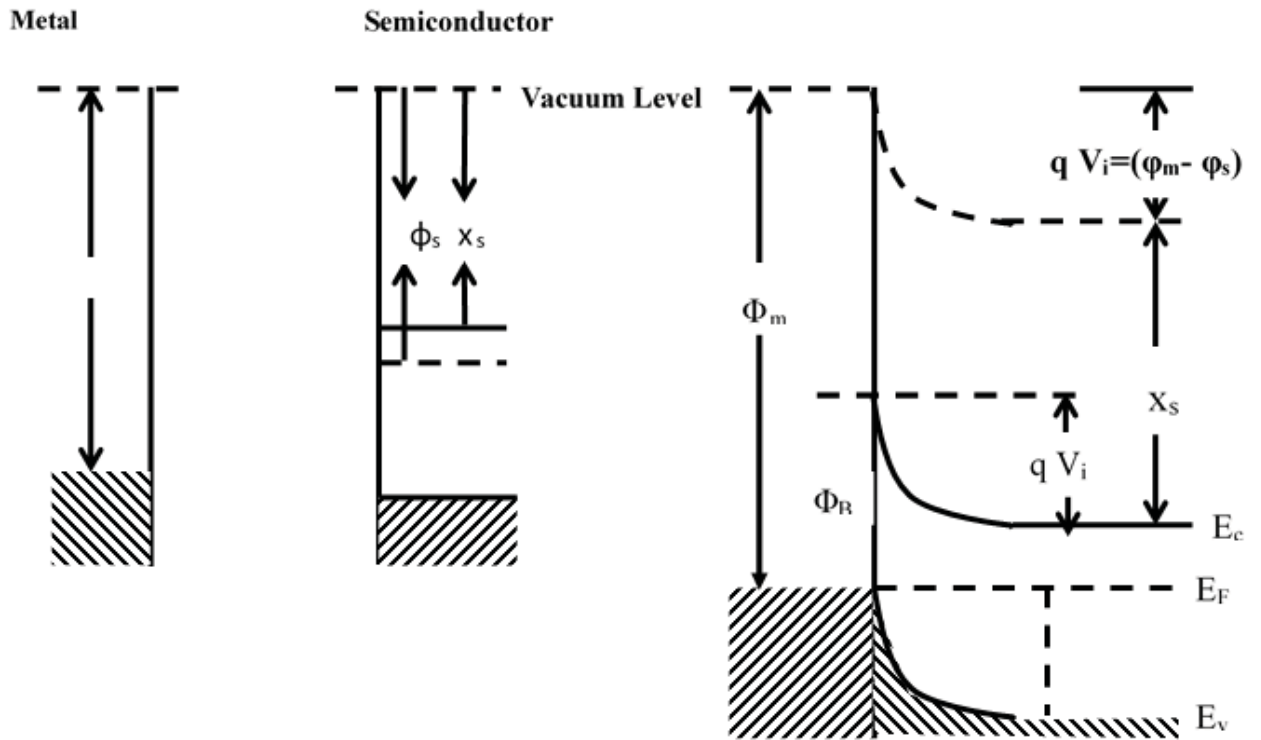
Figure 1.3: Energy band diagram of metal on n-type semiconductor Schottky contact (a) Neutral materials separated from each other and (b) thermal equilibrium situation after the contact has been made

since,

$$\phi_s = (\chi_s + \phi_n) \tag{1.2}$$

We have,

$$\phi_B = (qV_i + \phi_n) \tag{1.3}$$

where χ_s is electron affinity expressed in eV and $\phi_n = (E_C - E_F)$.

1.4.2   Ohmic contacts

The energy band diagrams of the MS contacts (n-type semiconductor) for $\phi_m < \phi_s$ as shown in Fig. 1.4. In this case a non rectifying ohmic contact is formed and

13
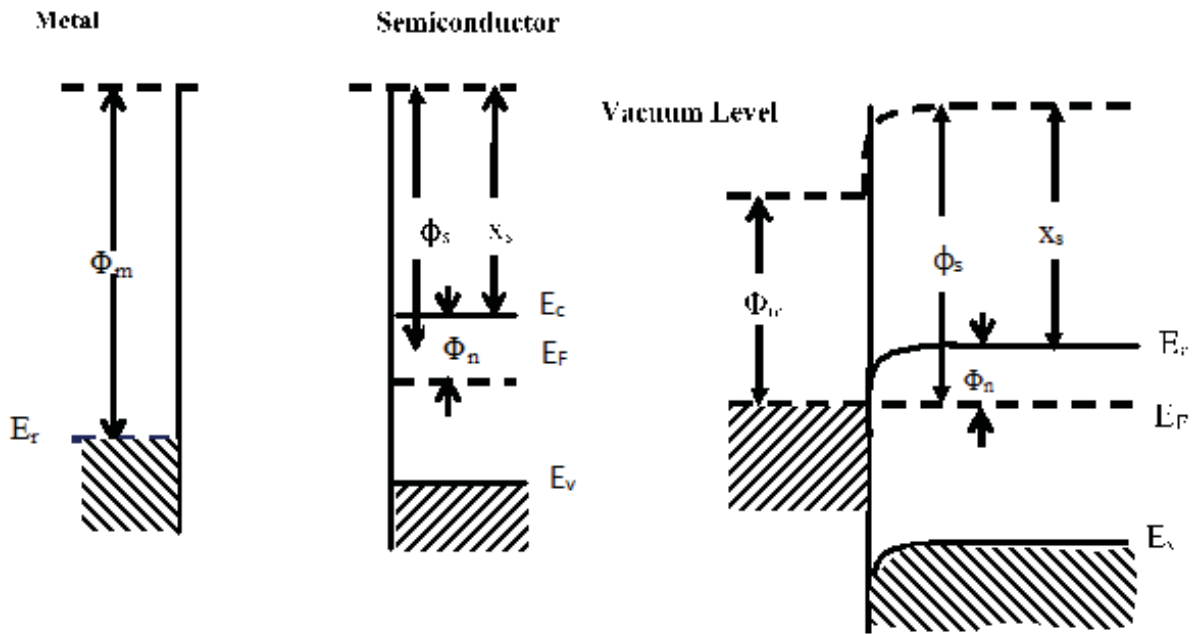
Figure 1.4: Energy band diagram of metal on n-type semiconductor ohmic contact (a) Neutral materials separated from each other (b) contact under thermal equilibrium

the current is determined by the resistance of the bulk region.

1.5   Need for UV sensors and their applications

Environment monitoring, ozone layer monitoring, missile detection, space communication, computer storage systems and various chemical & biological analysis and many other medical, defence and communication fields need sensors that operate in the UV range. These sensors have been developed in the past years with new semiconductor materials operating at low dark currents, high operational temperatures, higher photo responsivity at higher speed with a better efficiency. Currently single-crystalline silicon (Si), silicon carbide (SiC) or gallium nitride (GaN) based optical photo detectors are being used that are sensitive to both visible and infra-red radiation but are also costly and unsuitable for UV applications due to its low responsivity.

ZnO is another wide bandgap material (3.37 eV) with a large exciton binding energy (60 meV) at room temperature that makes it promising material for applications in laser diodes, light emitting diodes (LEDs) and UV photo detectors. It is also less susceptible to irradiation and has a high saturation velocity than the GaN for potential high speed UV light sensing for space applications.

1.6   Scope of the thesis

Chapter-2 presents the review of literature which is an integral part of any research that provides the future trends in a particular field. The state-of-the-art work in any particular research area helps us in forecasting the new devices. This chapter presents some important investigations reported by different researchers in the past decades in the area of ZnO thin film based Schottky contacts and TFTs. Electro-optical and micro-structural properties of the ZnO thin films , Schottky diodes and TFTs have been reviewed in this chapter along with the characterization techniques.

Firstly a brief review on ZnO thin film based Schottky diodes have been presented. Then the significance of UV detection in the context of increased solar radiation these days has been discussed. Finally, a exhaustive review on the present day UV detectors have been presented.

Chapter-3 presents numerical simulation and performance analysis of Pt/ZnO Schottky photo-diode using ATLAS. A program for Pt/ZnO Schottky photo-diode has been developed in ATLAS simulator from SILVACO international to study its various electrical and optical properties in ultra-violet region. Variation of current-voltage plot under dark and illumination condition has confirmed that Pt/ZnO Schottky diode is a potential candidate for ultra-violet light detection in variety of civil and military applications. Pt/ZnO Schottky photo-diode has exhibited a very good external quantum efficiency of in UV region. Value obtained for responsivity in UV region. Effect of temperature, ZnO thickness and doping concentration on the performance of Pt/ZnO Schottky photo-diode have also been analyzed and reported.

Numerical simulation performance Analysis of Pt/ZnO Schottky photo-diode has been done using ATLAS simulator(from SILVACO International) to study its various electrical and optical properties in ultraviolet region. Effect of temperature ZnO thickness and doping concentration of Pt/ZnO Schottky diodes have been analysed.

Chapter-4 compiles the fabrication and performance analyses of Schottky diodes with Au and Pd contacts on n-ZnO thin films as UV detector. RF magnetron sputtering technique has been used to deposit the nano-crystalline ZnO thin film. Characterization techniques, such as XRD, AFM, SEM and the UV measurement provided valuable information concerning the micro-structural, surface morphology, and optical properties of the ZnO thin film. The results show that the prepared thin film has good crystalline orientation and minimal surface roughness, with an optical band-gap of 3.1 eV. I-V and C-V characteristics were evaluated

that indicate non-linear behaviour of the diodes for both of the contacts with individual rectification ratio (IF/IR) for Au/ZnO and Pd/ZnO Schottky diodes, respectively. Responsivity of these Schottky photo-detectors, at room temperature, on being illuminated with a light of particular wavelength and bias. The detectivity and photoconductive gain of both Au and Pd based Schottky detectors were also found which indicate better performance of Pd based UV detector.

Chapter-5 presents the simulation and fabrication of different ZnO Bottom Gate Thin Film Transistors (TFTs).

This chapter presents numerical simulation and performance analysis of various electrical and optical properties of the ZnO bottom-gate TFTs, using three dimensional (3D) device simulator of VisualTCAD from Cogenda both under ambient and UV light conditions. The static performance of the TFTs with different W/L ratios have been investigated. Channel lengths were varied from 6 μm to 12 μm while keeping the width fixed at 40 μm. The thickness of both the ZnO channel and the dielectric SiO_2 were varied to observe the corresponding effects on the output and the transfer characteristics of the bottom-gate TFTs. Various electrical and optical parameters, such as ON-OFF current ratio, threshold voltage and field-effect mobility have been obtained. Intensity variation of the UV light was performed to find the current-voltage plots under ambient and illumination condition. The devices were also tested for different wavelength lights in the UV region. The simulations confirmed that ZnO TFTs are suitable detectors for ultra-violet light detection in variety of applications.

Fabrication of UV photo-detectors with staggered bottom gate ZnO Thin Film Transistors (TFT) structure, was undertaken thereafter. ZnO thin film was grown on silicon substrate with RF magnetron sputtering process, at room temperature. The static and dynamic performance of these devices have been explored by varying the channel lengths. The results show that the fabricated devices show a low leakage current in the nano-ampere region, a threshold voltage of 1.35 &

1.93 Volts and field effect mobility of 0.682 & 0.881 ($cm^2/V.s$) and sub-threshold swing of 8.896 & 10.679 mV/dec. They also exhibit superior electrical characteristics with a specific ON-OFF ratio, contrast ratio and bias-stress. The devices were tested for device stability by application of both positive and negative-stress. The devices were further tested for photo-response.

Chapter-6 concludes some major outcomes of the thesis. The chapter summarizes all the results presented in chapter 3-5. Finally, the future scope of the work is outlined in the end.

Chapter 2

ZnO Thin Films for Optoelectronic Devices: State of the Art

ZnO on silicon is emerging as a low-cost and low process temperature (room temperature) fabrication process, made possible by RF sputtering [4, 17]. With its capability for process integration with the present silicon technology, ZnO has become a prefered material of choice for wide range of electronic device applications, such as laser diode, thin film transistor (TFT), gas sensor, solar cell, piezo-electronic nano-generator, SAW resonator, and micro-electro mechanical devices [18–24].

The nano-crystalline ZnO thin films finds applications in a variety of semiconductor devices such as, UV detection, gas sensing, high performance active matrix for organic light emitting diodes (AMOLEDs) and transparent & flexible displays.

2.1   Introduction

Review of literature is an integral part of any research that provides the future trends in a particular field. The state-of-the-art work in any particular research area helps us in forecasting the new devices. This chapter presents some impor-

tant investigations reported by different researchers in the past decades in the area of ZnO thin film based Schottky contacts and TFTs.

This chapter contains a review of the fabrication and characterization techniques of ZnO thin films, in the first two sections. Next section contains a brief review of the ZnO thin film based devices: electrical contacts, Schottky diodes and TFTs. Finally, a review on UV photo-detectors with the special emphasis on the metal semiconductor contacts follows.

2.2   Fabrication Techniques

Fabrication of high quality epitaxial thin films of ZnO is needed for its application in opto-electronic devices. Even with latest advancements in fabrication technology, issues remain with p-type doping of the ZnO semiconductor material along with successful reproduction of reliable ZnO devices. These problems have been circumvented through the implementation of its nano-structures on a variety of wafers.

This section discusses the state of the art of ZnO nanostructure fabrication technologies, based on the published reports. The two major techniques to grow ZnO nano-structures are based on the gas-phase and the liquid phase. The liquid phase or the chemical solution approach is a low-cost technique that can be employed for large wafers for industrial production. Chemical bath deposition (CBD), electro-deposition (ED) and successive ion layer adsorption reaction (SILAR) are some of the methods of the liquid-phase techniques. Various gas-phase techniques such as the metal organic chemical vapour deposition (MOCVD), physical vapour transport (PVT) and pulsed laser deposition (PLD). Sophisticated ZnO nano-hetero-structures are fabricated with molecular beam epitaxy (MBE) and sputtering techniques [25].

A review of a few of these growth techniques are discussed in this chapter.

2.2.1 Liquid Phase

Liquid phase or the wet-phase method for nano-structure fabrication is a relatively low-cost process for large scale production of large wafers. This technique has a simple set-up that requires neither vacuum nor large process temperatures.

2.2.1.1 Chemical Bath Deposition (CBD)

The ZnO nano-crystals (seeds) attach to the surface of the substrates that is placed into reactor containing an aqueous solution of zinc nitrate and hexamethyleneteramine. The substrate is pre-treated for nucleation to take place for dense growth of nano-rods on its surface. The temperature and pH of the aqueous solution are controlled within a specified range. Different type of nano-pillars can be fabricated by varying the process parameters. This two-step growth process takes a very long time, typically, several hours to complete [26–28].

2.2.1.2 Electrodeposition (ED)

A similar reactor with controlled temperatures (70–90°C), as in the previous case of CBD, at ambient pressure contains the aqueous solution of zinc nitrate hydrate and hexamethylenetetramine in deionised water. Two electrodes maintained at a certain fixed bias are placed into this solution. The nano-rods can be grown in either of the following two ways. In the first method, the growth takes place on the conducting layer on the substrate surface. One of the commonly employed conducting layers on the surface substrates are (Ti(20 nm)/Au(200 nm), kept at a cathodic potential of 1V with respect to the Pt anode, acting as a counter-electrode. In the second method, nano-pillars can be grown between two conducting stripes that may be of Ti/Au and have been previously deposited with e-beam lithogra-

phy, for example. The bias voltage is applied between these stripes. It does not require another electrode, as in the previous case of electro-deposition. A dense growth of the nano-structures takes on the cathode side [29, 30].

2.2.1.3   Successive Ionic Layer Adsorption Reaction

Glass substrate is successively dipped in two different solutions with cation and anion precursors, at room temperature with heated water. The substrate is washed in between the two dips with a solvent, typically water and dried with N_2. Repeated immersion in this manner deposits thin films on the substrate with reported thickness of about 20 nm in 6 cycles. The reported grain size of the ZnO thin film are around 220–265 Å with hexagonal structure having a c-axis orientation. Very thin films can be deposited with this Successive Ionic Layer Adsorption Reaction (SILAR) deposition process [31, 32].

2.2.2   Gas Phase

In this technique inert carrier gas is used to transport pure elements, zinc and oxygen, in separate lines to the substrate in a reactor. Three separate zones permit maintaining different temperatures of the substrate and the source material for optimum conditions of growth of nano-pillars.

2.2.2.1   Physical Vapour Transport (PVT)

The growth of the nano-pillars/ nano-wires occurs with the bounding atoms that are adsorbed on the substrate surface. The temperate of the substrate has to be carefully controlled to provide optimal growth conditions.

An alternative catalyst assisted approach in which catalytic metal (Ag/Au/Pt) islands are initially deposited on the surface of the substrate. The growth of the nano-structures takes place at temperatures that exceed the melting point of

the catalyst. Impurity concentrations, due to the metal catalyst, in such nano-structures is significantly higher in this growth approach [33–35].

2.2.2.2 Metal Organic CVD

The Metal Organic Chemical Vapour Deposition (MOCVD) growth process initially involves transport of the precursor to the substrate, which are diethylzinc and nitrogen dioxide for zinc and oxygen, respectively for the growth of ZnO nano-pillars / wires. To grow ZnO thin films with this process, the precursors are changed to zinc hydrate and a mixture of oxygen and water. A chemical reaction takes place at the substrate surface that aids the adsorption at the surface. Finally, the precursor byproducts are transported from the substrate surface to the exhaust. The main advantage of this process that the precursors are not kept in the reactor, but are stored outside in stainless steel cylinders. The substrate is maintained within a temperature range of 800 to 1000° in the reactor. The pressure inside the reactor is maintained between 1–400 mbar [36–38].

2.2.2.3 Pulse Laser Deposition (PLD)

Pulsed Laser Deposition (PLD) process of growth is widely used for industrial fabrications of various types of ZnO nano-structures. Laser beam is used to evaporate the elemental materials from its target source in a vacuum chamber maintained at a pressure of around 100 mbar. Evaporation of the elemental zinc target into gas form by the laser beam is deposited on the substrate, under ambient oxygen environment in the reactor. Excimer lasers and Nd.Yag lasers operating at different wavelengths ranging from 193 nm to 355 nm , emitting pulses of 50 Hz through a lens have a typical spot size of about 0.1 mm^2 and angle of incidence of around 45° [39–42].

2.2.3 Alternative Techniques

Apart from the gas and liquid- phase techniques described above, various other approaches also exist to grow different nano-structure. A few of these techniques such as, spin coating make use of the nano-powders to fabricate nano-crystalline layers.

2.2.3.1 Spin coating

Spin coating technique is employed to deposit nano-particle layer over a substrate with a stabilized colloidal solution with added organic additives. This technique finds use for growth of nano-structures for sensing and photovoltaic applications. Layer homogeneity is enhanced with application of pressure that also improves the substrate attachment. Finally the substrate is subjected to heat that removes the unwanted organic contamination [43, 44].

2.2.3.2 Molecular Beam Epitaxy (MBE)

Molecular beam epitaxy (MBE) is a process to grow different nano-structures, including thin films, of various materials. Oxides, semiconductors and metals can be deposited with this technique. A beam of atoms/ molecules is targeted on a crystal in a heated state. A crystalline layer of the bombarding atoms/ molecules get deposited on the substrate forming unique nano-structures, in high level of cleanliness in the vacuum at lower temperatures. Oxygen plasma cell, at RF powers of 200-400W, is used to grow ZnO/ZnMgO heteo-structures as quantum-wells on ZnO nano-pillars that were deposited earlier on the substrate with CBD/VPT techniques. The hetero-structures growth process was optimized with reflection high energy electron diffraction (RHEED) oscillations. This process is widely employed for precise structures close to the ideal models for optoelectronic applications [45–50].

2.2.3.3 Sputtering

Sputtering is a flexible technique to grow nano-structures with control of its composition. ZnO thin films is done with the deposition of the ejected atom from the target source that has been hit with an ion source, that is usually a plasma, with energies in the range of a few tens of electron-Volts (eV). The sputtering yield depends on the sputtering threshold voltage, the plasma potential and the dc voltage applied to the target. The sputtering process is further divided into two groups, as per the applied electrode potentials, as DC sputtering and RF sputtering. Reactive and RF magnetron sputtering are further discussed that are also based on these two basic mechanisms of sputtering.

DC sputtering

DC sputtering is used to deposit metal films, the target is bound to the planar cathode and the substrate to the other planar electrode acting as the anode, with Argon as the ambient gas in the chamber. The chamber pressure is in the range of 10^{-6} mbar. The electric field ionizes the Argon atoms, creating more electrons resulting in a glow discharge. The target on being hit with the positively charged ions emits some atoms from its surface that reach the substrate surface as they travel randomly in the chamber. These source target atoms form a thin film on condensing at the substrate surface. Insulating materials cannot be deposited with this technique, due to positive charge build-up near the cathode creating an opposite electric field that stops the deposition process.

RF sputtering

In the RF sputtering, any conducting, semiconducting and insulating material can be deposited on the substrate. An ac voltage source operating at RF frequencies in the MHz range (around 13.56 MHz) to bombard the target alternately with ions and electrons to avoid charge build-up near the cathode. This happens as the high inertia of the ions, being heavier, cannot follow the RF switching, whereas the electrons are able to do so, thereby avoiding the positive build up near the cathode surface. This technique is much more effective than the DC sputtering and needs a lower operating voltages at requires reduced pressure. Optimal parameters lead to a uniform growth of the film with requisite thickness and structure. Adherence to the substrate is also of a very good quality. A optimised flow of oxygen gas is necessary for proper growth of semiconducting ZnO thin films. The substrate to target distance must also be optimised to obtain the required deposition rates.

Figure 2.1: RF Sputtering setup

RF magnetron sputtering

Permanent magnets placed on the back of the cathode, where the target is placed, are used in this process to alter the path of electrons. The electron paths now become helical, thereby increasing their path length which results in increase in the number of collisions with ambient Argon gas atoms. A denser plasma created in this manner increases the sputtering rate, at lower chamber pressures [51, 52].

Reactive sputtering

This is a sputtering process to deposit non-conducting thin films by mixing the reactive gases with inert gas in the chamber. Oxygen, hydrogen sulphide, nitrogen or any other gas, in a neutral or ionised phase, are mixed with the inert Argon gas in the process chamber. These gases react with the target, sputtered ions or the substrate to form films oxides, sulfides and nitrides on the substrate surface. The stoichiometry of the grown films can be controlled by varying the partial pressures of various gases in the chamber [52, 53].

2.2.4   Effect of Annealing

ZnO film are subjected to annealing after they have been grown with the sputtering techniques to relieve the in-built stresses and remove the surface defects such as micro-cracks, pin-holes etc. This also improves the crystal quality in the grown films and make the surface uniform. Annealing is done post deposition at temperatures ranging from 200°C to 400°C in the presence of forming/ oxygen gas. Increasing the temperatures above 400°C is known to cause micro-cracks in the grain structure, though these temperatures are good for improving the piezo-electric properties of the thin film. The substrate-to-target spacing and the gas flow rates are varied to optimize the nano-structure of the thin film. In the fabrication of the thin film transistors (TFTs) annealing significantly effects the thresh-

old voltage and mobility. Post deposition annealing plays an important role in the stability and reproducibility of the fabricated devices [54–57]. The experimental set-up is as shown in Fig. 2.2.

Figure 2.2: Annealing/ RTP

2.3   Characterization Techniques

Investigation of the fabricated nano-devices is done using a host of characterization techniques, at molecular levels. These can be broadly classified into various categories such as, structural and morphological (Ellipsometry, XRD, AFM, SEM, TEM etc.), optical (FTIR, UV-Vis, Raman etc.) and electrical (DC probe station). Some of these techniques have been briefly described here.

2.3.1   Structural and Morphological characterization Techniques

2.3.1.1   Ellipsometry

An ellipsometer is used to find layer thickness and the refractive index of thin transparent layers. This is an optical method that measures polarization change as the incident light is transmitted or reflected from the surface of the deposited

layer. The output response of the ellipsometer is dependent on the crystal structure, composition, doping concentrations and other properties of the material under test. Light emitted from the source is passed through a polarizer and its output is fed to an optical compensator that alters its polarization to circular. The accuracy of the ellipsometer is increased by the change in polarization. The reflected light from the device under test is fed to a compensator and another polarizer before being detected.

The ellipsometer used in this work uses a helium-neon laser as the light source with a spectral range of 245–1000 nm. The incident light radiates on the sample with an tilt angle of 70°C. Transparent films with a thickness of up to 10 μm can be measured, with a. The polarization state of the reflected light is determined by a rotating analyser. The experimental set-up is as shown in Fig. 2.3.

Figure 2.3: Ellipsometer

2.3.1.2   X-Ray Diffraction

The crystal structure of the thin films such as, lattice parameters, grain size, crystal orientation, chemical composition, stress and defects can be determined with the X-Ray diffraction technique. Electromagnetic waves with wavelengths of the

same order of magnitude as the spacing between the diffraction planes of the crystal structure (1-100 Å). The incident EM radiation interacts with the electrons of the sample under test, thereby scattered from the sample surface and reveals the important information about it.

We have used the highly flexible general purpose X-ray diffractometer system from Rigaku SmartLab. This system includes optics for both standard Bragg-Brentano and parallel-beam optics for use with poly crystalline thin films, powders and nano-materials. The experimental set-up is as shown in Fig. 2.4.

Figure 2.4: XRD

2.3.1.3 Scanning Electron Microscope (SEM)

The surface morphology of the fabricated ZnO thin films has been been done with the ultra high resolution SEM. In this technique, an incident high energy electron beam interact with the electrons of the sample under test. The electron beam is thermionically produced by high voltages in the range of 20 KV to 40 KV, which is then focussed using a condenser. The reflected beam includes secondary and backscattered electrons. The secondary electrons produced due to inelastic scattering are sensed by a a fully integrated Energy and angle selective Backscattered electron (EsB) detector, to produce an image with ultra high resolution images of

sub-nanometer resolution, below 1 KV. It has an integrated filtering grid to enhance image quality and requires no additional adjustments. The experimental set-up is as shown in Fig. 2.5.

Figure 2.5: SEM

2.3.1.4 Atomic Force Microscope

Surface morphology, magnetic and chemical properties of the test samples can also be analyzed with Atomic Force Microscope (AFM) technique. The interaction between the sharp tip as it scans the sample surface due to van der Waals and electrostatic forces causes deflection of the cantilever. A feedback mechanism avoids collisions between the tip and the sample surface. The deflection of the cantilevers causes change in the reflected laser which are detected by the photo-diodes. Different modes of operation of the AFM are contact and non-contact. In the contact mode of operation, the cantilever tip makes soft physical contact at a constant force with the surface of the test sample. The scanning of the sample can be done at a high speed with this method, but may cause damage to soft samples. In the tapping mode of operation, the cantilever oscillates near its resonant frequency which decreases as the tip is brought closer to the sample

surface, due to van der Waals force. The scanning is slower in this mode but, it causes less damage to the soft samples. In our work, we have used the AFM from Bruker Dimension Icon with a high resolution of less than 0.1 nm in the z-direction. The experimental set-up is as shown in Fig. 2.6.
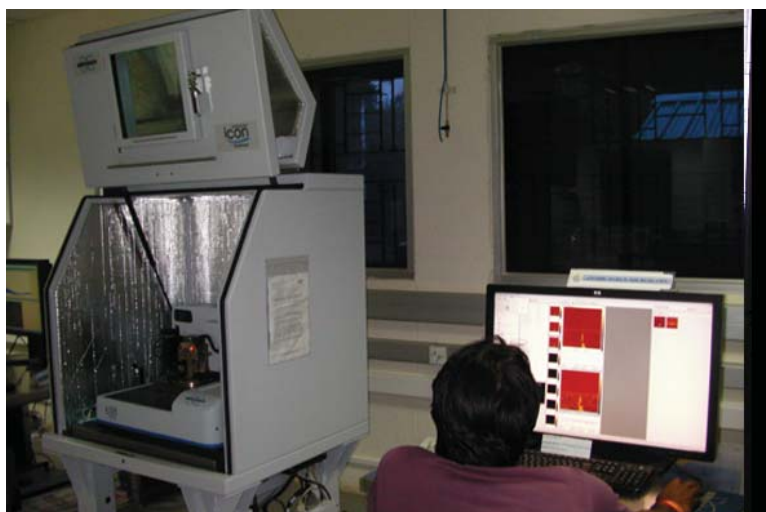
Figure 2.6: AFM

2.3.2 Optical characterization Technique

2.3.2.1 UV-VIS-NIR Spectrometer

UV-VIS-NIR Spectrometer is used to measure absorbance and transmittance of thin films, using integrating sphere. Kinetic studies can also be performed with this technique. Incident UV-VIS light, in the wavelength range of 200 nm to 3200 nm, on the sample is absorbed as per its typical material properties. The excited electrons from the ground state to higher excited states return back to the original state by vibrational transitions through smaller energy increments that are recorded by the UV-VIS-NIR Spectrometer. In this work, we have used the UV-VIS-NIR Spectrometer MPC3600 from Shimadzu, with a high spectroscopic resolution and a unique wavelength range capability and high performance [58]. The experimental set-up is as shown in Fig. 2.7.

Figure 2.7: UV-vis

2.3.3 Electrical characterization Technique

The electrical characteristics of the sample are measured with semiconductor device analyzer (SDA). The I-V and C-V measurements with a gate bias applied through the metal chuck with vacuum suction system to hold the wafer. The measuring tips are connected to the sample with micro manipulators that are connected to the source measurement units (SMUs), actings as either current or voltage sources. Precision in the range of 0.1 fA - 1 A and 0.5 μV - 200 V can be done that include both spot and sweep I-V measurements at sampling rates of 100 μs. It can also do pulse measurements with minimum pulse widths of 50 μs. Capacitance measurements such as C-V (capacitance versus voltage), C-t (capacitance versus time) and C-f (capacitance versus frequency) can also be done with the SDA, in the frequency range of 1 kHz to 5 MHz.

We have used the Semiconductor Device Analyzer with an opearting temperature range from 20–200°C. PC-based instrument with Windows–7 Professional operating system and EasyEXPERT software provided the results in the desired form. The experimental set-up is as shown in Fig. 2.8.

33

Figure 2.8: Semiconductor Parameter Analyzer

2.4 ZnO Thin Film Based Devices: Brief review

ZnO thin films can be used to fabricate passive, two and three terminal nano-devices. The passive devices include resistors, capacitors and inductors, whereas the p-n /Schottky diodes and thin film transistors are the two/three terminal devices, respectively.

2.4.1 Electrical Contacts

C. Coskum et al. [59] studied the effect of high energy electron radiation on ZnO thin film based ohmic and Schottky contacts. Al and Au were used as contacts. The effect of high electron energy has been investigated and It has been found that with increasing electron energy the ideality factor increases and Schottky barrier height decreases.

2.4.2 Schottky diodes

Literature review of some of the papers studied before proceeding for the simulation and fabrication of the Schottky diodes are mentioned below.

C. Periasamy et al. [60] fabricated the ZnO thin film on glass substrate using

thermal evaporation technique. Structural properties were obtained using X-ray diffraction method, atomic force microscopy. Further, MSM photo-diode was fabricated using Pd as contact material and detection was done using UV source of 365 nm wavelength. The responsivity of fabricated device was found to be 0.14 A/W.

Leonard J. Brillson et al. [18]investigated ZnO based Schottky barriers and ohmic contacts of In, Ti, Al and Pt. They discussed the role of surface cleaning, quality of crystal, chemical interactions for the Schottky diode. They also studied the importance of annealing for multilayer contacts, alloyed and ohmic contacts

S.K. Cheung et al. [61] reported a new method to obtain various diode parameters, such as ideality factor, barrier height and series resistance, using the forward I-V characteristics.

J.D. Hwang et al. [19] utilized the sol-gel or hydrothermal method to fabricate non-surface-treated ZnO thin film based Schottky contacts of Au metal. The seed layer was utilised to grow ZnO thin film and the effect of different seed layers on electrical behaviour of Schottky contacts had been investigated. Rectification ratio of around 8000 was measured, at a bias voltage of +2 V. Schottky contacts with sol-gel seed layer exhibits ohmic behaviour. C-V measurements were utilised to obtain the barrier height of 0.77 eV.

Y. N. Lee et al. [62] reported the fabrication, electrical and optical characterisation of Schottky contacts between Al and Phosphorous doped silicon layer. A higher quantum efficiency (0.397) has been reported, at 360 nm UV wavelength, as compared to the previously reported devices. Stable response time of 1.3 ms was obtained at 3 Volt.

S. Young et al. [63] investigated the ZnO nanorods based Schottky contacts for UV detection. The fabricated contacts were reported to possess a high responsivity of 104.14 A/W at -1 Volt which was attributed to the high surface-to-volume

ratio. It was observed that the increase in the power density is directly proportional to the photo current. Noise equivalent power and normalised detectivity were also obtained at -1 Volt.

S. Aydogan et al. [64] used the electrochemical deposition technique for deposition of ZnO on n-Si substrate with Au contacts. The fabricated device was characterized with I-V and C-V measurements. Cheung function and Norde methods were used to evaluate various characteristic parameters such as barrier height, ideality factor and series resistance. From the results, they concluded that the capacitance of Schottky diode is independent of frequency at lower frequencies but was seen to decrease at high frequencies.

A. B. Yadav et al. [65] utilised sol-gel based technique to fabricate highly sensitive Pd based Schottky contacts as a UV photo-detectors. The fabricated device showed very good contrast ratio of 5332 and responsivity of 8.39 A/W at a biasing voltage of -5 Volts, at room temperature.

Aniruddh, B.Y. et al. [66] determined the I-V characteristics of Pd based Schottky contacts on sol-gel-derived ZnO thin film. Effect of temperature on I-V characteristics was investigated and electrical parameters such as ideality factor, barrier height and reverse saturation current were obtained for different value of temperature.

C. Tsiarapas et al. [67] reported fabrication of ZnO thin film based Schottky diodes. ZnO with two different thickness was grown using RF-magnetron sputtering mechanism. I-V and C-V characteristics were measured at different temperature and two Schottky diodes were compared using electrical parameters such as rectification ratio, ideality factor, barrier height and series resistance.

S.J. Pearton et al. [10] reported ZnO based Schottky contacts used as UV light detector and gas sensor, as transparent device. They reported progress in controlling n-type and p-type doping, role of ion implantation for doping or isolation.

They have described about the ohmic and Schottky contact in detail.

H. Norde et al. [68] proposed a new method to obtain the barrier height in presence of series resistance. In this method forward I-V characteristics has been utilised to evaluate the barrier height with the proposed technique.

H.C. Chen et al. [21] reported n-type ZnO/p-type GaN hetro-junctions LEDs operated in reverse breakdown region. High quality n-ZnO layer was grown on GaN using atomic layer deposition technique. A theoretical model, based on the field assisted tunnelling, was applied to describe I-V characteristics in reverse breakdown region.

W. C. Liu et al. [22] described steady and transient state hydrogen sensing characteristics using Pd/InP MOS Schottky contacts, at room temperature and ambient pressure. The variation in I-V due to change in the hydrogen concentration was demonstrated for steady and transient states.

M. Prasad et al. [69] discussed the effect of relative humidity on the performance of ZnO based MEMS sensors. A ZnO layer was sandwiched in between the Al electrodes on a silicon diaphragm fabricated by bulk micro-machining process.

C. Periasamy et al. [24] fabricated the piezoelectric nano-generator using platinum contacts as ZnO nano-needle array. ZnO has been used to convert mechanical energy into electrical energy because of its suitable piezoelectric and semiconducting properties. Crystal structure has been studied using atomic force microscopy.

N. P. Herring et al. [70] demonstrated the fabrication of facile microwave irradiation (MWI). It was synthesised by using two different approaches. Transmission electron microscopy (TEM) and XRD were used for structural analysis. T. Varma et al. [71] simulated the fabrication ZnO based Schottky photo-diode of Pt using ATLAS software. Performance analysis using electrical and optical characteris-

tics have been done on ATLAS. Responsivity was found to be 0.32 A/W in UV region and has a good quantum efficiency of 88%. The effect of temperature, ZnO thickness and doping concentration on the performance of Schottky contacts have been studied.

2.4.3 Thin Film Transistors

The working of the thin film transistors can be understood with the corresponding NMOS silicon transistors. When a positive gate voltage is applied to the aluminium source/drain contact, the electrons are attracted to the interface between the ZnO and gate oxide layers to the form an accumulation channel. The work function difference between the metal and the semiconductor layer is the same as the threshold voltage that appears in the TFT, as the accumulation channel forms at low bias. In ZnO TFTs, there are trap states which can donate or accept electrons at the insulator semiconductor interfaces. The donor-like traps are neutral, naturally, but show a positive charge, otherwise. These donor-like traps have to be first filled with electrons to obtain switching operation of TFTs. For the case of acceptor-like traps, a reverse process of charge is present. They are negatively charged when filled with electrons, otherwise neutral. The donor-like traps, near the conduction band, have a dominant effect of shifting the threshold voltages in the n-type ZnO TFTs.

The operation of the ZnO TFTs can be classified into six different regions, as per the applied gate and drain bias voltages, namely turn-off, depletion, depletion-saturation, accumulation, accumulation-depletion and accumulation-saturation modes.

Literature review of some of the papers studied before proceeding for the simulation and fabrication of ZnO thin film based bottom gate TFTs are mentioned below.

Hoffman et al. [72] investigated ZnO-based thin-film transistors (TTFTs) fabricated with optical transmission of around 75% in the visible range of light. They observed from I-V measurements that the fabricated TFT was n-channel operating in enhancement-mode with excellent drain current saturation and a drain current on–off ratio of 10^7 with observable effect on the drain current to ambient light. The measured values of threshold voltages and channel mobilities of fabricated TFTs are reported to be in the range of 10 to 20 V and ; 0.3 to 2.5 cm^2 /V s, respectively. They found that changing the W/L ratio from 2:1 to 10:1 increases the drain current by a factor of about 5. They found that the required range of V_{GS} and V_{DS} used forTFT biasing are large in comparison to the silicon transistors and the operating voltages magnitudes are directly proportional to the gate insulator thickness. They deduced that the operating voltages can be reduced by a factor of 5–10 with a corresponding reduction in the gate insulator thickness. They also studied the effect of UV light and found that the TFTs possesses persistent photoconductivity, associated with the creation of electron-hole pairs by ultraviolet photons with energies greater than the ZnO band gap. H. Bae et al. [73] reported the fabrication of ZnO thin film based thin film transistor (TFT) and its application as a photo-detectors. TFT acted as a photo-detectors under zero gate bias. It has resistance of 100 M ohm, response time around 5 ms under 364 nm UV light confirming detecting behaviour of TFT.

 Pan, Zijian et al. [74] investigated ZnO-TFT with an integrated load resistance unit and the programmable ultraviolet (UV) detection integrated circuit unit. They found that the output current intensity was proportional to the UV intensity and possesses good switching characteristics with an ON/OFF ratio of around 100 under 365 nm UV light having an intensity of 1.224 mW/cm^2. They measured the rise and fall times of 35.0 & 43.9 ms, respectively when exposed to periodically switched UV light illumination. The UV PD has outstanding UV

photo-current characteristics, showing high sensitivity and fast response for UV detecting it works as a UV PD in the circuit unit. They have been able to achieve programmable measurement of UV.

Singh, Shaivalini et al. [17] investigated the ZnO thin film based TFT on silicon substrate with a W/L ratio of 4:1. They have reported simulation studies (done with software from ATLAS from Silvaco-International) along with the fabrication of the bottom gate TFT grown with the RF magnetron sputtering technique. They found that the characterization results show threshold voltage of 3.1 Volts, saturation field-effect to be 0.6134 cm^2 /V.s with ON OFF ratio of 10^2, at room temperature.

Cross, R. B. M. et al. [75] investigated the stability of ZnO thin film transistors grown with RF magnetron sputtering . They tested the device under gate bias stress, both positive and negative and found that the positive stress resulted in a positive shift of the transfer characteristics, while negative stress resulted in a negative shift. No effect was observed by them on the sub-threshold for low bias stress. They concluded that the instability to be a consequence of charge trapping at/near the channel/insulator interface. Also, the higher biases and longer stress times cause degradation of the sub-threshold slope, which is thought to arise as a consequence of defect state creation within the ZnO channel material. The devices were found to recover to their original characteristics, without any annealing process.

2.5 Application of ZnO thin films based devices as UV photo-detector: Recent review

S. J. Young et al. [76] reported ZnO thin film based Schottky nano-rods grown with RF sputtering, as UV photo-detectors.They observed that the photo-currents do not show any saturation at high value of biasing but is seen to increase with an increase in the incident power density. They have reported high value of responsivity of 104.14 A/W at - 1 Volt, so as to be used as a good UV photo-detector.

Kewei Liu et al. [20] studied Zinc Oxide based UV photo-detectors. Zinc Oxide thin film have been fabricated using different techniques such as PLD, MOCVD, RF Sputtering, MBE, P-MBE, Sol-gel and RF sputtering. ZnO-based p-n heterojunction photo diodes have been fabricated and compared. I-V characteristics under dark and UV conditions have been studied and compared.

T. Chen et al. [77] Schottky contact was grown on glass substrate. current-voltage plots were obtained under dark and UV conditions. photo-current under UV condition was found to be 6.5 µA, UV-to-visible ratio was reported 780.8 at -1 V, further the low frequency noise characteristics of ZnO nanorod-based Schottky contacts were also obtained.

Mian Wei et al. [23] investigated the ZnO based Nickel RF Micro-mechanical Resonators for monolithic wireless communication applications. In this research, fabrication of thin-film piezoelectric rectangular plate resonator and a piezoelectric-on-structural layer rectangular plate resonator have been discussed, further localised annealing techniques have also been discussed.

G. Cheng et al. [78] studied the highly sensitive ZnO based UV photo-detectors having fast response time. Optical parameters such as sensitivity, photo-current gain and on/off ratio were calculated and found to be 2.6×10^3 A/W, 8.5×10^3 and 4×10^5, respectively.

G.M. Ali et al. [79] reported characterization of ZnO thin film based metal-semiconductor-metal (MSM) and metal-insulator-semiconductor-insulator-metal (MISIM) UV photo-detectors. Sol-gel technique was used to grow ZnO thin film on a p-type Si substrate. Electrical and optical parameters were calculated from measured data.

Divya Somvanshi et al. [80] have reported the ultraviolet (UV) detection characteristics of Pd/ZnO Schottky contacts that were grown on tin coated n-Si substrates by thermal evaporation method. They measured the electrical characteristics of these diodes, with the applied bias voltages varying from 3 to 3 V, under both the dark and UV illumination at a wavelength of 365 nm. The as-fabricated photo-diodes were reported to have a high-contrast ratio of 541.34, quantum efficiency of 68% and responsivity of 0.20 A/W, at a reverse bias voltage of 3 Volt.

2.6   Summary and concluding remarks

Various nano-structures can be fabricated, with desired characteristics, as large single crystals or polycrystalline thin films. The single crystals of ZnO can be deposited with various wet & gas-phas deposition techniques such as, hydrothermal growth, vapour-phase transport, and CBD. Deposition of ZnO thin films can be realized by using chemical vapour deposition (CVD), molecular-beam epitaxy and RF magnetron sputtering. The RF magnetron sputtering has an additional advantage of fabricating ZnO thin films at room temperature, so as to permit different type of substrate structures. Such devices are known to possess high mobilities.

ZnO has provided new frontiers for emerging electronic devices, to replace the existing silicon technology. Its large exciton binding energy makes it suitable for opto-electronic applications to replace the existing GaN based UV sensors.

Chapter 3

Simulation and performance analysis of Schottky diode based on ZnO thin film

3.1 General Introduction of Performance Analysis of ZnO based Schottky Photodiodes

In recent years, ZnO has emerged as a promising material for variety of nano-electronic and piezoelectronic device applications. Its wide bandgap (3.37 eV), excellent radiation hardness, high exciton binding energy (60 meV) that enhances light emission and inhibits thermal activation at room temperature, etching ability with wet chemicals, ease of forming nanostructures with efficient light emission and biocompatibility has ensured its usability in many optoelectronic device applications such as UV detectors, light emitting diodes, solar cells and energy harvesting applications [20, 81–84]. High quality nanostructures and thin films of ZnO with low processing temperature has attracted researchers to use it in flexible electronic device applications. This increased popularity of ZnO

thin films and nanostructures for next generation optoelectronic device applications has motivated the researchers to study its electrical(metal) contact properties [64, 85–87].

Either it is, transparent electronics, flexible electronics or spintronics, all require metal contacts and hence a detailed systematic study of ZnO-metal contact is important. Mead has reported first Schottky contact in 1965 [88]. Since then, different authors have reported different metals as Schottky contacts for ZnO. Recently, Brillson and Lu have reported a comprehensive review on the progress of ZnO ohmic/Schottky contacts that has taken place in last few decades [18]. They have reviewed the role of alloyed contacts, multilayer contacts, metallization schemes, charge transfer, crystal quality, surface cleaning, defect formations and chemical interactions on the performance of ZnO based ohmic / Schottky contacts. Work reported in past suggests that fabrication of stable and better quality Schottky contacts to ZnO is still an area of high interest for researchers. Study of Schottky contact behaviour under given biasing conditions is an aspect which needs a significant attention. Some reports on properties of metal contacts, at room temperature, are available in literature but only very few reports are available on performance analysis of ZnO Schottky diodes in terms of temperature, thickness and doping variations [64, 89–92].

This work reports the simulation study and analysis of Pt/ZnO Schottky photodiode using ATLAS simulator from SILVACO international. Various electrical and optical parameters such as dark/illumination current, quantum efficiency and responsivity have been obtained for UV wavelength region. Different temperature related electrical parameters such as ideality factor and barrier height have been evaluated. Effect of temperature, thickness and doping concentration variation on the performance of Pt/ZnO Schottky photodiode has also been analysed and reported.

Table 3.1: Set of parameters used for ZnO during ATLAS simulation of Pt/ZnO Schottky photo-diode.

Parameter	Values
Bandgap (eV)	3.37
Electron affinity (χ)	4.35
Effective density of states in the conduction band (N_c) [cm^{-3}]	4×10^{18}
Effective density of states in the valence band (N_v) [cm^{-3}]	7×10^{19}
τ_h and τ_n (sec.)	1×10^{-9}
Dielectric constant (ε)	8.5
$\mu_n (cm^2 /V.s)$	60
$\mu_p (cm^2 /V.s)$	10

3.2   Simulation Setup

The 2D structure of Pt/ZnO Schottky photodiode is shown in Fig. 3.1.
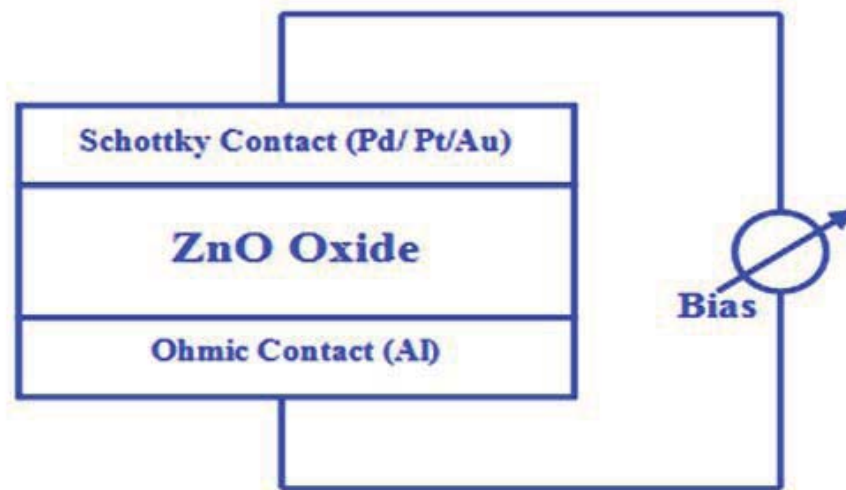
Figure 3.1: Simulation setup

Thickness of ZnO is taken as 500nm. A program of ZnO based Schottky photodiode have been developed in DECKBUILD interface with ATLAS simulator. Material properties of ZnO used during the simulation are listed in Table 3.1 [20,64,82,83,83,85,86,86,87,93,94].

Effect of bandgap narrowing, field dependent mobility and concentration dependent lifetime models have been considered during the simulation. Schockley-

Read-Hall (SRH) model has been used to consider recombination effects [95,96]. SRH also simulates the leakage current which exists due to thermal generation. Direct recombination model (AUGER) has been used to consider the presence of interface traps at interface. Thermionic emission model and concentration dependent mobility model which obeys simple power temperature dependence have also been used. Inclusion of thermionic emission model considers non equality of quasi fermi levels (ϕ_n and ϕ_p) with applied biasing voltage. Therefore, current boundary conditions of these parameters at the surface can be written as follows [97,98]:

$$J_{sn} = qv_n(n_s - n_{eq}) \exp\left(\frac{\Delta\phi_b}{kT}\right) \tag{3.1}$$

$$J_{sp} = qv_p(p_s - p_{eq}) \exp\left(\frac{\Delta\phi_b}{kT}\right) \tag{3.2}$$

where J_{sn} and J_{sp} are electron and hole currents at the surface, respectively q is charge of electron, n_s and p_s are surface electron and hole concentrations respectively, n_{eq} and p_{eq} are electron and hole concentrations, at equilibrium, assuming infinite surface recombination velocity ($V_{applied} = \phi_n = \phi_p$). v_n and v_p are the mean thermal velocity for electrons and holes respectively, and their values have been obtained using following equations [97,98]:

$$v_n = \frac{A_n^* T^2}{qN_c} \tag{3.3}$$

$$v_p = \frac{A_p^* T^2}{qN_v} \tag{3.4}$$

where A_n^* and A_p^* are effective Richardson constant for electrons and holes respectively, T is the lattice temperature, N_c and N_v are effective density of states for electrons and holes respectively.

Consideration of Schottky thermionic emission model also includes the effect of field dependent barrier lowering. Image forces and static dipole layers at metal semiconductor interface are responsible for this mechanism. The amount of energy with which this barrier height reduces can be written as [97, 98]:

$$\Delta\phi_b = \beta\sqrt{\frac{q}{4\pi\epsilon_s}}\sqrt{E} + \phi E^{\gamma} \tag{3.5}$$

where E is the electric field at the interface and α is the linear dipole barrier lowering coefficient.

3.3   Results and Discussion

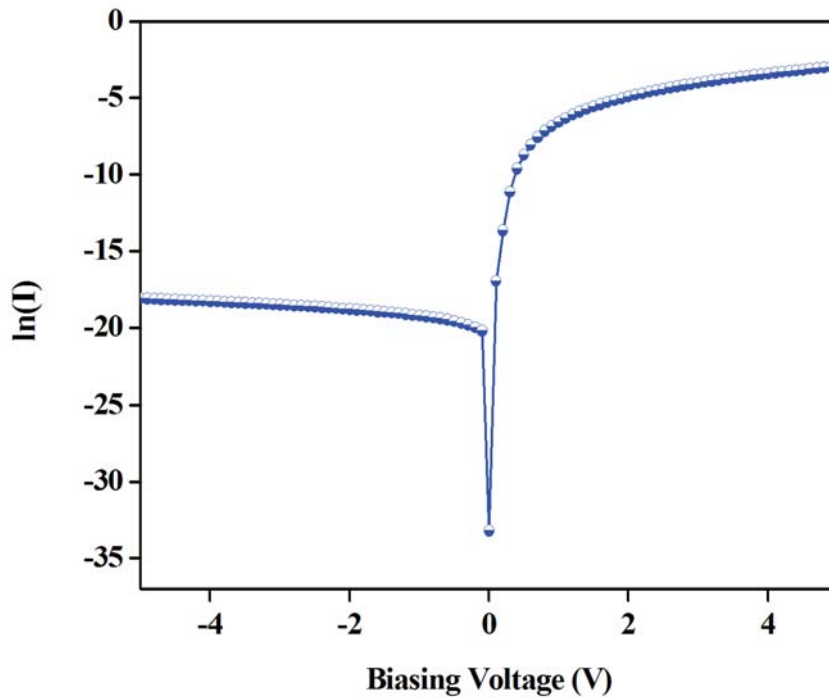Fig.3.2 shows the I-V plot for Pt/ZnO Schottky photodiode.

Figure 3.2: Current-voltage characteristics for Pt/ZnO Schottky photodiode.

Metal work function value for Pt has been taken as 5.65eV during the simu-

lation [98]. It is clear from Fig.3.2 that current-voltage characteristic of Pt/ZnO Schottky photodiode has shown Schottky nature. Ohmic and Schottky nature of metal-semiconductor contacts depends upon two parameters i.e. (i) work function of metal and (ii) electron affinity of semiconductor material. According to Bardeens model barrier height can be written as follows: [18]

$$\phi_{SB}^n = \phi_M - \chi_n - \Delta\chi \tag{3.6}$$

where ϕ_M is the work function of metal , χ_n is the electron affinity of semiconductor and $\Delta\chi$ is interface dipole. For ideal ohmic contact the potential barrier formed by the contact should be zero. Since work function of Pt is considerably higher than electron affinity of ZnO, Pt/ZnO contact has shown rectifying nature for current-voltage characteristics. The rectification ratio i.e. the ratio of forward current to backward current (IF/IR at ± 5V) for Pt/ZnO Schottky diode was found to be ~ 3.8×10^6.
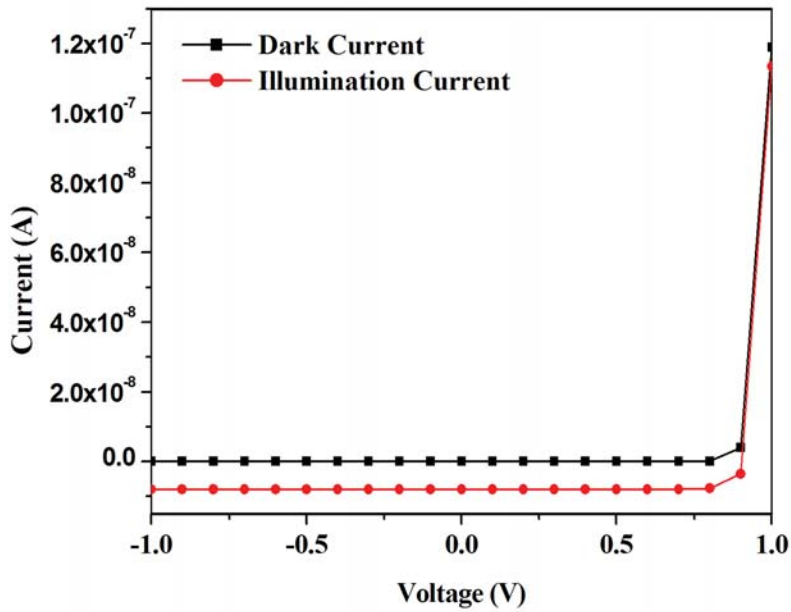

Figure 3.3: Variation of dark and illumination current as a function of biasing voltage

In low dimensional devices, Schottky barrier height not only depends upon work function of the metal but also depends upon image force lowering, field penetration and pinning of the fermi levels by surface states. All these parameters also affects Schottky barrier which varies with the absolute current value. Fig. 3.3 shows the variation of photocurrent with biasing voltage (-1 to 1 V) under dark and illumination conditions. When ultraviolet light falls over the photodetector, electron hole pairs get generated due to the absorption of photons in ZnO region. This generation of electron-hole pairs results in increased photocurrent under ultraviolet illumination which confirms the suitability of Pt/ZnO Schottky photodiodes for UV detection in variety of civil and military applications.
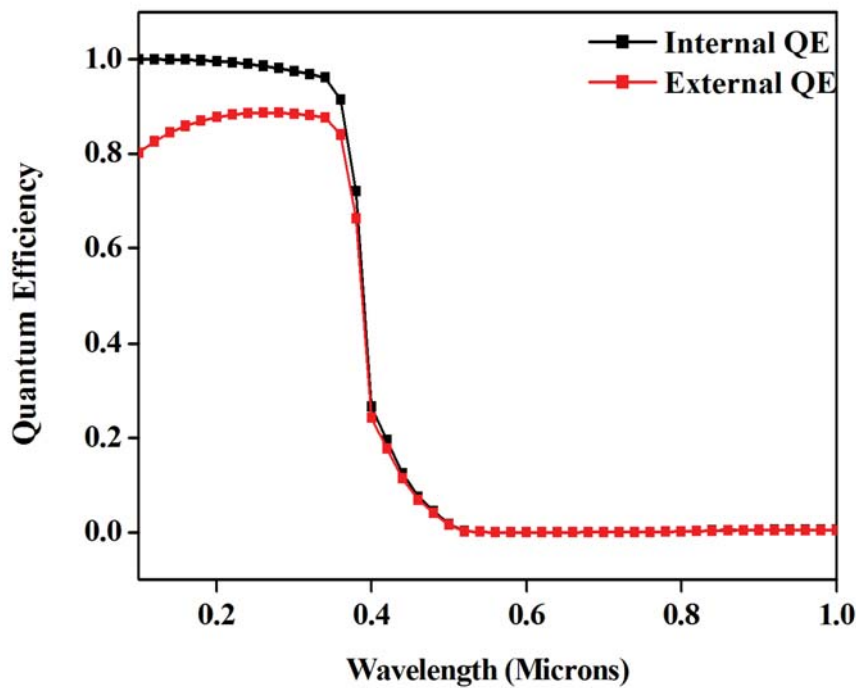

Figure 3.4: Variation of internal and external quantum efficiency as a function of optical wavelength

Fig. 3.4 demonstrates the variation of internal and external quantum efficiency of Pt/ZnO photodiode as a function of optical wavelength. Internal quantum efficiency has been obtained from the ratio of available photo current to the

source photocurrent whereas external quantum efficiency is the ratio of cathode current to the source photocurrent. It is clearly seen from the results that Pt/ZnO photodiode has exhibited a high internal and external quantum efficiency of ~98% and ~88% respectively for UV wavelength region which is attributed to high detectivity of the detector. High value of quantum efficiency in UV region with almost zero value in visible region confirms that Pt/ZnO Schottky photodiode can detect UV light very efficiently.
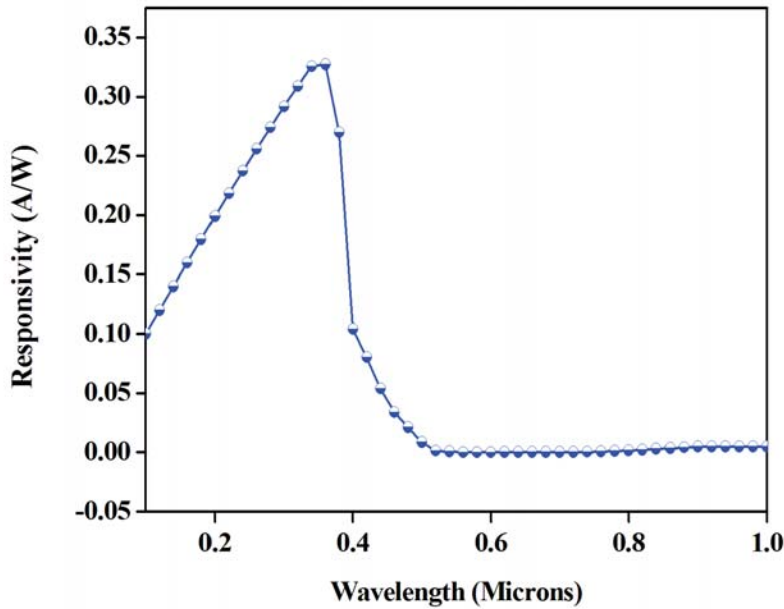
Figure 3.5: Responsivity spectra of the Pt/ZnO Schottky diode

Fig. 3.5 shows the responsivity spectra of Pt/ZnO Schottky photodiode that has been obtained using following equation.

$$R = \frac{q\eta\lambda}{hc} \tag{3.7}$$

where, η is quantum efficiency, λ is light wavelength and c is the velocity of light. The device has exhibited a good responsivity in ultraviolet wavelength region. Maximum responsivity of 0.32 A/W has been observed at 360 nm wavelength.

Figure 3.6: Effect of temperature on I-V characteristics of Pt/ZnO photodiode

Fig.3.6 depicts temperature dependent I-V variations of Pt/ZnO Schottky photo-diode. It can be seen that device has shown rectifying behaviour for all temperature ranges, and current has increas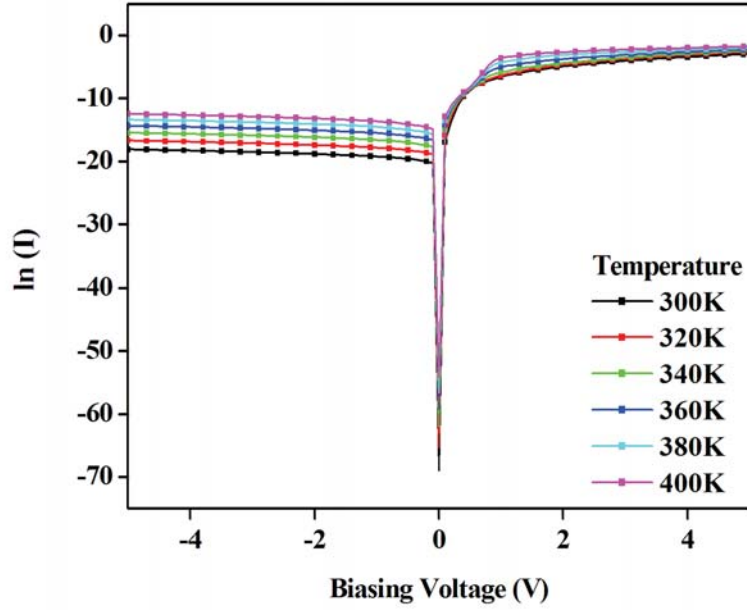ed with increasing temperature. Variation of ideality factor with temperature has been obtained using following equation [99].

$$n = \frac{q}{kT}\frac{\partial V}{\partial \ln(I)} \tag{3.8}$$

where q is the charge of electron, k is the Boltzmann constant, T is the lattice temperature. $\frac{\partial \ln(I)}{\partial V}$ can be obtained from the linear region slope of ln(I)-V plot. Ideality factor has shown a variation of 1.3-1.9 for 300-400 K temperature variation. In temperature dependent electrical characterization of Schottky contacts, barrier height also plays an important role and can be obtained using following equation [99].

$$\phi_{B,eff} = \frac{kT}{q}\ln\left(\frac{AA^*T^2}{I_0}\right) \tag{3.9}$$

where A is the contact area which is taken as unity during the simulation, A^*

51

is the effective Richardson constant ($A^* = 32 A cm^{-2} k^{-2}$ for $m_e^* = 0.27 m_0$) and I_0 is reverse saturation current. Variation of barrier height with temperature is demonstrated in Fig. 3.7, which has shown a linear increase in barrier height with temperature for Pt/ZnO Schottky photodiode.
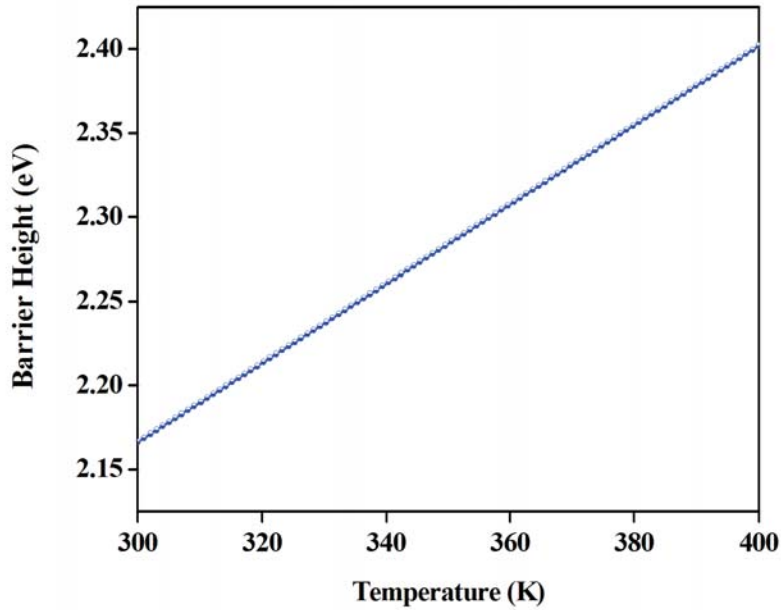

Figure 3.7: Variation of barrier height with temperature for Pt/ZnO photodiode

Increase in available charge carriers across the barrier for fermi level equalization may be the probable reason for increase in barrier height with temperature. Effect of ZnO thickness variation on responsivity of Pt/ZnO Schottky diode is demonstrated in Fig. 3.8. It has been observed that as thickness of ZnO increases, resistivity of ZnO layer also increases which results in increased responsivity of the photodiode. Fig. 3.9 shows effect of doping concentration variation on responsivity of the Pt/ZnO photodiode.

It is clearly seen that responsivity for Pt/ZnO photodiode has decreased with increased doping concentration. Analysis reveals that as doping increases, resistivity of ZnO layer decreases which results in reduced responsivity of the photodiode.
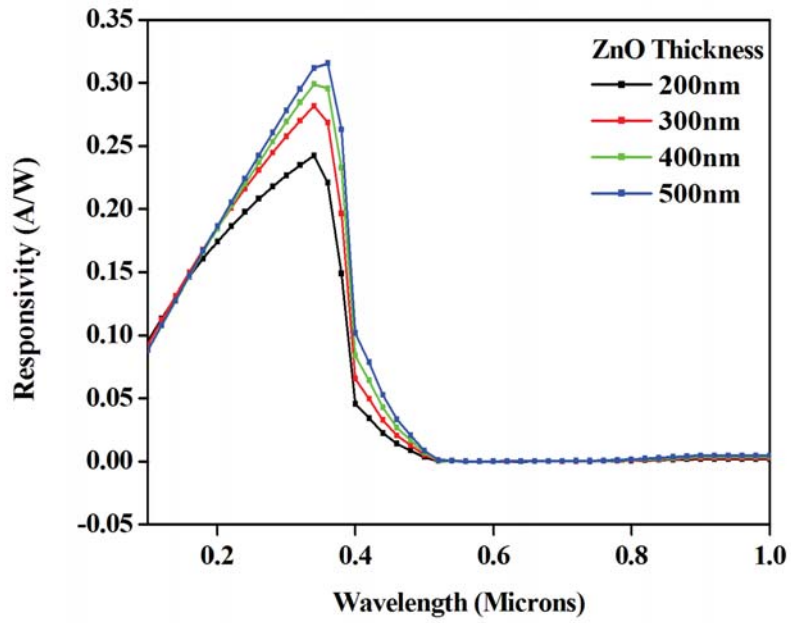
Figure 3.8: Effect of variation of thickness on I-V characteristics of ZnO Schottky contacts
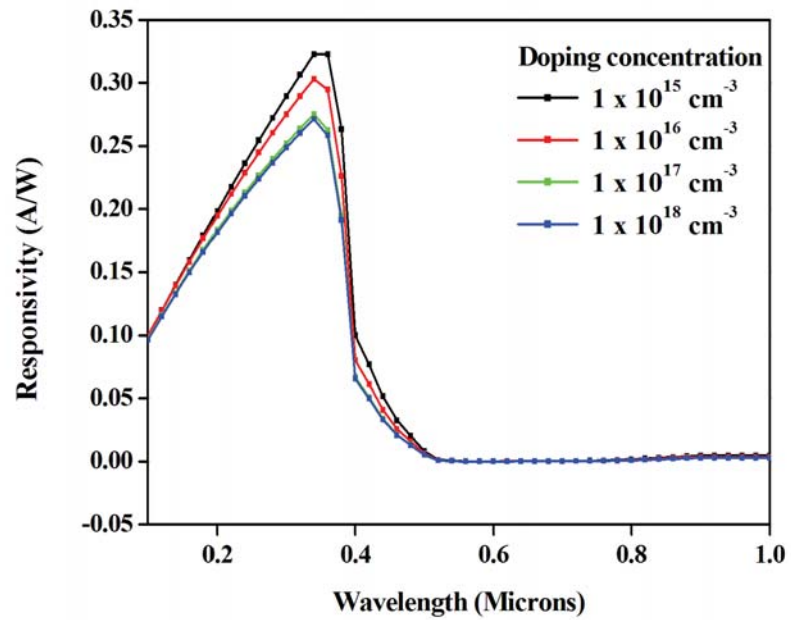
Figure 3.9: Effect of variation of doping concentration on I-V characteristics of ZnO Schottky contacts

3.4 Conclusion

This chapter presents simulation study and performance analysis of Pt/ZnO Schottky photodiode using ATLAS simulator from SILVACO international. Various important electrical and optical parameters of Pt/ZnO photodiode such as dark/illumination current, quantum efficiency and responsivity have been reported. The variation of responsivity as a function of wavelength has been obtained for different thickness and doping concentrations. Effect of temperature on current-voltage characteristics of Pt/ZnO Schottky photodiode has been studied. Temperature dependency of ideality factor and barrier height for Pt/ZnO Schottky photodiode has also been analyzed and reported.

Chapter 4

Fabrication and characterization of ZnO thin film based Schottky diodes and its application as UV detector

This chapter presents the fabrication and performance analyses of Schottky diodes with Au and Pd contacts on n-ZnO thin films as UV detector. RF magnetron sputtering technique has been used to deposit the nano-crystalline ZnO thin film. Characterization techniques, such as XRD, AFM, SEM and the UV measurement provided valuable information concerning the micro-structural, surface morphology, and optical properties of the ZnO thin film. I-V and C-V characteristics were evaluated for both Au/ZnO and Pd/ZnO Schottky diodes. Other important device parameters such as, ideality factor, barrier height, responsivity, photoconductive gain and detectivity were evaluated and compared.

4.1   Introduction

Solar UV radiation affects human beings adversely in variety of ways, causing cataract, lesions, photoaging, skin cancer and damage to the DNA structure. Var-

ious other artificial UV sources in medicine and industry also pose the same hazard. Although the atmosphere absorbs a significant portion of the solar UV radiation, the depletion of the stratospheric ozone is exposing humans to its harmful spectra with an higher intensity. It underscores the need to design and develop efficient and highly sensitive photo sensors at lower costs. Nano-crystalline Zinc Oxide (ZnO) thin films, with a wide band gap (3.37 eV), large exciton binding energy (60 meV) and high surface to volume ratio, are being developed as an alternative to the existing Gallium Nitride (GaN) based sensors that have low responsivity with a high cost. ZnO thin film is also a suitable semiconductor material for wide range of electronic device applications, such as, laser diode, thin film transistor (TFT), gas sensor, solar cell, piezo-electronic nano-generator, SAW resonator, and micro-electro mechanical devices [18–24], due to its excellent semiconductor and piezo-electrical properties. Moreover, realization of homogeneous ZnO thin film based opto-electronic devices require both p and n type material, although it is difficult to fabricate stable and reliable p-type ZnO thin film [70]. To realize the ZnO thin film based devices, different UV detector structures such as MSM, p-n, TFT, Schottky diode have been reported by researchers in the recent past [73, 78, 79, 100]. All these studies have explored possibilities of developing high performance ZnO UV photo detectors. A Schottky photo-diode has many advantages in various aspects such as high efficiency, low-dark current, high contrast ratio, simple structure and low cost. Fabrication of the ZnO thin films on silicon substrates helps us in achieving an integrated approach with the existing silicon technology. In this study, we demonstrate low power UV photo detectors based on ZnO thin films with gold (Au) and palladium (Pd) Schottky contacts on silicon wafer. The electroptical properties, along with structural, surface and optical properties, of both these detectors with thermally stable high Schottky barriers have been studied and compared.

4.2 Experimental Details

4.2.1 Preparation of ZnO thin film

In order to study the electroptical properties of the proposed devices, a nano-crystalline ZnO film was grown on a n-type silicon (Si) (101) substrate using RF magnetron sputtering, at room temperature. The process of cleaning the Si wafer was done in two steps- RCA-1 (10 minutes boiling in NH_3 + H_2O_2 + $6H_2O$) and RCA-2 (10 minutes in HCl + H_2O_2 + $6H_2O$ at 60°C), before deposition of the ZnO thin film. The deposition of ZnO thin film (340 nm) was carried out in 30 minutes and the following process parameters were maintained: a base vacuum of 5×10^{-6}T, pressure of 7.5×10^{-3}T and RF power of 100 Watts. The target to substrate distance was 7.5 cm. The basic structural, surface morphological, and optical properties of ZnO thin film were characterized by X-ray diffractometer (XRD) (Rigaku, Smartlab-3KW), Atomic Force Microscope (AFM) (Bruker, Multimode8-HR), Scanning Electron Microscope (SEM) (Nova Nano FE-SEM, 450) and UV-VIS-NIR Spectrometer (Shimadzu MPC3600).

4.2.2 Fabrication of Schottky diode

Schematic diagram of the proposed structure is shown in Fig. 4.1. Aluminium layer of thickness of ~100 nm was deposited on the back side of the Si wafer by vacuum coating technique, to act as an ohmic contact. Circular Schottky contacts of Ti (20nm) followed by Au/Pd (80nm) were deposited on the ZnO thin film through shadow mask, using E-beam technique. Top-view of the corresponding SEM image is shown in Fig. 4.2 with individual Schottky diode area of 0.74 mm^2. To improve the conductivity of the fabricated contacts, a rapid thermal process (RTP) was subsequently performed, at 450°C, in Argon atmosphere at 50 sccm for 5 minutes. Semiconductor Parameter Analyzer (Agilent B1500A), with probe

station, has been used to evaluate the electrical (I-V, C-V) and photo-response characteristics of both the Schottky contacts.
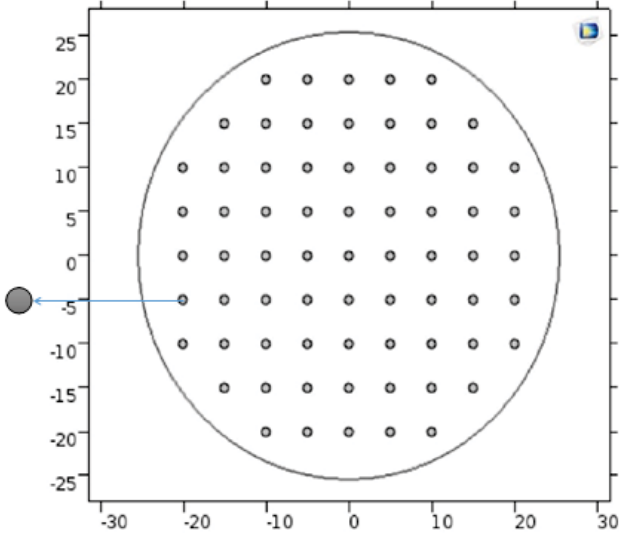

Figure 4.1: Grid of the Fabricated Schottky Contacts
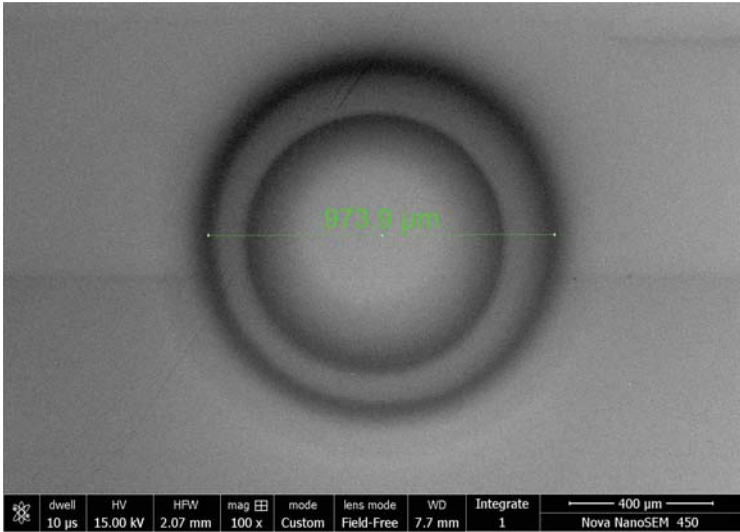
Figure 4.2: Schottky Contact

4.3 Results and Discussion

4.3.1 Structural and optical properties of RF sputtered ZnO thin film

Fig. 4.3 depicts the XRD spectra of the ZnO thin film prepared on n-type silicon substrate of 1-10 Ω-cm resistivity. The hexagonal wurtzite structure of the ZnO

Figure 4.3: XRD image of the ZnO thin film on silicon substrate

Figure 4.4: SEM image of the ZnO thin film on silicon substrate

thin film of polycrystalline nature with (002) c-axis orientation is verified by the strong diffraction peak observed at $2\theta = 34.4°$ of the XRD spectra and a weak diffraction peak at $2\theta = 62.8°$. The crystal size of 22.6 nm was computed for the

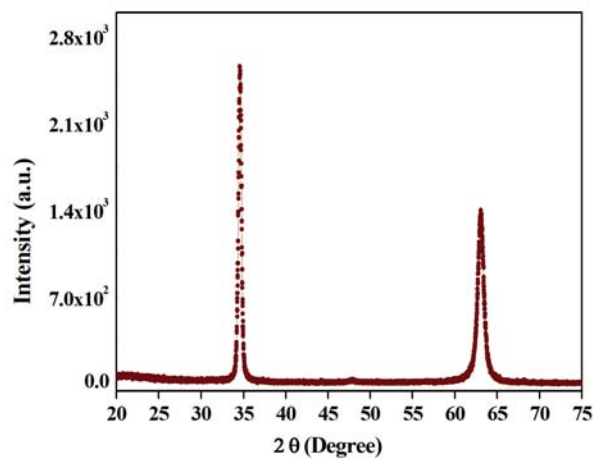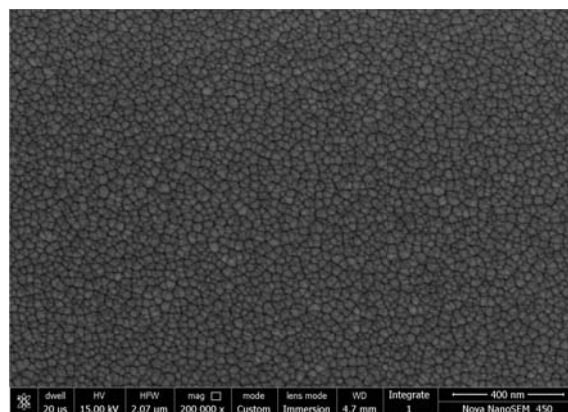(002) orientation peak, using the Scherrer's relation [101].

Fig. 4.4 shows the SEM image of the ZnO thin film on n-Si substrate. It confirms that the grown film is uniform with no cracks or pin holes. The average grain size was found to be in the range of 20-25 nm. Fig. 4.5 and Fig. 4.6 shows the 2-D
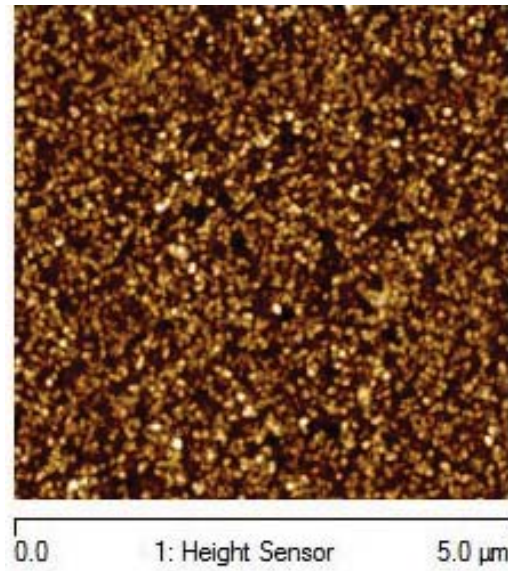

Figure 4.5: 2D-AFM image of the ZnO thin film on silicon substrate

and 3-D AFM images of the ZnO thin film on silicon substrate. It reveals that the grown RF sputtered ZnO thin film is uniform with an average grain size of 20-30 nm, which is in good agreement with the XRD and SEM results.
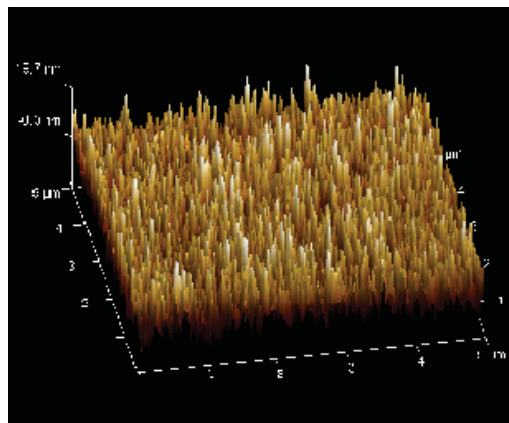

Figure 4.6: 3-D AFM image of ZnO thin film on Si substrate
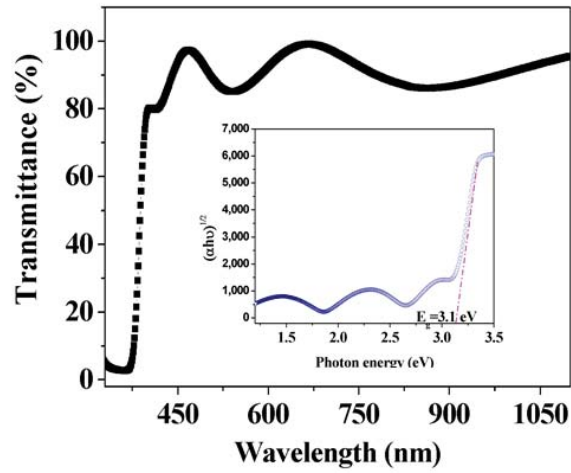
Figure 4.7: Optical transmission spectra of ZnO thin film. Inset shows the plot of $(\alpha h\nu)^{\frac{1}{2}}$ versus $(h\nu)$

Such nano-crystalline thin films are well suited for UV detection application owing to their high surface to volume ratio. Fig. 4.7 shows the transmittance spectra of the ZnO thin film with a sharp band edge absorption at 375 nm and a good optical transmittance of around 94%, as observed in the visible range. The optical band gap of the ZnO thin film was evaluated by extrapolating the linear region of $(\alpha h\nu)^{\frac{1}{2}}$ versus $(h\nu)$ plot, as shown in the inset of Fig. 4.7 and found to be 3.1 eV [67].

4.3.2 Electrical characteristics of Au/ZnO and Pd/ZnO Schottky diodes

The experimentally measured current-voltage (I-V) characteristics of both Au/ZnO and Pd/ZnO devices, are depicted in Fig. 4.8, under dark conditions. I-V characteristics shows a typical non-linear behaviour of both these contacts with rectification (IF/IR) ratios of 19 and 427 for Au/ZnO and Pd/ZnO Schottky diodes, respectively, at a bias of ±4 V. This supports the results that we obtained from the
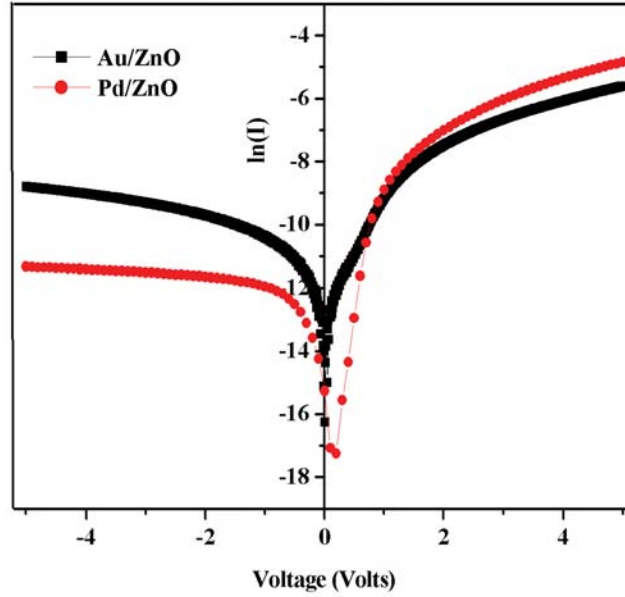
Figure 4.8: I-V characteristics of both Au/ZnO and Pd/ZnO Schottky diodes, under dark condition

TCAD simulation done in Chapter 3 [71]. Generally, the major current transport mechanism of the thin film Schottky contacts can be described by the thermionic emission theory [60, 64]. The important diode parameters of both the devices have been evaluated from the I-V characteristics by using the following equations [61, 64]

$$I = I_0 \exp\left(\beta \frac{V - IR_s}{n}\right) \tag{4.1}$$

$$I_0 = AA^* T^2 \exp(-\beta \phi_b) \tag{4.2}$$

$$\beta = \frac{q}{kT}$$

where, V is the applied bias voltage, k is the Boltzmann constant, T is the temperature, n is the ideality factor, ϕ_b is the effective barrier height at zero bias, A is the effective area of the Schottky diode, A^* is the Richardson constant (0.15 A/cm^{2}K^2 for ZnO) [59] and R_s is the series resistance. According to (4.2), the sat-

uration currents I_0, which are defined by the value of the I-V characteristics near zero bias voltage, are found to be 8.69×10^{-8}A and 3.24×10^{-8}A for Au/ZnO and Pd/ZnO Schottky diodes, respectively. The effective barrier height ϕ_b and the ideality factor n have been evaluated without considering R_s, for the ideal case, from the (4.3) and (4.4), respectively.

$$\phi_b = \frac{1}{\beta} \ln\left(\frac{AA^*T^2}{I_0}\right) \tag{4.3}$$

$$n = \beta \frac{dV}{d(\ln I)} \tag{4.4}$$

The measured diode parameters of both the Schottky diodes in dark conditions, at room temperature, are listed in Table 4.1. The obtained high value of the ideality factor and the low value of barrier height may be due to the interfacial defects, different current transport mechanisms, inhomogeneities in the interface oxide layer and also the series resistance of the diode [59].
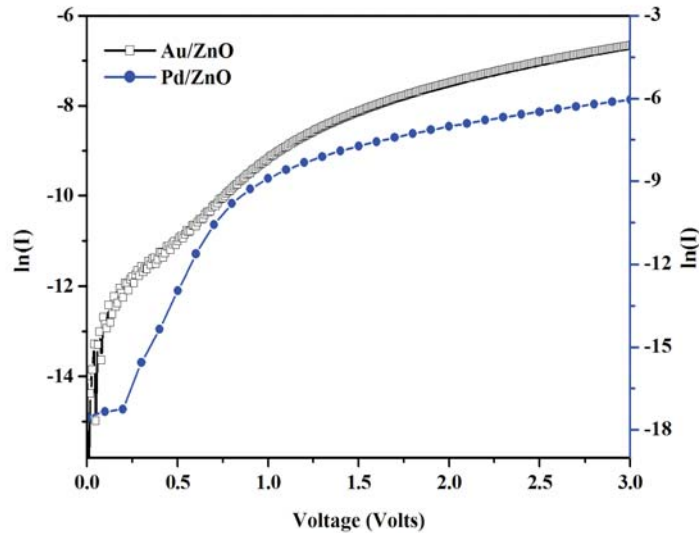
Figure 4.9: Logarithmic plot of the I-V characteristics under forward bias for both of the Au and Pd Schottky contacts

The current transport behaviour of both the Schottky diodes has further been

Table 4.1: Comparison of electrical parameters of ZnO thin film Schottky diodes at room temperature

Device structure	Ideality factor, n		Barrier height, ϕ_b (eV)				Series resistance, R_s (Ω)		
	I-V	Cheung & Cheung	I-V	Cheung & Cheung	Norde	C-V	I-V	Cheung & Cheung	Norde
Our study, Au/ZnO	2.27	5.6	0.54	0.21	0.50	0.68	620	1181	3858
Our study, Pd/ZnO	2.68	2.75	0.57	0.62	0.73	0.79	2.54	523	931
Au/ZnO, [64]	1.53	2.10	0.59	0.54	0.61	0.73	1525	1531	1836
Pd/Zno, NR [102]	1.46	-	0.81	-	0.81	-	-	-	412.5×10^3

investigated with the forward I-V logarithmic plot, as shown in Fig. 4.9. From this figure, it is seen that, low forward voltages (0-0.5 V) with an approximately unit slope accounts for the first region, due to the tunneling effect. Space charge limited current regions, due to the presence of traps, account for the diode behaviour at higher bias voltages [64,67]. The series resistance, R_s, is an important
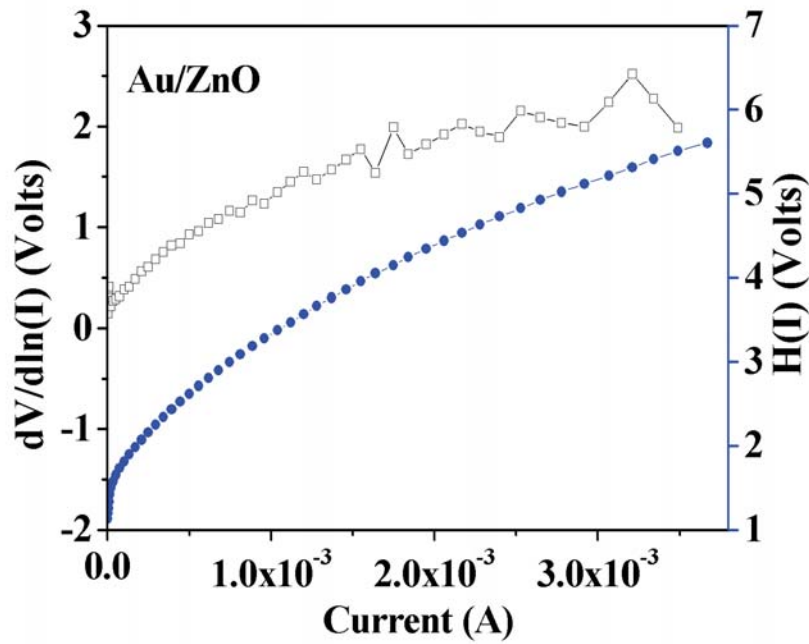
Figure 4.10: Plot of $\frac{dV}{d\ln(I)} - I$ and $H(I) - I$ in the forward bias for Au/ZnO Schottky diode

parameter which causes the I-V behaviour to deviate from that of the ideal diode. The electrical properties of the fabricated diodes have been further studied by using the Cheung & Cheung and modified Norde' techniques [61,68]. The Cheung & Cheung's relations are described, as below

$$\frac{dV}{d(\ln I)} = \frac{n}{\beta} + IR_s \tag{4.5}$$

$$H(I) = V - \frac{n}{\beta}\frac{I}{AA^*T^2} \tag{4.6}$$

$$H(I) = n\phi_b + IR_s \tag{4.7}$$

65
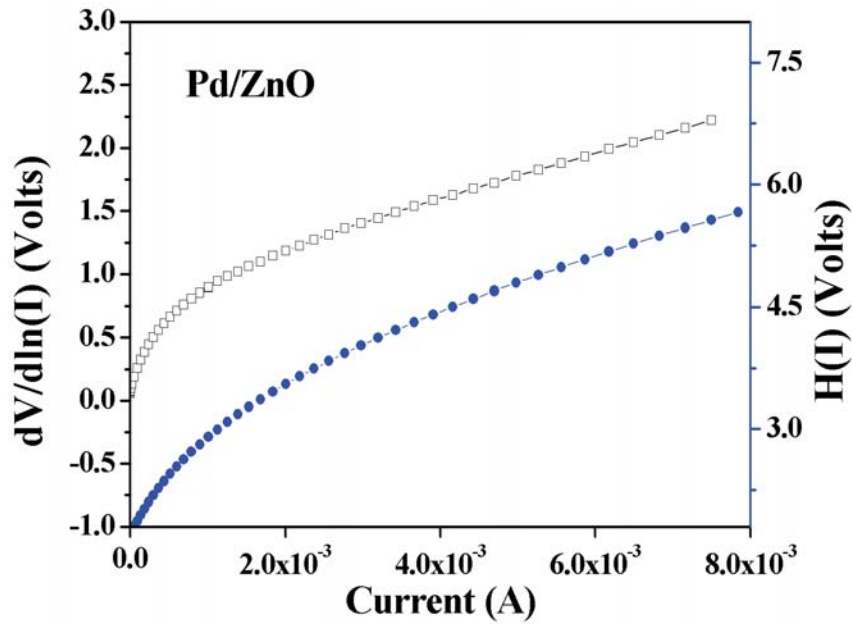
Figure 4.11: Plot of $\frac{dV}{d\ln(I)} - I$ and $H(I) - I$ in the forward bias for Pd/ZnO Schottky diode

Fig. 4.10 and Fig. 4.11 show the plots of $\frac{dV}{d\ln(I)} - I$ and $H(I) - I$ of both the Au/ZnO and Pd/ZnO Schottky diodes, respectively. Series resistance, ideality factor and barrier height are obtained from the slope and the y-intercept of Fig. 4.10 and Fig. 4.11. The measured values of all of these parameters are listed in Table 4.1 and found to be in good agreement with the results reported by other researchers [64, 102]. It is observed that the value of n computed by Cheung & Cheung method, for the Au/ZnO Schottky diode, is significantly higher than that obtained from the corresponding I-V plot. The reason may be that the ideality factor calculated by Cheung & Cheung method, with the downward curvature region of I-V characteristics, shows a higher value than the one obtained from the conventional thermionic emission model, where we used in the low voltage linear region of I-V characteristics. Furthermore, it is also noted that the series resistance, computed with both the methods, show different values. For the case of Pd/ZnO Schottky diode, the values are comparable.

66

Further, to gain more insight into the behaviour of the fabricated Schottky diodes, we calculated the series resistance and the barrier height with an alternate method, as proposed by Norde and given below [68]

$$F(V) = \frac{V}{\gamma} - \frac{1}{\beta} \ln\left(\frac{I(V)}{AA^*T^2}\right) \tag{4.8}$$

$$\phi_b = F(V_0) + \frac{V_0}{\gamma} - \frac{1}{\beta} \tag{4.9}$$

$$R_s = \frac{\gamma - n}{\beta I} \tag{4.10}$$

γ in equation (4.8) being the first integer greater than n, as evaluated with the I-V method. The $F(V) - V$ plots of both the Schottky diodes are shown in Fig. 4.12. From this figure, the minimum value of $F(V_0)$ and V_0 are 0.48, 0.15 V, 0.59,
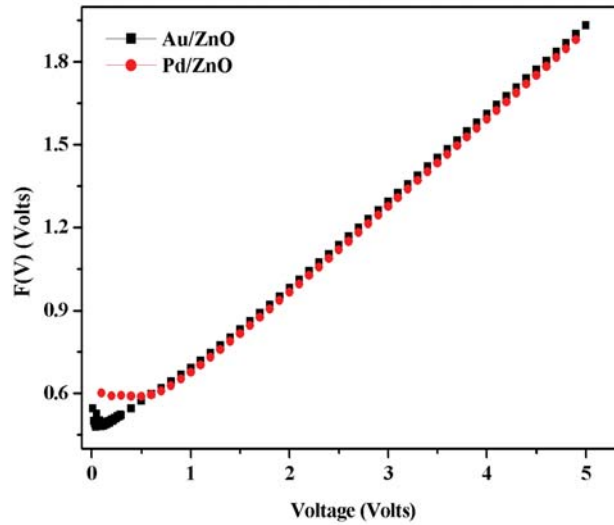
Figure 4.12: F(V) versus bias voltage plot of both Au and Pd Schottky contacts

0.5 V for Au/Zno and Pd/ZnO diodes, respectively. Values obtained are substituted in (4.9) and (4.10) to determine the barrier height and the series resistance of both the fabricated Schottky diodes. The computed values of ϕ_b and R_s are listed in Table 4.1. The values of series resistance, R_s calculated from the modi-

fied Norde's are higher than those obtained from Cheung & Cheung method for both diodes. The ideality values evaluated from both the methods for Pd/ZnO are comparable, whereas, for Au/ZnO the values obtained from Cheung & Cheung method are much higher. For comparison, the Schottky diodes have been
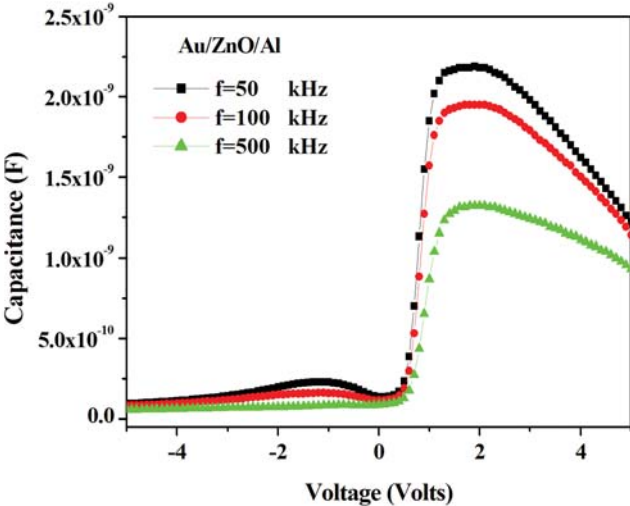
Figure 4.13: C-V characteristics of the Au/ZnO Schottky diode at different frequencies
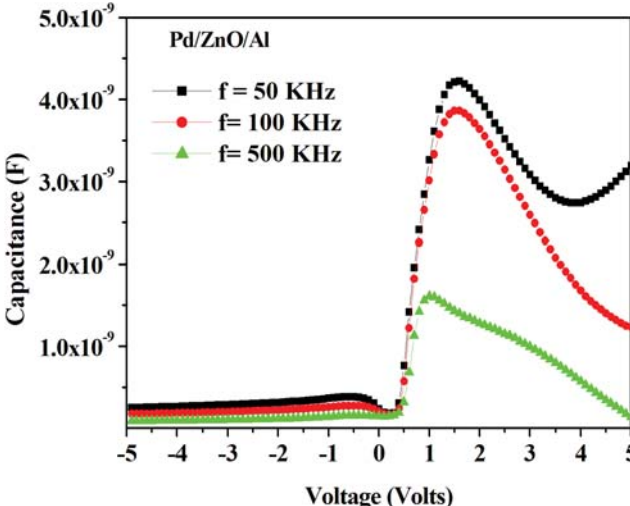
Figure 4.14: C-V characteristics of the Pd/ZnO Schottky diode at different frequencies

further investigated with the capacitance-voltage (C-V) measurements done at different frequencies and depicted in Figs. 4.13 & 4.14, from which it is clearly

observed that an increase in frequency results in fall of capacitance values.
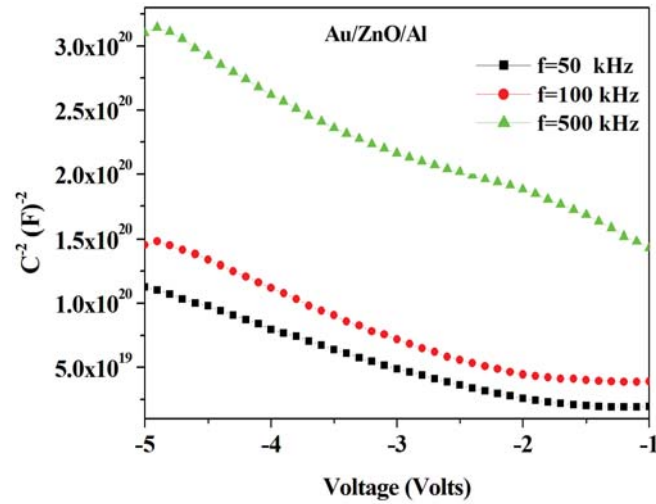
Figure 4.15: $(\frac{1}{C^2} - V)$ characteristics of the Au/ZnO Schottky diode at different frequencies
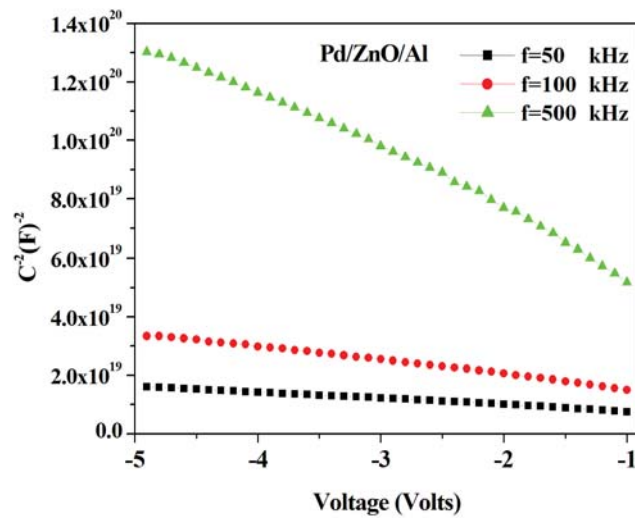
Figure 4.16: $(\frac{1}{C^2} - V)$ characteristics of the Pd/ZnO Schottky diode at different frequencies

A similar trend is obtained for ZnO thin film Schottky diode, as reported by others [64]. A peak is observed in the forward-bias region, at lower bias values, that gradually disappears as the the frequency is increased, which may be due to presence of deep-states in the energy band, interfacial defects or the series

resistance of the devices [64].

Plots of $(\frac{1}{C^2} - V)$ for these devices have been shown in Figs. 4.15 & 4.16, derived from C-V characteristics, for different frequencies. The built-in potential, V_{bi} and the barrier height values of the devices are computed from Figs. 4.15 and 4.16, along with the following relations

$$\frac{1}{C^2} = \frac{2(V_{bi} - V - \frac{1}{\beta})}{\epsilon_{ZnO} q N_D(W) A^2} \tag{4.11}$$

$$\phi_b = q\left[V_{bi} + \frac{1}{\beta} \ln\left(\frac{N_C}{N_D}\right)\right] \tag{4.12}$$

where, $\epsilon_{ZnO} (= 9\epsilon_0)$ is the permeability of the ZnO thin film, $N_D(W)$ is the carrier concentration at a distance $x = W$ and $N_C = 4.98 \times 10^{18} cm^{-3}$ in the conduction band [61,102]. The carrier concentration N_D versus depth plots are shown in Fig. 4.17. The measured values of carrier concentration, as calculated from Fig. 4.17, and the barrier height are $1.579 \times 10^{16} cm^{-3}$ & 0.765 eV and $3.58 \times 10^{16} cm^{-3}$ & 0.86 eV, respectively for Au/ZnO and Pd/ZnO Schottky diodes at a frequency of 500 kHz.
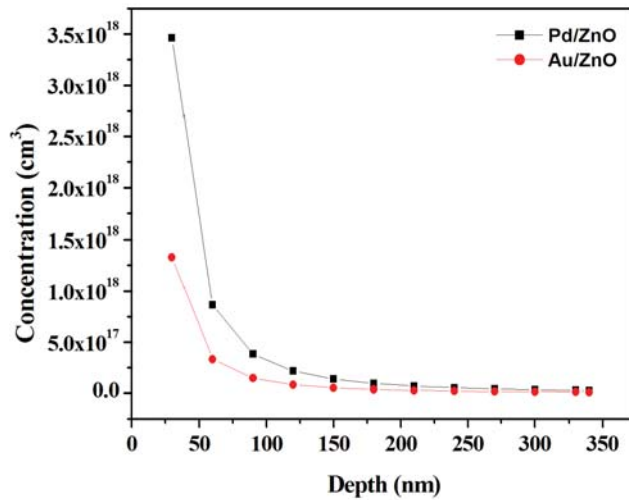
Figure 4.17: Depth profile of the carrier concentration versus the depletion width

The obtained values of the barrier height from the C-V characteristics of both the devices are high as compared to the values computed from the I-V measurement. These differences may be due to the presence of barrier height inhomogeneities and interface defect states at the Schottky junction [61,68].

4.3.3 UV Detection of the Schottky diodes

In order to evaluate the feasability of both these fabricated diodes, as UV detectors, tests were subsequently conducted to evaluate their photo-detector response in the UV region.The experimental setup is shown in Fig. 4.18. The I-V measurements were performed under UV light of wavelength 365 nm and the results are shown in Figs. 4.19 and 4.20. The UV detector and photo-response of the ZnO thin film based Schottky contacts have already been described by other researchers elsewhere [65, 80]. The photo-detection mechanism of these Schot-
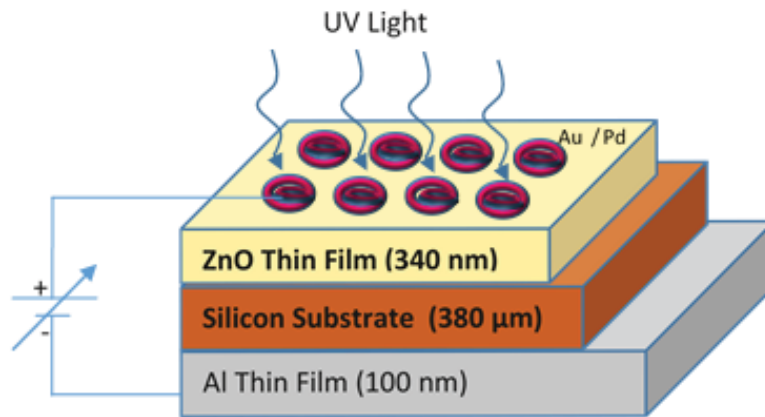
Figure 4.18: Experimental Setup for IV Characterization under UV Exposure.

tky diodes is mainly governed by adsorption and desorption of oxygen on ZnO thin film surface. Under dark condition, oxygen is adsorbed by capturing a free electron from the surface of the ZnO thin film, as per (4.13).

$$O_2(g) + e^- = O_2^-(ad) \tag{4.13}$$

71

where, $O_2(g)$ is oxygen (gas form). This adsorption creates a depletion layer near the surface of the film which results in a decrease in conductivity of the ZnO thin film. Under UV illumination, one absorbed photon results in a photogenerated electron-hole pair: $h\nu \rightarrow h^+ + e^-$, where, $h\nu$ and e^- represent hole and electron respectively. Consequently, photogenerated holes move towards the surface and neutralize the adsorbed oxygen, as per (4.14)

$$O_2^-(ad) + h^+ = O_2(g) \tag{4.14}$$

Thus, the oxygen atoms are desorbed near the ZnO thin film surface. Since, it is the reverse process of the adsorption, the oxygen desorption results in an increase in the photoconductivity near the surface. The total photo-response of the detector is also due to the following reasons: separation of holes and electrons in the depletion region and the modulation of the sheet conductance. This in turn, enhances the photoresponse of the detectors in the UV region. From the I-V
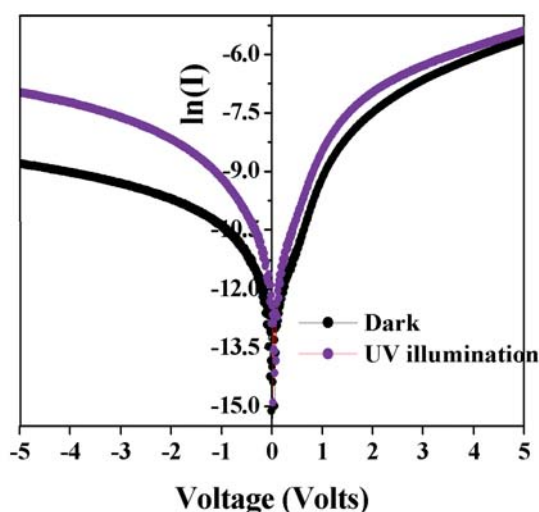
Figure 4.19: I-V characteristics of the Au/ZnO Schottky diode under dark and UV illumination

plots, shown in Figs. 4.19 & 4.20, we can easily see that the reverse currents of
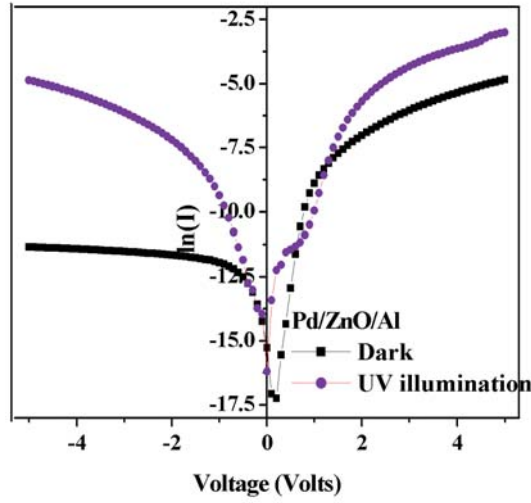
Figure 4.20: I-V characteristics of the Pd/ZnO Schottky diode under dark and UV illumination

both the Schottky diodes show a clear enhancement when illuminated with the UV light. Further, the responsivity R and the quantum efficiency η have been evaluated using the following relations

$$R = \eta \frac{\lambda(\mu m)}{1.24} \qquad (4.15)$$

$$\eta = \frac{I_{ph}}{P_{opt}} \frac{h\nu}{q} \qquad (4.16)$$

where, I_{ph} is the photon current and P_{opt} is the incident optical power. The measured values are listed in Table 4.2 and it is observed that Pd/ZnO diode shows better photo-detection capabilities towards UV light than the Au/ZnO based Schotkky diode.

The detectors were also tested for different optical powers and the results are shown in Figs. 4.21 and 4.22. An increase in current is observed, as the optical UV power intensity is increased from 2.16 to 4.46 mW/cm^2. The Pd/ZnO Schottky diode was found to exhibit a good contrast ratio ($\frac{I_{ph}}{I_{dark}}$), of 86.14, at a reverse bias of -2 V, whereas a very low value, 4.65, was obtained for Au/ZnO Schottky

73
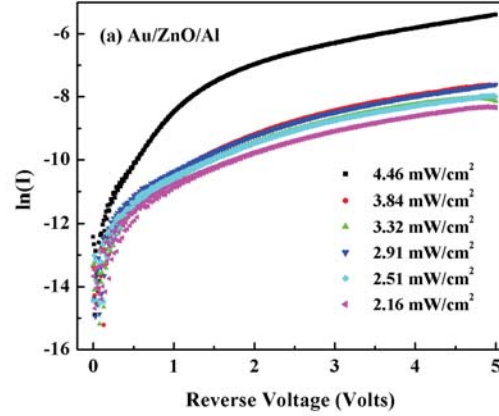
Figure 4.21: I-V characteristics of Au/ZnO/Al Schottky UV detector with different light intensities.
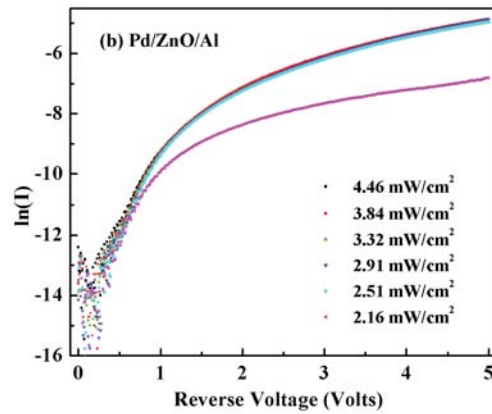
Figure 4.22: I-V characteristics of Pd/ZnO/Al Schottky UV detector with different light intensities.

diode, as depicted in Fig. 4.23. The computed responsivity of both the detectors, measured at -2 V, are found to be 10.16 and 22.7 A/W for Au/ZnO and Pd/ZnO detectors, respectively. Detectivity, D and photoconductive gain, G, are the other important parameters that determine the capability of UV sensor to detect the weakest light signal, which have been evaluated using following relations

$$D = \frac{\lambda \eta q}{hc} \sqrt{\frac{R_0 A}{4kT}} \qquad (4.17)$$
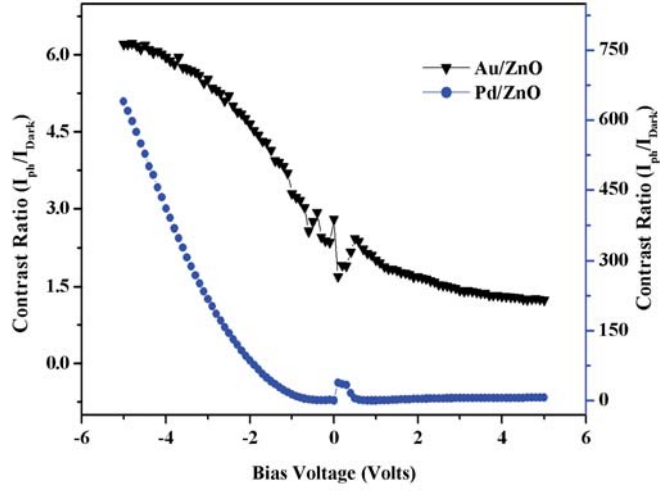
Figure 4.23: Contrast Ratio versus Bias Voltage plot of the Schottky contacts

$$R_0 A = \left(\frac{dJ}{dV}\right)^{-1} \tag{4.18}$$

$$G = \frac{N_e}{N_p} = R\frac{1.24}{\lambda(\mu m)}\frac{1}{\eta} \tag{4.19}$$

where $R_0 A$ is the resistance-area product, at zero bias, λ is the wavelength (in μm), N_e and N_p are the total number of electrons and photons collected per unit time. The values of obtained gain and detectivity of both the Au/ZnO and Pd/ZnO Schottky photo-detectors are 34.5 & 77.18 and 1.23×10^{10} & $1.95 \times 10^{10} cm.Hz^{0.5}/W$, respectively, assuming $\eta = 1$. These experimental results indicate better performance of Pd based UV detector, over the Au based. A possible reason of degradation of the performance of the Au based detector may be due to its being a very effective recombination center in Si substrate and its fast diffusion into the Si substrate during annealing process at 450°C, in the present study. The photo-electrical properties of both the Schottky detectors have been compared and presented in Table 4.2.

75

Table 4.2: PERFORMANCE PARAMETERS FOR UV DETECTION OF Au/ZnO AND Pd/ZnO Schottky DIODES

	Responsivity A/W at -2V bias	Photo-conductive Gain G	Detectivity, at -2V bias mHz$^{0.5}$/W
Au/ZnO	10.16	34.5	1.23×10^{10}
Pd/ZnO	22.72	77.18	1.95×10^{10}

4.4 Conclusion

ZnO thin film has been prepared by RF magnetron sputtering technique. The structural, surface and optical properties of the grown ZnO thin films are reported. The ZnO thin film was subsequently used to fabricate both the Au/ZnO and Pd/ZnO Schottky photo-diodes for UV detection at 365 nm. The results show that the prepared thin film has good crystalline orientation and minimal surface roughness, with an optical bandgap of 3.1 eV. The results confirm deposition of a high quality ZnO thin film by the RF magnetron sputtering process.

I-V and C-V characteristics were evaluated that indicate non-linear behaviour of the diodes for both of the contacts with individual rectification ratio (IF/IR) of 19 and 427, at ±4V, for Au/ZnO and Pd/ZnO Schottky diodes, respectively. Responsivity of these Schottky photo-detectors, at room temperature, on being illuminated with a light of wavelength 365 nm and applied bias of -2 V, were found to be 10.16 and 22.7 A/W, for Au and Pd contacts, respectively.

The detectivity and photoconductive gain of both Au and Pd based Schottky detectors were found to be 1.23 $\times 10^{10}$ & 34.5 and 1.95 $\times 10^{10}$ cm.Hz$^{0.5}$/W & 77.18, respectively, which indicate better performance of Pd based UV detector. The evaluated device parameters indicate Pd/ZnO detector to be superior than the Au/ZnO Schottky detector. The above experimental results can provide a good platform for future researchers to explore low cost UV photo-detectors, operating at room temperature, as an alternate to the existing GaN based UV detectors.

Chapter 5

Design and development of Thin Film Transistors based on ZnO thin film

This chapter presents the simulation, fabrication and characterisation of UV photo-detectors with staggered bottom gate ZnO Thin Film Transistors (TFTs), grown on silicon at room temperature using RF magnetron sputtering process. The static performance of these detectors have been explored by varying the channel lengths (6 μm and 12 μm). The TFT device parameters such as, leakage current, threshold voltage, field-effect mobility and sub-threshold swing are evaluated. The devices were investigated for stability with application of both positive and negative-stress. The fabricated TFTs are further tested for UV detector applications.

5.1 Introduction

ZnO based thin film transistors (TFT) being quite similar to MOSFET devices, both in terms of operation and also the composing layers, has another application

in the emerging field of UV detectors [74].

5.2 Simulation and performance analysis of ZnO Thin Film Transistors

5.2.1 General Introduction of Performance Analysis of ZnO Thin Film Transistors

Simulation study and performance analysis of ZnO Thin Film Transistors (TFTs) have been done. Static performance of the TFTs with different W/L ratios have been evaluated. Channel lengths were varied from 6 μm to 12 μm while keeping the width, W, to be 40 μm. The thickness of both the ZnO channel and the dielectric SiO_2 were varied to observe the corresponding effects on the output and the transfer characteristics of the bottom-gate TFTs. Various electrical and optical parameters, such as ON-OFF current ratio, threshold voltage and field-effect mobility have been obtained.

Three-dimensional (3D) device simulator of VisualTCAD from Cogenda was used to gain insight into the various electrical and optical properties of the ZnO bottom-gate TFTs. Further the TFTs were also investigated under the presence of ultraviolet light. The current-voltage characteristics, under ambient and illumination conditions, were plotted for varying intensities of the UV light. The detectors were also tested for light of different wavelengths in the UV region from 40-400 nm. The simulations confirmed that ZnO TFTs are suitable detectors for ultraviolet light detection in variety of applications.

5.2.2 Simulation Setup

The three-dimensional structure of the thin flim transistor is shown in Fig. 5.1. The drift-diffusion, energy valence, carrier transportation, Poisson's and continuity equations are involved in the device simulation. Drift Diffusion Model
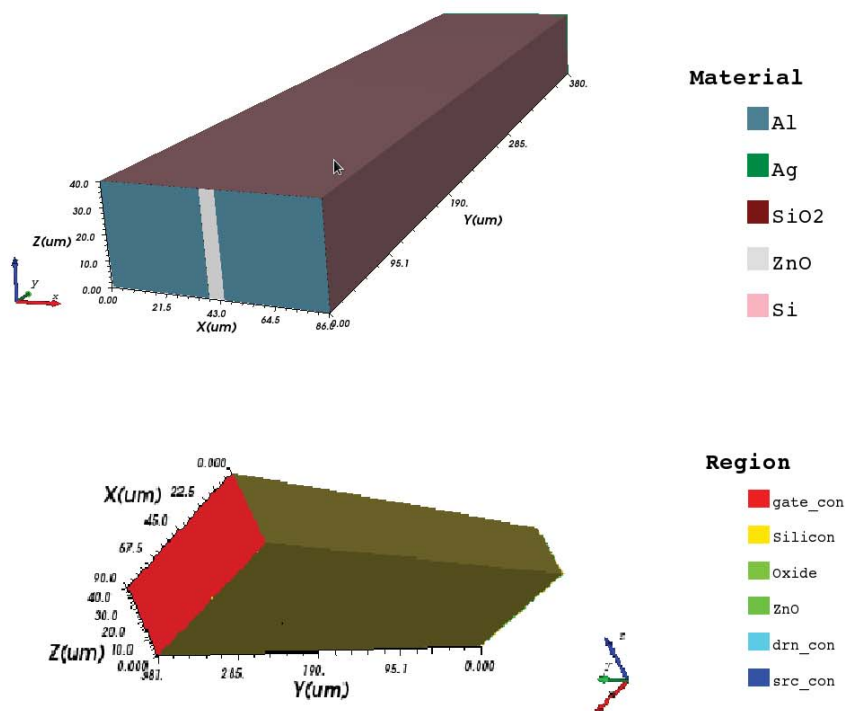
Figure 5.1: Top and bottom view of the simulated bottom gate TFT structure

Level-1 (DDML1) that has been chosen for the simulation, approximates the hydrodynamic model to consider the recombination effects, as under

- Light speed is much faster than carrier speed.

- All the collisions are elastic.

- Band-gap does not change during collisions.

- Carrier temperature equals to lattice temperature and keeps equilibrium.

- The gradient of driving force should keep small.

- Carrier degeneration can be neglected.
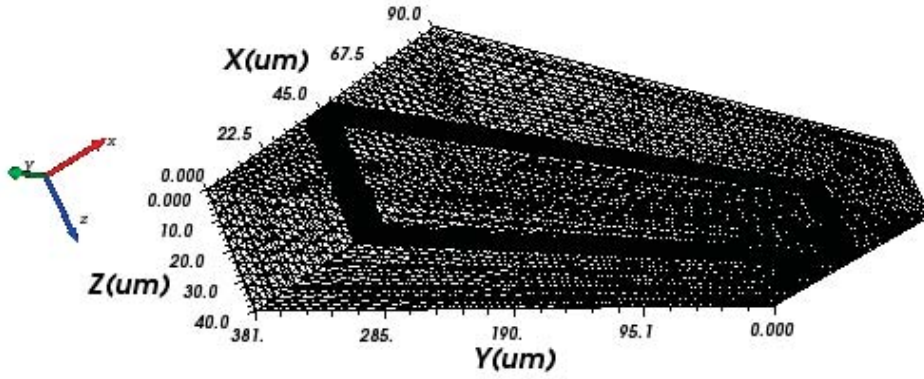
Figure 5.2: 3D mesh view of the simulated bottom gate TFT structure

By substituting DDM into the current density expressions and combining with Poisson's equation, the following basic equations for DDML1 are obtained:

$$\frac{\partial n}{\partial t} = \nabla . \left(\mu_n n \overrightarrow{E_n} + \mu_n \frac{K_b T}{q} \nabla n \right) - \left(U - G \right) \tag{5.1}$$

$$\frac{\partial p}{\partial t} = -\nabla . \left(\mu_p p \overrightarrow{E_p} - \mu_p \frac{K_b T}{q} \nabla p \right) - \left(U - G \right) \tag{5.2}$$

$$\nabla . \epsilon \nabla \psi = -q(p - n + N_D{}^+ - N_A{}^-) \tag{5.3}$$

where, p and n are hole and electron concentrations, $\overrightarrow{E_n}$ and $\overrightarrow{E_p}$ are the effective driving electrical field to electron and hole, U and G are recombination and generation rates for electron and hole respectively, ψ is the electrostatic potential, q is electron charge, $N_D{}^+, N_A{}^-$ are ionized impurity concentrations.

5.2.3   Simulation of Bottom Gate TFTs

Simulation of the bottom-gate ZnO TFT has been done using VisualTCAD 3D simulator from Cogenda, the mesh view of the proposed structure is shown in Fig. 5.2. The device dimensions for the simulated and fabricated TFT structure, are illustrated in Fig. 5.3. Various models are available for simulation studies
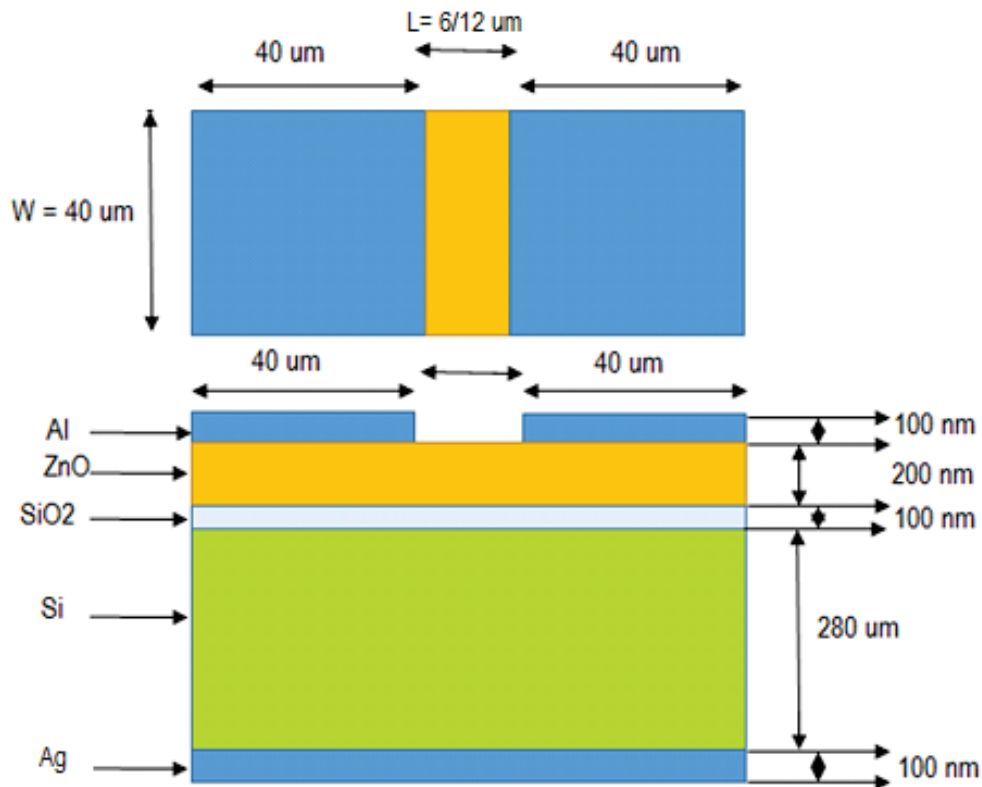
Figure 5.3: Schematic of the bottom gate TFT structure (top and cross-sectional views)

such as, Drift Diffusion, Density gradient, Band structure along with other Mobility models (Bulk, Analytic, Masetti analytic, Phillips, Lomabardi surface, Lucent high field etc.). Drift Diffusion model has been chosen in our study. As all the parameters are not defined in the VisualTCAD library so Mob, Band and Basic models are utilized to define the various parameters of ZnO. Fermi-Dirac model is used for the distribution of carriers. Various electrical and optical parameters such as OFF current, drain current ON-OFF ratio, threshold voltage and

field-effect mobility have been obtained, both under ambient light and UV illumination conditions. The assumed material parameters for simulation of the bottom-gate TFT devices are given in Table 5.1.

Table 5.1: Set of Parameters used for ZnO during VisualTCAD simulation of Bottom gate TFT

Parameters	Values
Bandgap	3.37 eV
Dielectric constant, ϵ_s	8.12
Electron mobility, μ_n	0.015 m²/V.s
Hole mobility, μ_p	0.003 m²/V.s
Effective mass of electron, m_e^*	$0.24 \times m_0$
Effective mass of hole, m_h^*	$0.59 \times m_0$
Electron mobility (μ_n)	1500 cm²/V.s
Electron affinity, ζ	4.35 eV
Work function, ϕ_s	4.45 eV
Effective density of states in the conduction band, N_c	$2.94 \times 10^{24} \mathrm{m}^{-3}$
Effective density of states in the valence band, N_v	$11.36 \times 10^{24} \mathrm{m}^{-3}$
DDML Lifetime for electrons, τ_{n0}	4.19×10^{-6} s
SRH/Drift-diffusion Lifetime for holes, τ_{p0}	6.57×10^{-6} s

5.2.4 Simulation Results

Various electrical and optical parameters, such as ON-OFF current ratio, threshold voltage and field-effect mobility have been obtained. The two important electrical parameters, namely, the threshold voltage (V_T) and the field-effect mobility (μ_{FE}) have been extracted from the transfer characteristics, when the device is operating in the saturation region. The output current is given as

$$I_{D,sat} = \frac{W}{2L} \mu_{FE} C_{OX} (V_{GS} - V_T)^2 \tag{5.4}$$

where C_{OX} is the gate-oxide capacitance per unit area.

The threshold voltage V_T can be evaluated from the output characteristics from the intersection of the linear extrapolation from the I_D versus V_{GS} plot, for lower V_{DS}.

The channel mobility for the ZnO TFTs under consideration here can be determined by various methods. The field-effect mobility μ_{FE}, has been evaluated from the transconductance (g_m) with low V_{DS}, to account for the efficiency of the carrier transport in the ZnO thin film as below

$$\mu_{FE} = \frac{g_m}{C_{OX}\frac{W}{L}V_{DS}} \tag{5.5}$$

5.2.4.1 Electrical Characteristics

The electrical characteristics of the simulated Zno based TFTs have been investigated in this section. First the effect of thickness variation of the ZnO channel layer and the oxide layer of SiO_2 was examined. It was found that as the oxide layer thickness is doubled, the output currents decrease by half. No effect of ZnO layer thickness was observed on either of the electrical characteristics.
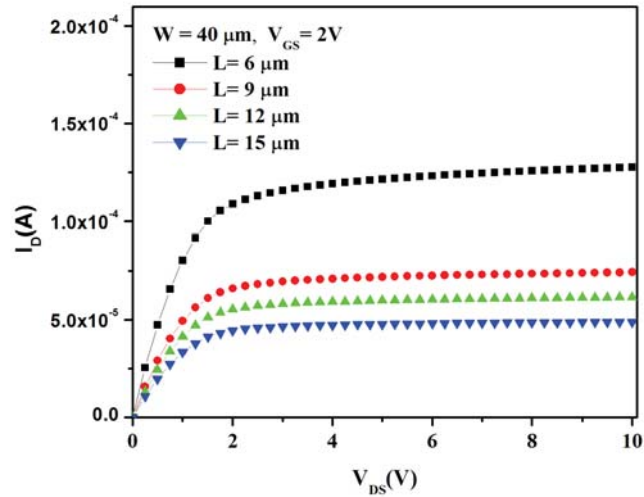
Figure 5.4: Output characteristics of Bottom gate TFT for various channel lengths

The output and the transfer characteristics for the TFT for W=40 μm and varying channel lengths of L = 6, 9, 12 & 15 μm are as shown in Fig. 5.4 & Fig. 5.5 which clearly show the currents increase linearly for lower V_{DS} (ohmic region)
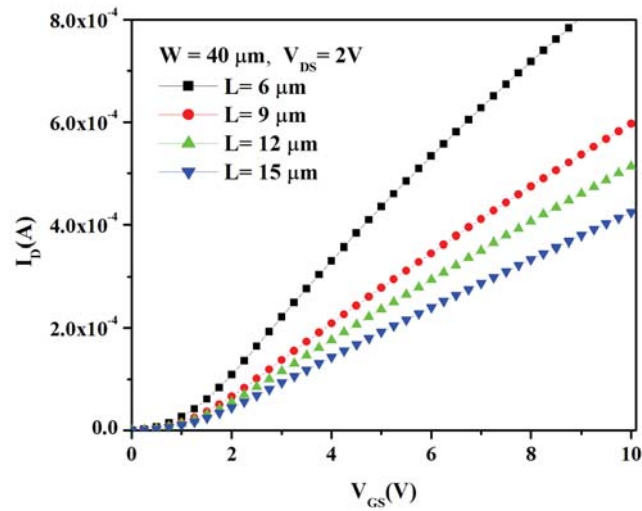
Figure 5.5: Transfer Characteristics of Bottom gate TFT for for various channel lengths

and saturates for higher values of V_{DS} (Constant current region). The TFT behaviour is evident from these curves.

5.2.4.2 UV Characteristics

The intensities and wavelength of the UV light have been varied to study their effects on the electrical characteristics of the ZnO TFTs.

Figure 5.6: Output Characteristics of Bottom gate TFT for different intensity of UV light at $V_{GS} = 2V$
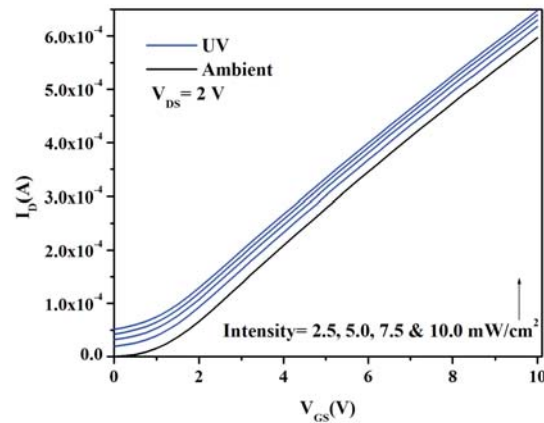
Figure 5.7: Transfer Characteristics of Bottom gate TFT for different intensity of UV light at V_{DS} = 2V

Intensity variations

The effect of UV light on the output and the transfer characteristics for the TFT has been investigated for channel width W=40 μm and length of L = 9 μm, as the UV illumination intensity is varied from 25, 50, 75 & 100 mW/cm^2, are as shown in Figs. 5.6 & 5.7. The output currents show a significant increase of 2-4 times as compared to the ambient currents.

Wavelength variations

The effect of UV light on the output and the transfer characteristics for the TFT has been investigated for channel width W=40 μm and length of L = 9 μm, as the UV illumination wavelength is varied from 100, 200 & 300 nm, are as shown in Fig. 5.8 & Fig. 5.9. The output currents show a significant increase of 2-4 times as compared to the ambient currents. The TFT behaviour under UV illumination

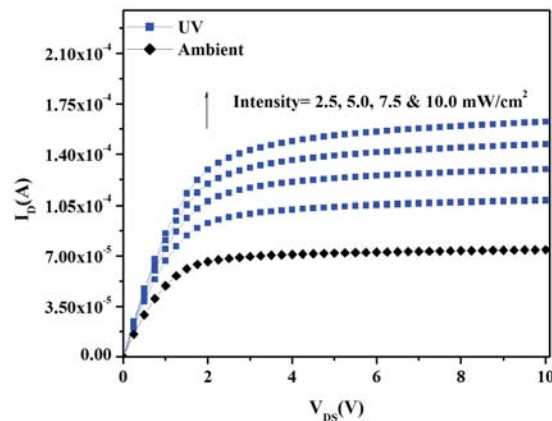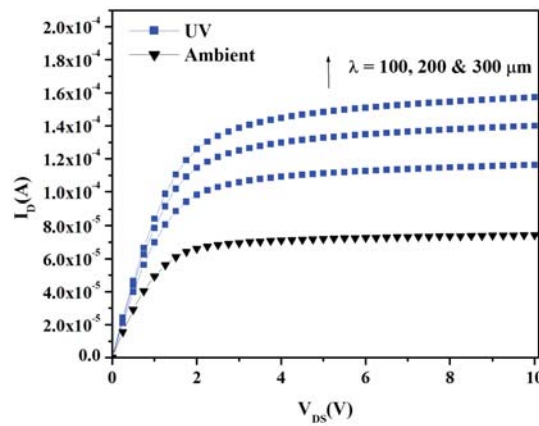
Figure 5.8: Output Characteristics of Bottom gate TFT for different wavelengths at V_{GS} = 2V
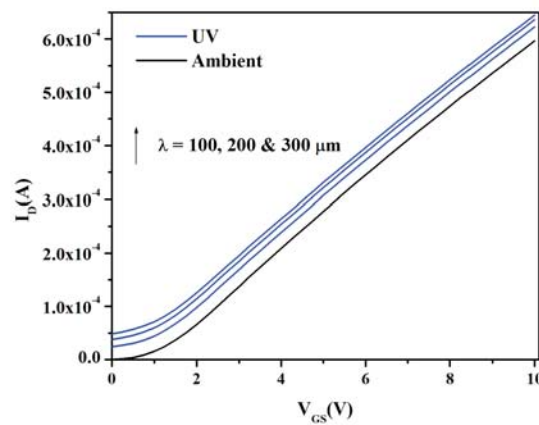
Figure 5.9: Transfer Characteristics of Bottom gate TFT for different wavelengths at V_{DS} = 2V

shows that it is suitable for UV applications.

5.3 EXPERIMENTAL DETAILS

5.3.1 Fabrication of Bottom Gate TFTs

The bottom gate ZnO TFT was fabricated in 5 processing steps. Initially, the surface of a 4 inch Si (100) wafer with a thickness of 380 μm and resistivity of 1-10 Ω-cm., was cleaned with standard RCA-1 method (10 minutes boiling in NH_3 + H_2O_2 + $6H_2O$) followed by RCA-2 (10 minutes in HCl + H_2O_2 + $6H_2O$ at 60°C). These processes cleared its surface of the organic and metallic contaminants. SiO_2 layer, 100 nm thick, was grown by dry oxidation, to act as a gate insulator layer (5.16). The sample was then cleaned with acetone, IPA (C_3H_8O) and DI water sequentially, followed by soft baking for 5 minutes, to prepare it for lithography. The top-side of the wafer with SiO_2 layer was immediately coated with a positive photo-resist S1813 (Shipley) with spin coating technique at 4000 rpm. Mask preparation for patterning the different layers was done with opto-lithographic process of mask writer Heidelberg Instruments (Model μ PG-501). Transfer of

Figure 5.10: Mask writer

the mask on the wafer was done in vacuum with a UV dosage of 45 mJ/cm^2 for 7 seconds, using SUSS MicroTec (Model MJB4) mask aligner, with a resolution of 0.5μm. Each of the patterned layers were developed using MF26A for 24 sec-

onds. A nano-crystalline ZnO film was grown on this SiO_2 layer with a thickness 200 nm, as a channel layer, by RF sputtering process, at room temperature in 22 minutes with the following process parameters: a base vacuum of 5.0×10^{-6}T, pressure of 4.1×10^{-6}T, RF power of 100 Watts, ZnO target (iTASCO) of 99.99% purity and target to substrate distance of 7.5 cm. The ZnO film step height was measured with the Dektak XT surface profiler, as shown in 5.11.
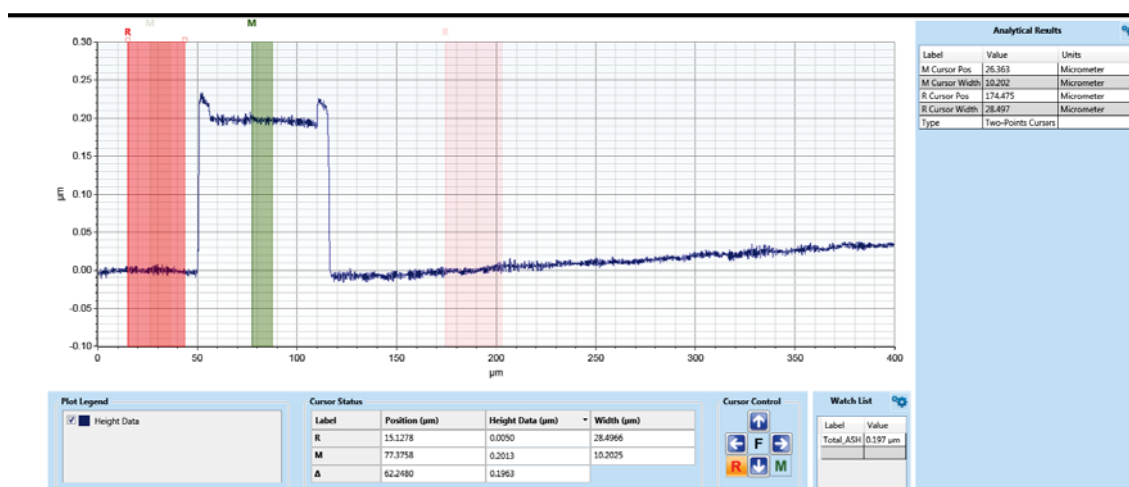
Figure 5.11: ZnO layer thickness measurement done with DEKTAK

Lift off process was done at the chemical wet bench (FELCON), to remove the unwanted ZnO. Annealing was done at 450° in oxygen for 1 hour to achieve the surface uniformity and upgrade the stoichiometry of zinc and oxygen. The same process of mask deposition was done to prepare the wafer for deposition of aluminium to act as source and drain electrodes, for two different channel lengths of 6 μm and 12 μm, both having a width of 40 μm. Finally, wet-etching was performed with buffered HF to remove SiO_2 layer on the back side of the wafer before deposition of silver (Ag), thickness 140 nm, with DC sputtering to act as gate electrode. The wet bench setup is as shown in Fig. 5.12. Rapid Thermal Annealing (RTA) at 350°C in argon for 1 minute was done to improve the electrical characteristics of the fabricated device.

The corresponding photo-image of the fabrication process steps of the ZnO thin

Figure 5.12: Wet Bench setup

film on SiO_2 /Si substrate is shown in Fig. 5.13.

Semiconductor Parameter Analyzer (Agilent B1500A), with probe station, was used to perform the electrical characteristization of the TFTs. X-ray diffractometer (XRD) (Rigaku, Smartlab-3KW) provided valuable information concerning the micro-structural properties of the ZnO thin film. Characterization with Atomic Force Microscopy (AFM) (Bruker, Multimode8-HR)and Scanning Electron Microscope (SEM) (Nova Nano FE-SEM, 450) was done to find the surface morphology. The transmittance/ absorption of the film was measured with UV-VIS-NIR Spectrometer (Shimadzu MPC3600). UV lamp with a wavelength of 365 nm and an input optical intensity of 1.28 mW/cm^2 was used to find the photo-response of the TFTs. The transfer characteristics of the fabricated device were further investigated for their behaviour under different bias stress conditions, at room temperature, with the Semiconductor Parameter Analyzer.

Bottom Gate TFT: Fabrication Process

Step 1: Patterned ZnO on SiO$_2$ layer by RF Sputtering

Step 2: Patterned Source/ Drain Al contact on ZnO
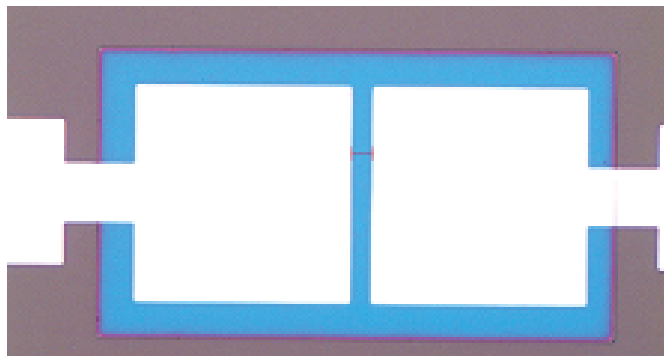
Step 3: Bottom Gate Ag Contact
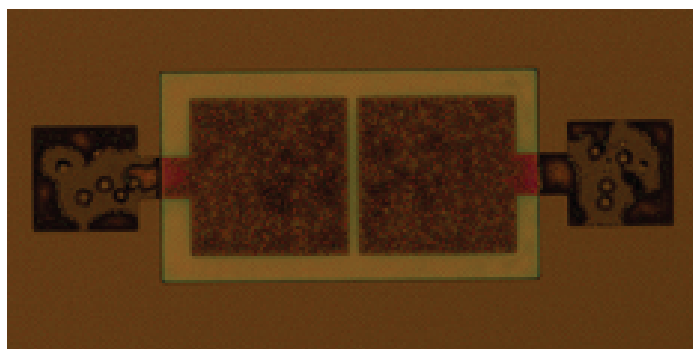
Figure 5.13: Schematic of the bottom gate TFT fabrication process
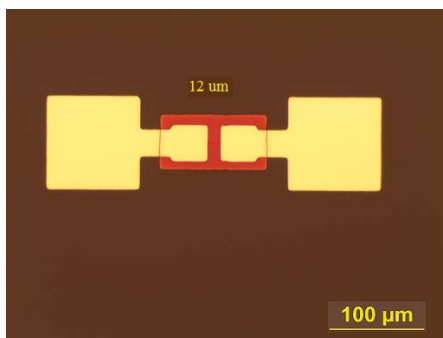
Figure 5.14: Microscope image of the bottom gate fabricated TFT with L =12 μm
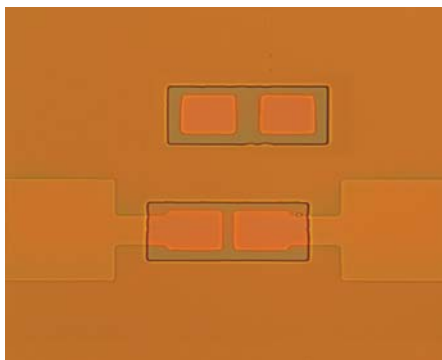
Figure 5.15: Microscope images of the fabricated TFT
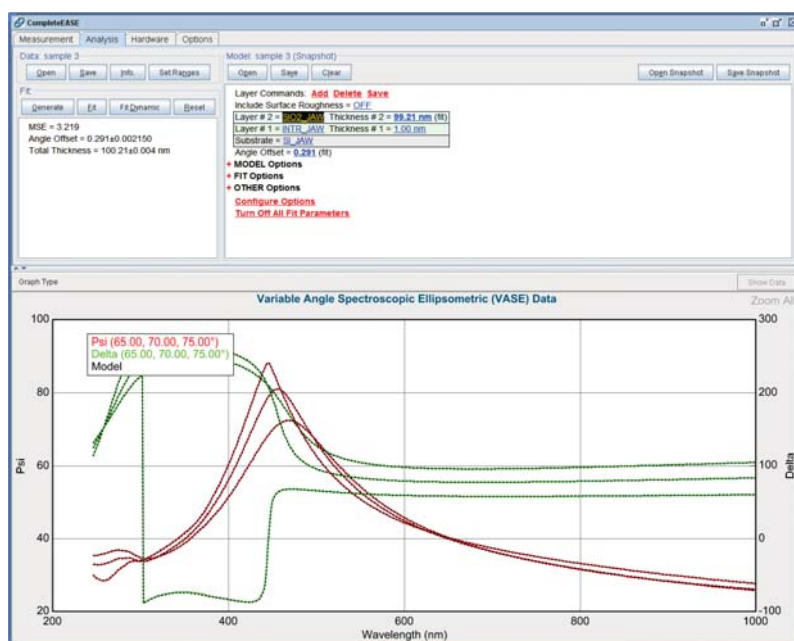
Figure 5.16: SiO$_2$ layer thickness measurement done with ellipsometer

5.4   RESULTS AND DISCUSSION

5.4.1   ZnO Thin Film Characterisation

The detailed structural and optical characteristics of the ZnO thin film has been described in [103], however some of the important properties are discussed here. The XRD spectra of the ZnO thin film deposited on the silicon substrate is shown in the Fig. 5.17, that shows a strong diffraction peak at $2\theta= 34.4°$ and also a weak diffraction peak at $2\theta= 62.8°$. The result confirms the deposited ZnO thin film is polycrystalline with hexagonal wurtzite structure and possesses (002) c-axis orientation.
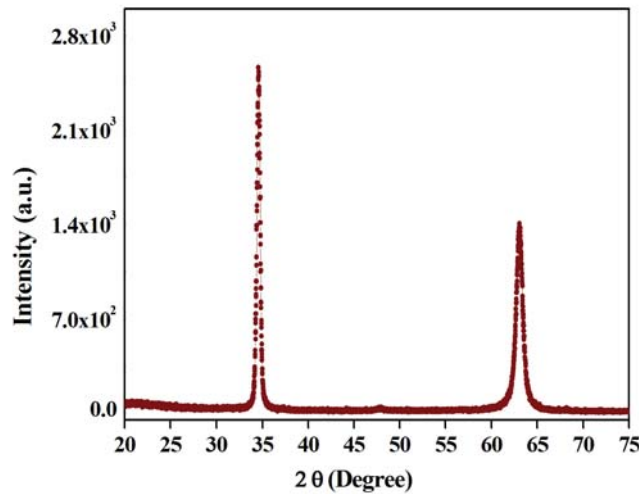
Figure 5.17: XRD pattern of ZnO thin film

The optical transmittance of the deposited ZnO thin film is shown in Fig. 5.18 for the wavelength ranging from 300 nm to 1100 nm. The obtained transmittance in excess of 80% for the wavelength for the visible range (400-700 nm) permits us to fabricate the bottom gate TFT based on the ZnO channel layer to act as a UV (100 - 400 nm) detector.
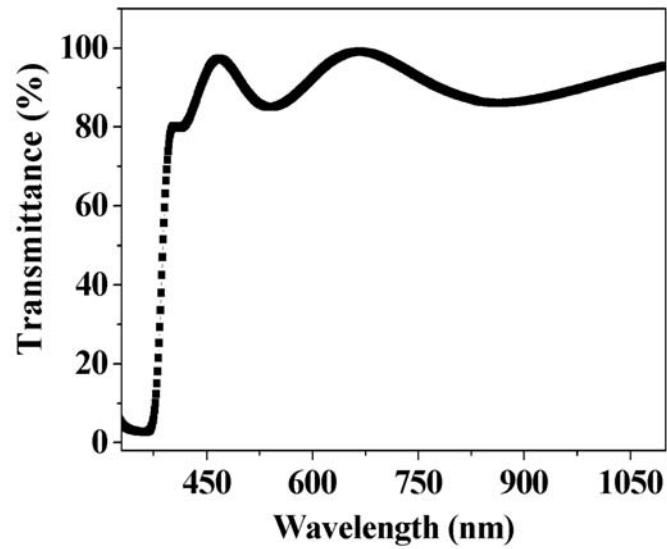
Figure 5.18: Transmittance of the ZnO thin film

5.4.2 TFT performance

The output characteristics of the fabricated bottom gate TFT detector are shown in Fig. 5.19 for the two different channel lengths, L, of 6 and 12 μm. From the
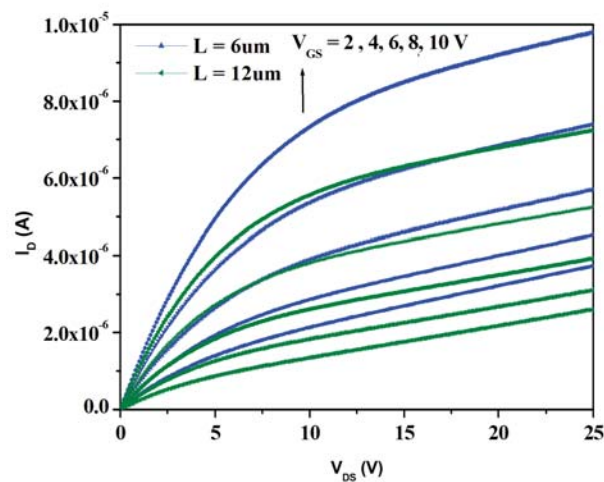
Figure 5.19: Output characteristics for the two different channel lengths

plots, we see that the drain current, I_D increases as the drain voltage, V_{DS}, is increased from 0 to 25 Volts. The curves plotted for different positive gate bias

in Fig. 5.19 clearly show the device to be operating in the enhancement mode, achieving saturation at high values of V_{DS}. The gate leakage currents are shown in Fig. 5.20.
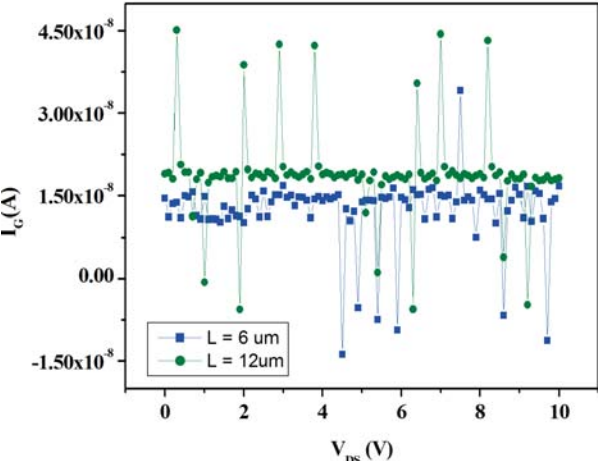
Figure 5.20: The gate leakage current for the two different channel lengths of the fabricated TFTs
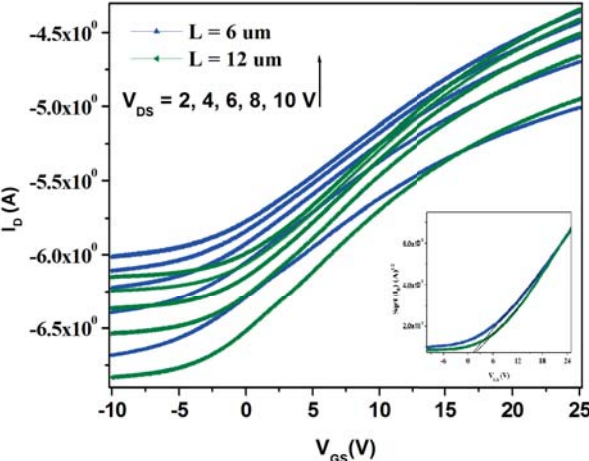
Figure 5.21: Transfer characteristics for the two different channel lengths of the fabricated TFTs

The transfer characteristics for the device operating in the saturation region/ mode, for different applied V_{DS} of 2, 4, 6, 8 & 10 Volts, are shown in Fig. 5.21.

Both the output and transfer characteristics show a marked increase in the output currents, as the channel length, L, is decreased from 12 μm to 6 μm. The minimum and maximum values of the drain current I_D depends upon the gate leakage current along with the system noise of the measuring device and the capacitive injection due to the applied field in the ZnO channel, respectively. The evaluated ON-OFF ratios, for the TFTs of L = 6 μm and L = 12 μm, are of the order of 4 and 5, that suggest that the fabricated TFTs possess good switching characteristics for electronic applications.

The two important parameters, namely, the threshold voltage V_T and the mobility, have been extracted from the transfer characteristics. These have been evaluated from the curves when the devices are operating in the saturation region and the output current follows the relation, as below

$$I_{D,sat} = \frac{W}{2L} \mu_{FE} C_{OX} (V_{GS} - V_T)^2 \qquad (5.6)$$

where C_{OX} is the capacitance per unit area. The threshold voltage V_T can be evaluated from the output characteristics as the intersection of the linear extrapolation either in the $\sqrt{I_D}$ versus V_{GS} plot, for higher V_{DS}, or from the I_D versus V_{GS} plot, for lower V_{DS}. The threshold voltage have been extracted from the transfer characteristics for lower V_{DS} in this paper. From the output and the transfer characteristics, it is observed that as the channel length of the TFT is decreased the drain current increases.

As in [72], the mobility characteristics being non-ideal as compared to the MOSFET structures, the channel mobility can be determined in various ways, for the ZnO TFTs under consideration here. We have evaluated the field-effect mobility μ_{FE}, the obtained transconductance values, g_m, with low V_{DS}, to account for the efficiency of the carrier transport in the ZnO thin film [4], as below

$$\mu_{FE} = \frac{\left(\frac{d\sqrt{I_D}}{dV_{GS}}\right)^2}{\frac{1}{2}C_{OX}\frac{W}{L}} \tag{5.7}$$

A comparison of the simulated and fabricated normalised transfer characteris-
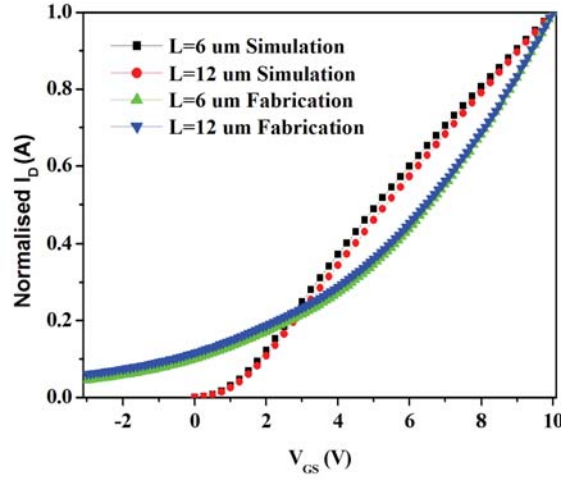
Figure 5.22: Comparison of the simulated and fabricated normalised transfer characteristics for the two different channel lengths

tics of the TFTs for the two different channel lengths is shown in Fig. 5.22. The difference in the simulation and fabrication results may be due to defects in the ZnO channel, contact resistances at the source and drain terminals and also the imperfections in the ZnO-SiO$_2$ layer interface. The evaluated values for these parameters are shown in Table 5.2.

Table 5.2: Extracted parameters

Channel Length	Threshold Voltage, V_T (V)		Mobility, μ_{FE} (cm^2/V.s)	
	Fabrication	Simulation	Fabrication	Simulation
6 µm	1.18	0.77	0.62	0.47
12 µm	2.33	1.62	1.61	1.20

From Table 5.2, higher values of the threshold values, V_T, have been obtained for the fabrication results, as compared to the simulation results. The inconsistency in the results may be due to the ZnO-SiO$_2$ layer interface defects. The ex-

perimentally obtained values of the field-effect mobility, though still at the lower end of the reported values (comparable to those obtained in [17]) but are better than those obtained, as in [74]. The experimental results indicate good quality of the fabricated ZnO thin film with low scattering effects.

Another important parameter to evaluate the TFT is its sub-threshold swing, S that reflects its speed of operation and power consumption. It conveys the information regarding the change in gate voltage required for a decade change in drain current in the sub-threshold region ($V_{GS} < V_T$). The sub-threshold swing, S, is the inverse of the maximum slope of transfer characteristics that is essential for the gate voltage V_G to increase the drain current by a decade

$$S = \left(\frac{d\log(I_D)}{dV_{GS}} \bigg|_{max} \right)^{-1} \tag{5.8}$$

Valuable information regarding the density of the trap states can also be extracted from this parameter from the equation, as below [104]

$$N_t = \left(\frac{S\log(e)}{\frac{kT}{q}} - 1 \right) \frac{C_{gi}}{q} \tag{5.9}$$

where C_{gi} is the gate insulator capacitance per unit area.

We can also evaluate the minimum gate voltage that is required to turn on a TFT from its OFF state, as under [105]

$$\Delta V_{GS,min} = S . \frac{I_{ON}}{I_{OFF}} \tag{5.10}$$

The obtained values of sub-threshold swing, S, of the TFT of W = 40μm and L = 6 μm & L = 12 μm are 13.5 and 12.8 V/dec, respectively. It is observed that the sub-threshold swing becomes better as the channel length increases. These values are better than the reported values [3, 106, 107].

97

5.4.3 Device Stability

The active layer of the TFT has trapped charges, due to impurities, between the fermi level and the minimum energy level of the conduction band, whose distribution alters with the application of gate bias stress. Both the positive and negative stress of ±8 Volts were induced on the fabricated device for different durations of 5 minutes and 10 minutes. It was observed that as the stress duration is increased from 5 minutes to 10 minutes, a perceptible shift in subthreshold slope results, along with a change in the threshold voltage. Also, the transfer characteristics of the TFTs got shifted on application of both positive and negative-stress but was mostly deteriorated by the negative stress. This behaviour is in agreement to the reported logarithmic time dependence [75] and indicates that the charge trapping process diminishes because of creation or removal of defects, on being subjected to stress.
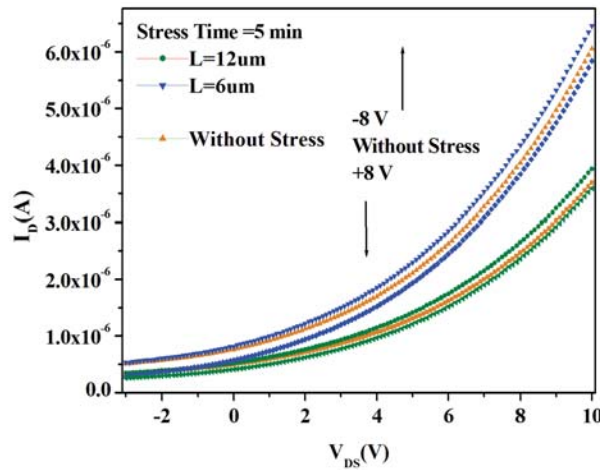
Figure 5.23: Stress test transfer characteristics of the TFTs with L = 6 μm

Figs. 5.23 and 5.24 show the experimental results for the transfer characteristics under different gate bias stress of ±8 Volts for 5 and 10 minutes on the fabricated bottom-gate ZnO TFTs, at room temperature. The unstable nature of the
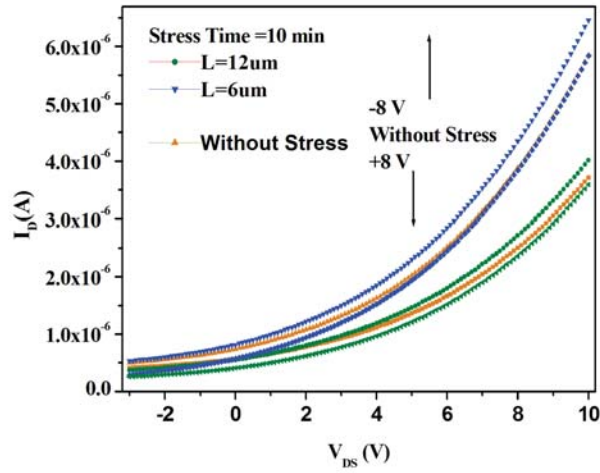
Figure 5.24: Stress test transfer characteristics of the TFTs with L = 12 μm

TFT characteristics may be due to the presence of high grain boundary concentration of the sputtered ZnO thin film, the ZnO-SiO$_2$ interface layer defects or a combination of both of these.

5.4.4   UV Detection
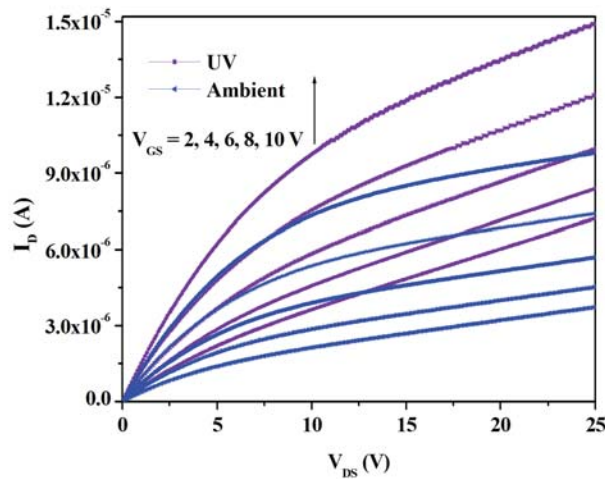
Figure 5.25: Output characteristics under UV light for the TFT with L = 6 μm

The UV detector and photo-response of the ZnO thin film based Schottky contacts have already been described by other researchers elsewhere [65, 80]. The
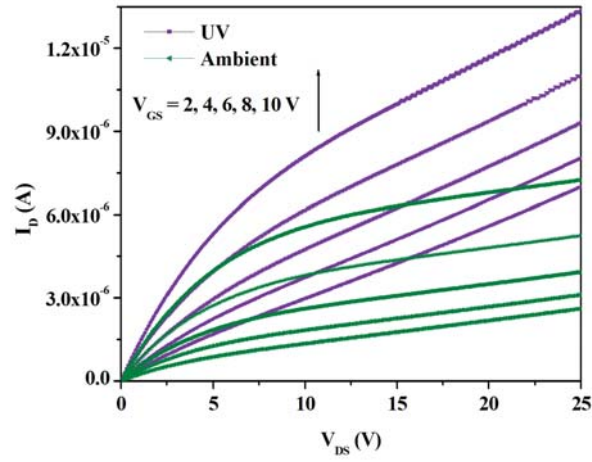
Figure 5.26: Output characteristics under UV light for the TFT with L = 12 μm

photo-detection mechanism of these TFTs is due to the effect of oxygen adsorption and desorption by the ZnO thin film surface. Under dark condition, oxygen is adsorbed by capturing a free electron from the surface of the ZnO thin film, as reported in our work [103].
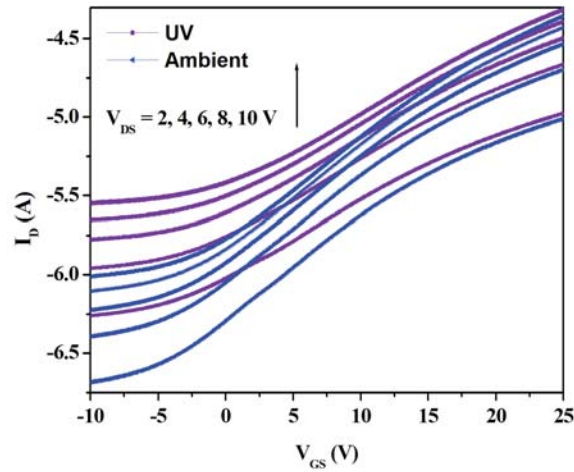
Figure 5.27: Transfer characteristics under UV light for the TFT with L = 6 μm

The output and transfer characteristics for the bottom gate TFT on illumination with the UV light of intensity of wavelength 365 nm 1.28 mW/ cm^2, are plotted in Figs. 5.25, 5.26, 5.27 and 5.28 with symmetrical curves indicating a good
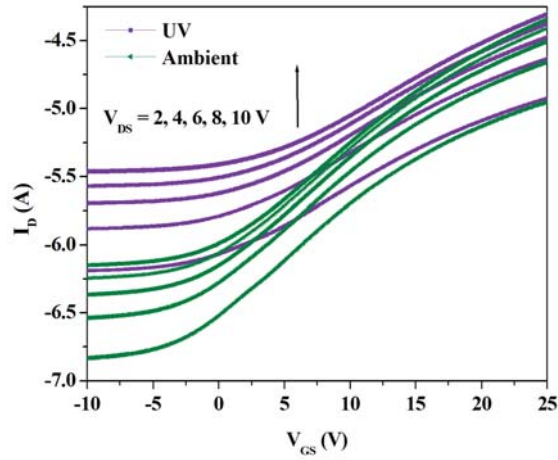
Figure 5.28: Transfer characteristics under UV light for the TFT with L = 12 μm

quality ohmic contact between the ZnO thin film and the electrodes. Compared with the values reported by others [106], the obtained low photo-response (approx. 1.5 times) of the fabricated TFTs, is possibly due to low operating voltages and possible electron-hole pair recombinations. The marked increase in the observed response of the TFT on illumination with the UV light of wavelength 365 nm indicates that the device can be used for UV detection. Fig. 5.29 shows the variation of output characteristics under different applied UV power. It was observed that the drain current increases by almost 50% under UV illumination at an applied gate voltage of +10 V and V_{DS} = 25V under UV power of 4.3 mW/cm^2. Increasing the UV powers above this value does not generate additional carriers thereby producing a negligible effect on these characteristics.
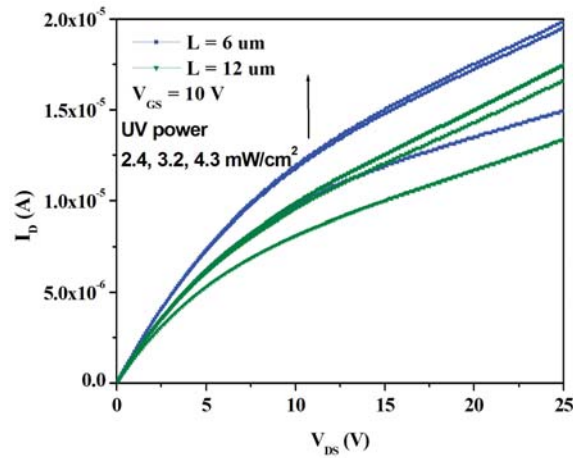
Figure 5.29: UV power variation on the output characteristics for the two different channel lengths

5.5 Conclusion

Bottom-gate ZnO Thin Film Transistors of two different channel lengths, 6 μm and 12 μm, were fabricated on silicon substrate, at room temperature, using RF magnetron sputtering technique, after conducting detailed simulation studies. The ON/OFF ratio obtained are of the order of 3. Leakage currents in the nano-ampere range and mobilities of 0.62 and 1.61 ($cm^2/V.s$) have been obtained for L = 6 μm and 12 μm, respectively. The response of the fabricated device was verified with the simulation results that are within ±10% range for lower voltages and match nicely as the transistor moves down into the saturation region. From the TFT characteristics, it is observed that as the channel length of the TFT is decreased the drain current increases. The detector was also tested for device stability with the transfer characteristics of the TFTs which got shifted on application of both positive and negative-stress, mostly deteriorated by the negative stress. Other important device parameters were compared with the simulation results and found to be in good agreement. The fabricated TFTs were subsequently tested for UV detection applications, with variation of UV power. The TFTs exhibit a high photo-response with increase of about 50% in the output current.

Chapter 6

Conclusion and future Work

6.1   Conclusion

Zinc Oxide thin film based Schottky Diodes and TFTs were designed and fabricated. Their application as UV Detectors was demonstrated. Before actual fabrication, simulation studies were undertaken with various software tools to optimize the device characteristics and improve the performance. ZnO based Schottky diodes were evaluated with different types of metal contacts, such as Gold (Au), Platinum (Pt) and Palladium (Pd) under different temperature conditions, doping concentrations and channel thickness. The variation of responsivity as a function of wavelength have been simulated for different thickness and doping concentrations. Effect of temperature on current-voltage characteristics of Pt/ZnO Schottky photodiode has been studied. Temperature dependency of ideality factor and barrier height for Pt/ZnO Schottky photodiode has also been analyzed.

 Further their UV responses were investigated with various performance parameters such as, contrast ratio, responsivity, photo-conductive gain and detectivity to extract the working performance of these Schottky photo-diodes.

Simulations studies were also carried out to evaluate the optimized parameters for the bottom-gate TFTs, with varying channel lengths. Simulation and performance analysis of ZnO bottom gate TFTs was done to plot the output and transfer characteristic curves for different W/L ratios. Effect of UV light of different intensities and wavelengths was investigated on current-voltage characteristics. The simulated devices were found to exhibit suitable photo-response for UV detection applications.

After optimization of electrical and optical properties of both Schottky photo-diodes (PD) and Thin Film Transistors (TFTs), the actual fabrication was carried out to validate the simulation results. The important parameters of both devices observed from the fabrication results as follows:

Schottky Diodes

a. ZnO thin film was prepared by RF magnetron sputtering technique.

b. Characterization techniques, like Atomic Force Microscopy (AFM), Scanning Electron Microscopy (SEM), X-ray Diffraction (XRD) and UV visible spectroscopy were used to analyse the structural and optical properties of the grown film.

c. It is observed that the prepared thin film has good crystalline orientation and minimal surface roughness, with an optical band-gap of 3.1 eV.

d. Subsequently, Au/ZnO and Pd/ZnO based Schottky photo-diodes were fabricated.

e. From I-V and C-V experimental results both the devices indicate non-linear behaviour with rectification ratio (IF/IR) of 19 and 427, at ±4 V, for Au/ZnO and Pd/ZnO Schottky diodes, respectively.

f. Both of the fabricated diodes show good response to UV light and the responsivities were found to be 10.16 and 22.7 A/W, for Au and Pd contacts, respectively.

g. The detectivity and photoconductive gain of both Au and Pd based Schottky detectors were found to be 1.23 $\times 10^{10}$ & 34.5 and 1.95 $\times 10^{10}$.Hz$^{0.5}$/W & 77.18, respectively, which indicate better performance of Pd based UV detector.

h. The above experimental results can provide a good platform for future researchers to explore low cost UV photo-detectors, operating at room temperature, as an alternate to the existing GaN based UV detectors.

Thin Film Transistors

a. After conducting detailed simulation studies, fabrication of bottom-gate ZnO Thin Film Transistors with two different channel lengths, 6 μm and 12 μm, was undertaken, on silicon substrate, at room temperature, using RF magnetron sputtering technique.

b. The static performances of these devices have been explored by varying the channel lengths. The devices show low leakage currents of 14 & 19 nA and exhibit superior electrical characteristics with an ON-OFF ratio of the order of 3.

c. Threshold voltages of 1.35 & 1.93 Volts and sub-threshold swings of 8.896 & 10.67 mV/dec have been obtained for the TFTs with L = 6 μm and L = 12 μm, respectively.

d. Mobilities of 0.682 and 0.881 (cm^2/V.s) have been obtained for TFTs with L = 6 μm and 12 μm, respectively.

e. The response of the fabricated device was verified with the simulation results that were within ±10% range for lower voltages and match nicely as the transistor moves down into the saturation region.

f. The devices were also tested for their stability.

g. The fabricated prototype TFTs were also successfully demonstrated for UV detection applications.

6.2   Future work

The future of ZnO thin film based nano-structures will be fully realized only when a stable p-type doping will be possible. Only then fully functional devices will be achieved and the optoelectronic and electronic applications will be thoroughly accomplished for commercial applications. The present hetero-structures have problems of lattice mismatch between the ZnO and SiO$_2$ substrate, thereby inducing defects and deterioration in the electrical performance.
Measurements still need to be done for the

- the radiation hardness of the fabricated devices is to be investigated for space applications.

- wavelength dependent sensitivity and noise analysis.

- gas sensing and bio-sensing for bio-medical applications and environmental studies.

Bibliography

[1] Z. L. Wang, "Zinc oxide nanostructures: growth, properties and applications," p. R829R858, Jun 2004. [Online]. Available: http://dx.doi.org/10.1088/0953-8984/16/25/R01

[2] Ü. Özgür, Y. I. Alivov, C. Liu, A. Teke, M. A. Reshchikov, S. Doğan, V. Avrutin, S.-J. Cho, and H. Morkoç, "A comprehensive review of zno materials and devices," p. 41301, Aug 2005. [Online]. Available: http://dx.doi.org/10.1063/1.1992666

[3] R.-J. Lyu, H.-C. Lin, and T.-Y. Huang, "Fabrication and Characterization of Film Profile Engineered ZnO TFTs With Discrete Gates," *IEEE J. Electron Devices Soc.*, vol. 3, no. 3, pp. 260–266, May 2015.

[4] E. Fortunato, P. Barquinha, and R. Martins, "Oxide Semiconductor Thin-Film Transistors: A Review of Recent Advances," vol. 24, no. 22, pp. 2945–2986, May 2012.

[5] T. P. Chow and R. Tyagi, "Wide bandgap compound semiconductors for superior high-voltage unipolar power devices," *IEEE Transactions on Electron Devices*, vol. 41, no. 8, pp. 1481–1483, Aug 1994.

[6] U. Ozgur, Y. I. Alivov, C. Liu, A. Teke, and M. A. Reshchikov., "A comprehensive review of ZnO materials and devices." *J. Appl. Phys.*, vol. 98, no. 4, p. 041301, 2005.

[7] S. Adachi, "Properties of group iv, iii-v, and ii-vi semiconductors. 2005."

[8] D. R. Lide, *Hdbk of Chemistry & Physics 73rd Edition*. CRC, 1992, vol. 73.

[9] D. C. Look, B. Claflin, Y. I. Alivov, and S.-J. Park, "The future of zno light emitters," *physica status solidi (a)*, vol. 201, no. 10, pp. 2203–2212, 2004.

[10] O. Lopatiuk, W. Burdett, L. Chernyak, K. Ip, Y. Heo, D. Norton, S. Pearton, B. Hertog, P. Chow, and A. Osinsky, "Minority carrier transport in p-type zn 0.9 mg 0.1 o doped with phosphorus," *Applied Physics Letters*, vol. 86, no. 1, p. 012105, 2005.

[11] S. E. Harrison, "Conductivity and hall effect of zno at low temperatures," *Physical Review*, vol. 93, no. 1, p. 52, 1954.

[12] K. Hagemark, "Defect structure of zn-doped zno," *Journal of Solid State Chemistry*, vol. 16, no. 3-4, pp. 293–299, 1976.

[13] H. Morkoç and Ü. Özgür, "Optical properties," *Zinc Oxide: Fundamentals, Materials and Device Technology*, pp. 131–244, 2009.

[14] A. Janotti and C. G. Van de Walle, "Hydrogen multicentre bonds," *Nature materials*, vol. 6, no. 1, p. 44, 2007.

[15] S. Fonash, "Solar cell device physics academic," *New York*, 1981.

[16] M. Tyagi, "Physics of schottky barrier junctions," in *Metal-Semiconductor Schottky Barrier Junctions and Their Applications*. Springer, 1984, pp. 1–60.

[17] S. Singh and P. Chakrabarti, "Simulation, Fabrication and Characterization of ZnO Based Thin Film Transistors Grown by Radio Frequency Magnetron Sputtering," *J. Nanosci. Nanotechnol.*, vol. 12, no. 3, pp. 1880–1885, Mar. 2012.

[18] L. J. Brillson and Y. Lu, "ZnO Schottky barriers and Ohmic contacts," *J. Appl. Phys.*, vol. 109, no. 12, p. 121301, Jun. 2011.

[19] J.-D. Hwang, C.-Y. Kung, and Y.-L. Lin, "Non-Surface-Treated Au/ZnO Schottky Diodes Using Pre-Annealed Hydrothermal or Sol-Gel Seed Layer," *IEEE Trans. Nanotechnol.*, vol. 12, no. 1, pp. 35–39, Jan. 2013.

[20] K. Liu, M. Sakurai, and M. Aono, "ZnO-Based Ultraviolet Photodetectors," *Sensors*, vol. 10, no. 9, pp. 8604–8634, Sep. 2010.

[21] H. C. Chen, M. J. Chen, Y. H. Huang, W. C. Sun, W. C. Li, J. R. Yang, H. Kuan, and M. Shiojiri, "White-Light Electroluminescence From n-ZnO/p-GaN Heterojunction Light-Emitting Diodes at Reverse Breakdown Bias," *IEEE Trans. Electron Devices*, vol. 58, no. 11, pp. 3970–3975, Nov. 2011.

[22] W.-C. Liu, H.-J. Pan, H.-I. Chen, K.-W. Lin, S.-Y. Cheng, and K.-H. Yu, "Hydrogen-sensitive characteristics of a novel Pd/InP MOS Schottky diode hydrogen sensor," *IEEE Trans. Electron Devices*, vol. 48, no. 9, pp. 1938–1944, Sep. 2001.

[23] M. Wei, A. Avila, I. Rivera, M. Baghelani, and J. Wang, "ZnO on nickel RF micromechanical resonators for monolithic wireless communication applications." *J. Micromech. Microeng.*, vol. 27, no. 5, p. 055006, Mar. 2017.

[24] C. Periasamy and P. Chakrabarti, "Time-dependent degradation of Pt/ZnO nanoneedle rectifying contact based piezoelectric nanogenerator," *J. Appl. Phys.*, vol. 109, no. 5, p. 054306, Mar. 2011.

[25] M. Willander, *Zinc Oxide Nanostructures: Advances and Applications*. Pan Stanford Publishing, 2014.

[26] M. Sahal, B. Hartiti, A. Ridah, M. Mollar, and B. Mari, "Structural, electrical and optical properties of zno thin films deposited by sol–gel method," *Microelectronics Journal*, vol. 39, no. 12, pp. 1425–1428, 2008.

[27] B. Postels, M. Kreye, H.-H. Wehmann, A. Bakin, N. Boukos, A. Travlos, and A. Waag, "Selective growth of zno nanorods in aqueous solution," *Superlattices and Microstructures*, vol. 42, no. 1, pp. 425–430, 2007.

[28] L. Vayssieres, "Growth of arrayed nanorods and nanowires of zno from aqueous solutions," *Advanced Materials*, vol. 15, no. 5, pp. 464–466, 2003.

[29] A. Wagner, A. Behrends, A. Waag, and A. Bakin, "Two step deposition method with a high growth rate for zno nanowire arrays and its application in photovoltaics," *Thin Solid Films*, vol. 520, no. 14, pp. 4637–4641, 2012.

[30] B. Postels, A. Bakin, H.-H. Wehmann, M. Suleiman, T. Weimann, P. Hinze, and A. Waag, "Electrodeposition of zno nanorods for device application," *Applied Physics A: Materials Science & Processing*, vol. 91, no. 4, pp. 595–599, 2008.

[31] A. Jimenez-Gonzailez and P. Nair, "Photosensitive zno thin films prepared by the chemical deposition method silar," *Semiconductor science and technology*, vol. 10, no. 9, p. 1277, 1995.

[32] O. Lupan, S. Shishiyanu, L. Chow, and T. Shishiyanu, "Nanostructured zinc oxide gas sensors by successive ionic layer adsorption and reaction method and rapid photothermal processing," *Thin solid films*, vol. 516, no. 10, pp. 3338–3345, 2008.

[33] A. Bakin, A. C. Mofor, A. El-Shaer, and A. Waag, "Vapour phase transport growth of zno layers and nanostructures," *Superlattices and Microstructures*, vol. 42, no. 1, pp. 33–39, 2007.

[34] P. Liu, Y. Li, Y. Guo, and Z. Zhang, "Growth of catalyst-free high-quality zno nanowires by thermal evaporation under air ambient," *Nanoscale research letters*, vol. 7, no. 1, p. 220, 2012.

[35] M. H. Huang, Y. Wu, H. Feick, N. Tran, E. Weber, and P. Yang, "Catalytic growth of zinc oxide nanowires by vapor transport," *Advanced Materials*, vol. 13, no. 2, pp. 113–116, 2001.

[36] X. Wang, S. Yang, X. Yang, D. Liu, Y. Zhang, J. Wang, J. Yin, D. Liu, H. Ong, and G. Du, "Zno thin film grown on silicon by metal-organic chemical vapor deposition," *Journal of Crystal Growth*, vol. 243, no. 1, pp. 13 – 18, 2002. [Online]. Available: http://www.sciencedirect.com/science/article/pii/S0022024802013726

[37] X. M. Ma, X. T. Yang, C. Wang, J. Yang, X. H. Gao, J. E. Liu, H. Jing, G. T. Du, B. Y. Liu, and K. Ma, "Zno thin film grown on glass by metal-organic chemical vapor deposition," in *2008 2nd IEEE International Nanoelectronics Conference*, March 2008, pp. 833–835.

[38] S. T. Tan, B. Chen, X. Sun, W. Fan, H. S. Kwok, X. Zhang, and S. Chua, "Blueshift of optical band gap in zno thin films grown by metal-organic chemical-vapor deposition," *Journal of Applied Physics*, vol. 98, no. 1, p. 013505, 2005.

[39] M. Tsoutsouva, C. Panagopoulos, D. Papadimitriou, I. Fasaki, and M. Kompitsas, "Zno thin films prepared by pulsed laser deposition," *Materials Science and Engineering: B*, vol. 176, no. 6, pp. 480 – 483, 2011, 6th International Conference on Nanosciences & Nanotechnologies, 13-15 July 2009, Thessaloniki, Greece. [Online]. Available: http://www.sciencedirect.com/science/article/pii/S092151071000214X

[40] R. Kumar, G. Kumar, and A. Umar, "Pulse laser deposited nanostructured zno thin films: A review," *Journal of nanoscience and nanotechnology*, vol. 14, no. 2, pp. 1911–1930, 2014.

[41] V. Craciun, J. Elders, J. G. Gardeniers, and I. W. Boyd, "Characteristics of high quality zno thin films deposited by pulsed laser deposition," *Applied physics letters*, vol. 65, no. 23, pp. 2963–2965, 1994.

[42] A. Ohtomo and A. Tsukazaki, "Pulsed laser deposition of thin films and superlattices based on zno," *Semiconductor science and technology*, vol. 20, no. 4, p. S1, 2005.

[43] B. Norris, J. Anderson, J. Wager, and D. Keszler, "Spin-coated zinc oxide transparent transistors," *Journal of Physics D: Applied Physics*, vol. 36, no. 20, p. L105, 2003.

[44] S. Ilican, Y. Caglar, and M. Caglar, "Preparation and characterization of zno thin films deposited by sol-gel spin coating method," *Journal of optoelectronics and advanced materials*, vol. 10, no. 10, pp. 2578–2583, 2008.

[45] Y. Heo, D. Norton, and S. Pearton, "Origin of green luminescence in zno thin film grown by molecular-beam epitaxy," *Journal of Applied Physics*, vol. 98, no. 7, p. 073502, 2005.

[46] Y. Chen, D. Bagnall, Z. Zhu, T. Sekiuchi, K.-t. Park, K. Hiraga, T. Yao, S. Koyama, M. Shen, and T. Goto, "Growth of zno single crystal thin films on c-plane (0 0 0 1) sapphire by plasma enhanced molecular beam epitaxy," *Journal of Crystal Growth*, vol. 181, no. 1-2, pp. 165–169, 1997.

[47] P. Zu, Z. Tang, G. K. Wong, M. Kawasaki, A. Ohtomo, H. Koinuma, and Y. Segawa, "Ultraviolet spontaneous and stimulated emissions from zno microcrystallite thin films at room temperature," *Solid State Communications*, vol. 103, no. 8, pp. 459–463, 1997.

[48] Y. Chen, D. Bagnall, H.-j. Koh, K.-t. Park, K. Hiraga, Z. Zhu, and T. Yao, "Plasma assisted molecular beam epitaxy of zno on c-plane sapphire:

growth and characterization," *Journal of Applied Physics*, vol. 84, no. 7, pp. 3912–3918, 1998.

[49] T. Voss, J.-P. Richters, and A. Dev, "Surface effects and nonlinear optical properties of zno nanowires," *physica status solidi (b)*, vol. 247, no. 10, pp. 2476–2487, 2010.

[50] G. Chu, Z. Xiong, and S. Zhao, "Growth of zn1- xmgxo and zn1- xcdxo nanowires and the application in light emitting devices," *Journal of nanoscience and nanotechnology*, vol. 10, no. 8, pp. 4893–4896, 2010.

[51] J. L. Vossen and W. Kern, "Thin film processes ii academic press," 1991.

[52] W. Steckelmacher, "Sputtering by particle bombardment iii: Characteristics of sputtered particles, technical applications: Edited by r behrisch and k wittmaack, with contribution by r behrisch, w hauffe, wo hofer, n laegreid, ed mcclanaham, bur sundquist, k wittmaack and ml yu (topics in applied physics, vol 64), springer, berlin, 1991. isbn 3-540-53428-8, xv+ 410 pp. dm 120." 1992.

[53] R. Hong, H. Qi, J. Huang, H. He, Z. Fan, and J. Shao, "Influence of oxygen partial pressure on the structure and photoluminescence of direct current reactive magnetron sputtering zno thin films," *Thin Solid Films*, vol. 473, no. 1, pp. 58–62, 2005.

[54] V. Gupta and A. Mansingh, "Influence of postdeposition annealing on the structural and optical properties of sputtered zinc oxide film," p. 10631073, Jul 1996. [Online]. Available: http://dx.doi.org/10.1063/1.362842

[55] S. K. Arya, S. Saha, J. E. Ramirez-Vick, V. Gupta, S. Bhansali, and S. P. Singh, "Recent advances in zno nanostructures and thin films for biosensor applications: Review," *Analytica Chimica Acta*,

vol. 737, no. Supplement C, pp. 1 – 21, 2012. [Online]. Available: http://www.sciencedirect.com/science/article/pii/S0003267012008148

[56] J. Zhang, G. He, L. Zhu, M. Liu, S. Pan, and L. Zhang, "Effect of oxygen partial pressure on the structural and optical properties of zno film deposited by reactive sputtering," *Applied surface science*, vol. 253, no. 24, pp. 9414–9421, 2007.

[57] R. Hong, J. Huang, H. He, Z. Fan, and J. Shao, "Influence of different post-treatments on the structure and optical properties of zinc oxide thin films," *Applied Surface Science*, vol. 242, no. 3, pp. 346–352, 2005.

[58] S. Singh and P. Chakrabarti, "Optical characterization of zno thin films grown by thermal oxidation of metallic zinc," *Advanced Science, Engineering and Medicine*, vol. 5, no. 7, pp. 677–682, 2013.

[59] C. Coskun, N. Gedik, and E. Balca, "The effect of high-energy electron irradiation on ZnO-based ohmic and Schottky contacts." *Semicond. Sci. Technol.*, vol. 21, no. 12, p. 1656, Oct. 2006.

[60] C. Periasamy and P. Chakrabarti, "Electrical and optical characterization of ZnO based nano and large area Schottky contacts," *J. Appl. Phys.*, vol. 11, no. 4, pp. 959–964, Jul. 2011.

[61] S. K. Cheung and N. W. Cheung, "Extraction of Schottky diode parameters from forward current-voltage characteristics," *Appl. Phys. Lett.*, vol. 49, no. 2, pp. 85–87, Jul. 1986.

[62] Y.-N. Lee, J.-K. Shin, Y.-T. Lee, M. Ishida, and W. Lee, "SOI-Based Schottky Barrier Diode Array for Ultraviolet Line-Scanner," *IEEE Sensors J.*, vol. 15, no. 3, pp. 1727–1731, Mar. 2015.

[63] S.-J. Young, "Photoconductive gain and noise properties of zno nanorods schottky barrier photodiodes," *IEEE Journal of Selected Topics in Quantum Electronics*, vol. 20, no. 6, pp. 96–99, 2014.

[64] Ş. Aydoğan, K. Çınar, H. Asıl, C. Coşkun, and A. Türüt, "Electrical characterization of Au/n-ZnO Schottky contacts on n-Si," *J. Alloys Compd.*, vol. 476, no. 1-2, pp. 913–918, May 2009.

[65] A. B. Yadav, A. Pandey, D. Somvanshi, and S. Jit, "Sol-Gel-Based Highly Sensitive Pd/n-ZnO Thin Film/n-Si Schottky Ultraviolet Photodiodes," *IEEE Trans. Electron Devices*, vol. 62, no. 6, pp. 1879–1884, Jun. 2015.

[66] A. B. Yadav, A. Pandey, and S. Jit, "Pd Schottky Contacts on Sol-Gel Derived ZnO Thin Films With Nearly Ideal Richardson Constant," *IEEE Electron Device Lett.*, vol. 35, no. 7, pp. 729–731, Jul. 2014.

[67] C. Tsiarapas, D. Girginoudi, and N. Georgoulas, "Electrical characteristics of Pd Schottky contacts on ZnO films," *Mater. Sci. Semicond. Process.*, vol. 17, pp. 199–206, Jan. 2014.

[68] H. Norde, "A modified forward I?V plot for Schottky diodes with high series resistance," *J. Appl. Phys.*, vol. 50, no. 7, pp. 5052–5053, Jul. 1979.

[69] M. Prasad, V. Sahula, and V. K. Khanna, "Long-Term Effects of Relative Humidity on the Performance of ZnO-Based MEMS Acoustic Sensors," *IEEE Trans. Device Mater. Rel.*, vol. 14, no. 2, pp. 778–780, Jun. 2014.

[70] N. P. Herring, L. S. Panchakarla, and M. S. El-Shall, "P-Type Nitrogen-Doped ZnO Nanostructures with Controlled Shape and Doping Level by Facile Microwave Synthesis," *Langmuir*, vol. 30, no. 8, pp. 2230–2240, Mar. 2014.

[71] T. Varma, S. Sharma, C. Periasamy, and D. Boolchandani, "Performance Analysis of Pt/ZnO Schottky Photodiode Using ATLAS." *J. Nanoelectron. Optoelectron.*, vol. 10, no. 6, pp. 761–765, Dec. 2015.

[72] R. L. Hoffman, B. J. Norris, and J. F. Wager, "ZnO-based transparent thin-film transistors," *Appl. Phys. Lett.*, vol. 82, no. 5, pp. 733–735, Feb. 2003.

[73] H. Bae, S. Im, and J. Song, "Low-Voltage Ultraviolet Detectors Using ZnO Thin-Film Transistor Isolated by B Ion Implantation," *Jpn. J. Appl. Phys.*, vol. 47, no. 7R, p. 5362, Jul. 2008.

[74] Z. Pan, X. Zhao, W. Peng, X. Qi, and Y. He, "A ZnO-Based Programmable UV Detection Integrated Circuit Unit," *IEEE Sensors J.*, vol. 16, no. 22, p. 79197923, Nov. 2016.

[75] R. B. M. Cross and M. M. De Souza, "Investigating the stability of zinc oxide thin film transistors," *Appl. Phys. Lett.*, vol. 89, no. 26, p. 263513, Dec. 2006.

[76] S.-J. Young, "Photoconductive gain and noise properties of ZnO nanorods Schottky barrier photodiodes." *IEEE J. Sel. Topics Quantum Electron.*, vol. 20, no. 6, pp. 96–99, Nov. 2014.

[77] T.-P. Chen, S.-J. Young, S.-J. Chang, C.-H. Hsiao, L.-W. Ji, Y.-J. Hsu, and S.-L. Wu, "Low-Frequency Noise Characteristics of ZnO Nanorods Schottky Barrier Photodetectors," *IEEE Sensors J.*, vol. 13, no. 6, pp. 2115–2119, Jun. 2013.

[78] G. Cheng, X. Wu, B. Liu, B. Li, X. Zhang, and Z. Du, "ZnO nanowire Schottky barrier ultraviolet photodetector with high sensitivity and fast recovery speed," *Appl. Phys. Lett.*, vol. 99, no. 20, p. 203105, Nov. 2011.

[79] G. M. Ali and P. Chakrabarti, "ZnO-based interdigitated MSM and MISIM ultraviolet photodetectors," *J. Phys. D: Appl. Phys.*, vol. 43, no. 41, p. 415103, Sep. 2010.

[80] D. Somvanshi and S. Jit, "Pd/ZnO nanoparticles based Schottky ultraviolet photodiodes grown on Sn-coated n-Si substrates by thermal evaporation method," *IEEE Journal of Selected Topics in Quantum Electronics*, vol. 20, no. 6, pp. 120–125, 2014.

[81] K. Sundaram and A. Khan, "Work function determination of zinc oxide films," *Journal of Vacuum Science & Technology A: Vacuum, Surfaces, and Films*, vol. 15, no. 2, pp. 428–430, 1997.

[82] I. Saurdi, M. Mamat, M. Malek, and M. Rusop, "Preparation of aligned zno nanorod arrays on sn-doped zno thin films by sonicated sol-gel immersion fabricated for dye-sensitized solar cell," *Advances in Materials Science and Engineering*, vol. 2014, pp. 1–8, 2014.

[83] S. Sharma, S. Vyas, C. Periasamy, and P. Chakrabarti, "Structural and optical characterization of zno thin films for optoelectronic device applications by rf sputtering technique," *Superlattices and Microstructures*, vol. 75, pp. 378–389, 2014.

[84] S.-J. Young, L.-W. Ji, R. W. Chuang, S.-J. Chang, and X. Du, "Characterization of zno metal–semiconductor–metal ultraviolet photodiodes with palladium contact electrodes," *Semiconductor science and technology*, vol. 21, no. 10, p. 1507, 2006.

[85] A. Polyakov, N. Smirnov, E. Kozhukhova, V. Vdovin, K. Ip, Y. Heo, D. Norton, and S. Pearton, "Electrical characteristics of au and ag schottky contacts on n-zno," *Applied physics letters*, vol. 83, no. 8, pp. 1575–1577, 2003.

[86] C. Periasamy and P. Chakrabarti, "Fabrication and characterization of au/zno nano-schottky contacts," *Journal of Nanoelectronics and Optoelectronics*, vol. 5, no. 1, pp. 38–42, 2010.

[87] W. Park, G.-C. Yi, J.-W. Kim, and S.-M. Park, "Schottky nanocontacts on zno nanorod arrays," *Applied Physics Letters*, vol. 82, no. 24, pp. 4358–4360, 2003.

[88] C. Mead, "Surface barriers on znse and zno," *Physics Letters*, vol. 18, no. 3, p. 218, 1965.

[89] T. Kim, J. Lee, H. Kim, S. Kim, and W. J. Cho, "Effect of a pt substrate on the growth and fabrication of zno schottky diodes," *JOURNAL-KOREAN PHYSICAL SOCIETY*, vol. 50, no. 3, p. 594, 2007.

[90] M. Rusop, "Effect of film thickness on structural, electrical, and optical properties of sol-gel deposited layer-by-layer zno nanoparticles," *Transactions on Electrical and Electronic Materials*, vol. 13, no. 2, pp. 102–105, 2012.

[91] H. Kim, A. Sohn, Y. Cho, and D.-W. Kim, "Temperature-dependent electrical characteristics of ag schottky contacts to differently grown o-polar bulk zno," *Journal of Electronic Packaging*, vol. 135, no. 1, p. 011010, 2013.

[92] S. Chand, P. Kaushal, and J. Osvald, "Numerical simulation study of current–voltage characteristics of a schottky diode with inverse doped surface layer," *Materials Science in Semiconductor Processing*, vol. 16, no. 2, pp. 454–460, 2013.

[93] K. Sundaram and A. Khan, "J. of vac., sc. and tech," *A: Vacuum, Surfaces and Film*, vol. 15, p. 428, 2009.

[94] S. Sharma and C. Periasamy, "Effect of sputtering power on structural and optical properties of zno thin films grown by rf sputtering technique," *Journal of Nanoelectronics and Optoelectronics*, vol. 10, no. 2, pp. 205–210, 2015.

[95] S.-J. Young, L.-W. Ji, S.-J. Chang, Y. Chen, and S. Peng, "Zno schottky diodes with iridium contact electrodes," *Semiconductor Science and Technology*, vol. 23, no. 8, p. 085016, 2008.

[96] S. Sharma and C. Periasamy, "Simulation study and performance analysis of n-zno/p-si heterojunction photodetector," vol. 19, pp. 1633–1636, 2014.

[97] D. S. Atlas, "Atlas users manual," *Silvaco International Software, Santa Clara, CA, USA*, 2005.

[98] K. Yang, J. R. East, and G. I. Haddad, "Numerical modeling of abrupt heterojunctions using a thermionic-field emission boundary condition," *Solid-State Electronics*, vol. 36, no. 3, pp. 321–330, 1993.

[99] S. Sharma and C. Periasamy, "A study on the electrical characteristic of n-zno/p-si heterojunction diode prepared by vacuum coating technique," *Superlattices and Microstructures*, vol. 73, pp. 12–21, 2014.

[100] S. Sharma, B. C. Bayer, S. V., S. G., and C. Periasamy, "Structural, Electrical, and UV Detection Properties of ZnO/Si Heterojunction Diodes," *IEEE Trans. Electron Devices*, vol. 63, no. 5, pp. 1949–1956, May 2016.

[101] S. Sharma, T. Varma, K. Asokan, C. Periasamy, and D. Boolchandani, "Annealing Temperature Dependent Structural and Optical Properties of RF Sputtered ZnO Thin Films." *J. Nanosci. Nanotechnol.*, vol. 17, no. 1, pp. 300–305, Jan. 2017.

[102] D. Somvanshi and S. Jit, "Electrical and optical characterization of Pd/ZnO nanorods (NRs) Schottky diodes grown on n-Si substrates." *Solid State Physics.*, vol. 1591, no. 1, pp. 1425–1427, 2014.

[103] T. Varma, C. Periasamy, and D. Boolchandani, "Performance analyses of Schottky diodes with Au/Pd contacts on n-ZnO thin films as UV detectors (doi.org/10.1016/j.spmi.2017.08.060)," *Superlattices Microstruct.*, 2017.

[104] J. S. Park, W.-J. Maeng, H.-S. Kim, and J.-S. Park, "Review of recent developments in amorphous oxide semiconductor thin-film transistor devices," *Thin solid films*, vol. 520, no. 6, pp. 1679–1693, 2012.

[105] T. Kamiya, K. Nomura, and H. Hosono, "Present status of amorphous ingazno thin film transistors," *Science and Technology of Advanced Materials*, vol. 11, no. 4, p. 044305, 2010.

[106] H. S. Bae, M. H. Yoon, J. H. Kim, and S. Im, "Photodetecting properties of ZnO-based thin-film transistors," *Appl. Phys. Lett.*, vol. 83, no. 25, pp. 5313–5315, Dec. 2003.

[107] S. Dubey, P. K. Tiwari, and S. Jit, "A two-dimensional model for the subthreshold swing of short-channel double-gate metal–oxide–semiconductor field effect transistors with a vertical gaussian-like doping profile," *Journal of Applied Physics*, vol. 109, no. 5, p. 054508, 2011.

List of publications from this thesis work

Peer-reviewed International journals

- Tarun Varma, Shashikant Sharma, C.Periasamy and D. Boolchandani, Performance Analysis of Pt/ZnO Schottky Photodiode Using ATLAS, Journal of Nanoelectronics and Optoelectronics (SCI) Volume: 10/761-765/2015 ISBN:1555-1318.

- S. Sharma, Tarun Varma, K. Asokan, C. Periasamy, Dharmendar Boolchandani, "Annealing Temperature Dependent Structural and Optical Properties of RF Sputtered ZnO Thin Films", Journal of Nanoscience and Nanotechnology (SCI, Impact factor:1.55) Volume:1/1-5/2015.

- Tarun Varma, C. Periasamy and D. Boolchandani, "Performance Analyses of Schottky Diodes with Au/Pd Contacts on n-ZnO thin films as UV detectors", Superlattices and Microstructures journal, 2017 (SCI, Impact factor: 2.123)

- Tarun Varma, C. Periasamy and D. Boolchandani, "Performance Evaluation of Staggered Bottom Gate ZnO Thin Film Transistors with Different W/L Ratios for UV Sensing", Superlattices and Microstructures journal. (Communicated on 21st September, 2017 (under review))

Peer-reviewed International conference

- Tarun Varma, C.Periasamy, Dharmendar Boolchandani, "Electrical and UV Detection Properties of ZnO Thin Film Based Schottky Contacts Deposited by RF Magnetron Sputtering", IEEE conference on Emerging Devices and Smart Systems on 3rd and 4th March, 2017. (ICEDSS 2017)

Brief Curriculum-Vitae

Tarun Varma obtained his Bachelor of Engineering degree in Electronics & Communication Engineering from M.B.M. Engineering College, University of Jodhpur, in 1989. He obtained the Master of Engineering degree in Electronics & Communications Engineering from the erstwhile Regional Engineering College, now, Malaviya National Institute of Technology, Jaipur in 2003. He is currently Associate Professor in the Department of Electronics & Communications Engineering at Malaviya National Institute of Technology, Jaipur, India. His current research interests include nano material based optoelectronic devices. He is a member of IEEE since 1997.